The Role of Peptidyl Arginine Deiminases in Regulating Anti-tumor Responses in Immune Cells

By

Michael Reginald Pitter

A dissertation submitted in partial fulfillment
of the requirements for the degree of
Doctor of Philosophy
(Molecular and Cellular Pathology)
in the University of Michigan
2024

Doctoral Committee:

Professor Weiping Zou, Co-Chair
Professor Arul Chinnaiyan, Co-Chair
Professor Maria Castro
Assistant Professor Ilona Kryczek
Associate Professor Yongqing Li

Michael Reginald Pitter

mrpitter@umich.edu

ORCID iD: 0000-0002-1183-4217

Dedication

This dissertation is dedicated to my family, friends, colleagues, and mentors who supported me along my journey to producing this work. Importantly, it is dedicated to my father, the late Dr. Michael C. Pitter MD – a chemical engineer and gynecologic surgeon – who passed away from cancer shortly before my beginning my PhD studies. He played a major role in the development of who I am today and who I continue to become.

Acknowledgements

This work would not have been possible without the substantial support that I received from several people in different areas of my life. I took an academic turn, transitioning from my undergraduate studies in English literature and philosophy to the biomedical sciences. One semester after graduating from Boston University, I enrolled in a post-baccalaureate biomedical sciences program at Columbia University. There, I initially intended to attend medical school to become a physician. I completed all the necessary courses: biology I&II, inorganic chemistry I&II, organic chemistry I&II and physics I&II. During this time, I started to volunteer in a neurobiology laboratory (The Rae Silver Laboratory) where they studied circadian rhythms and behavioral neuroscience. Eventually, towards the end of my post-baccalaureate studies, I started to work there part-time and then upon finishing my studies, I started to work there full-time to continue the research in which I was engaged. The main projects to which I contributed the most focused on the mechanisms by which chronic methamphetamine use induced neuroinflammation in various regions of the brain which reinforced drug-seeking behavior. We approached the treatment of drug-seeking behavior or addiction via the treatment of neuroinflammation in the brain. I co-authored multiple publications and even presented our findings at the National Institutes on Drug Abuse (NIDA) Genetics Consortium in Washington D.C. The process of working in the laboratory, elucidating phenomena which may be applied towards the treatment of human disorders, the production of knowledge via the publication of our work and the sharing of ideas at conferences with peers and colleagues inspired me deeply to become a scientist and an investigator. After working in the Rae Silver Lab, I went onto work as a Research Technician in

the laboratory of Marcel van den Brink at the Sloan Kettering Institute. Here, I was exposed to the rigors of a high-impact, productive lab in which our work therein would be directly applied to patients with cancer at the Memorial Sloan Kettering Cancer Center across the street. This experience further motivated me to become more engaged as a researcher in immunology. Therefore, I pursued a PhD at the University of Michigan with the goal of working in the laboratory of Weiping Zou. Between the completion of my undergraduate studies and the matriculation at the University of Michigan, there are several individuals whom I would like to acknowledge.

During my time at Boston University as a liberal arts student, a number of experiences contributed to my ultimate pursuit in the sciences. Most profoundly, I was fortunate to have been able to study abroad in Haifa, Israel during my junior year of college and travel to several different places in the region, including parts of Turkey and parts of Ethiopia. This traveling experience moved me and it became crucial to me that my career would be dedicated to working in a universal space. I wanted my future work to be useful and beneficial for all humans regardless of language and ethnic background. Through medical research, I could contribute to human health and be a productive member of the wider world, which I found exciting and imperative. Importantly, as a college student, I had the privilege of having a number of mentors who contributed to my transition into the sciences. Professor Allison Blakely who lectured on Black History in Europe; Professor Victor Kestenbaum who lectured in various topics in philosophy including Human Nature; and Christopher Martin who lectured on Literary Criticism all contributed to the broadening of my perspective and my role in the world.

I began my scientific journey at Columbia University. With great compassion, I would like to acknowledge three critical mentors who were instrumental in my early development as a

scientist: Dr. Rae Silver, Dr. Joseph LeSauter and Dr. Carl Hart. As a post-baccalaureate student in the biomedical sciences, I contacted several principal investigators (PIs) to inquire whether I could conduct research in their labs. I felt that conducting research would be a necessary addition to my biomedical science courses as I could be exposed to the frontiers of science and understand better the importance and usefulness of scientific knowledge. Dr. Rae Silver was the only PI who responded to my email and invited me to volunteer in her lab. Eventually, I joined the lab and would work there for the next 2.5 to 3 years. During this time, I led and contributed to multiple projects. I also served as a mentor to undergraduate and some graduate students, instructing them on techniques including immunohistochemistry, microscopy, *in vivo* experiments, and concepts in behavioral neuroscience. Although I did not realize it at the time, Dr. Silver gave me the opportunity of a lifetime and I will always be grateful for this chance. Dr. Joseph LeSauter, also known as Joe, was the head Research Scientist in the Silver Lab. I worked with him daily, devising experiments, building research apparatuses, analyzing data, troubleshooting, composing research papers and proposing new research directions. I thrived in this environment because I felt no limits to my curiosity and I was motivated by my own certainty that the work that we were doing was important. As I mentioned above, one of the major research foci in the lab focused on the neuroinflammatory basis of methamphetamine addiction with the goal of treating drug-seeking behavior by reducing neuroinflammation. When I would leave the laboratory in Morningside Heights to return to my apartment in Bedford-Stuyvesant by train, I would unfortunately see individuals on the streets or in the subway who might have been victims of drug addiction of some kind which led them to pursue other self-destructive paths. Perhaps, for the first time, I felt that I was contributing to the development of solutions to a human problem. Finally, I must acknowledge Dr. Carl Hart. He was and continues

to be a close collaborator of Dr. Rae Silver. Dr. Carl Hart was among the very few Black professors in the sciences with tenure at Columbia University. As a neuropsychopharmacologist, he was also engaged in research studies investigating drug addiction in humans. He led a laboratory in the New York State Psychiatric Institute in which he studied human cognition under the influence of drugs including cocaine and methamphetamine. I would sometimes work in his lab. Dr. Carl Hart's research has been interpreted to be controversial as he sought to redefine "addiction" as it was traditional understood in society and how it was presented in the Diagnostic and Statistical Manual of Mental Disorders, 5th edition (DSM-5). Dr. Carl Hart continues to be an important mentor to me because he would always stress not to take for granted what is published or what is considered established knowledge: question everything. From my time at Columbia, I would also like to acknowledge Claudia Juárez Portilla and Rachel Kim from the Silver Lab; and Kirsten Frazer from the Hart Lab.

As mentioned above, I worked as a Research Technician in the laboratory of Dr. Marcel van den Brink at the Sloan Kettering Institute. I would like to acknowledge Dr. van den Brink for giving me the opportunity to work with his group. The van den Brink lab was a highly productive lab consisting mostly of post-doctoral fellows. I learned a great deal here in terms of immunology, translational research, wet lab techniques and how best to navigate a large, competitive lab. Working here was a necessary condition for any future endeavor I would engage in, I thought. In the van den Brink Lab, I must acknowledge Antonio Gomes, the Senior Computational Biologist there at the time. While we were colleagues, we also became good friends and soccer teammates. Importantly, he inspired me to pursue bioinformatics as I could see that the lab members, in large part, depended heavily on his expertise. I would also like to acknowledge Melody Smith MD, a physician-scientist in the lab from whom I received valuable

advice both professionally and scientifically. She also invited me to co-author a review article with her which simultaneously augmented my knowledge in the immunotherapy field and gave me the opportunity to inform a wide range of readers on the cutting edge of emerging immunotherapeutic strategies. Following this experience in the van den Brink Lab, I felt well prepared to enroll in a PhD program and to lead my own projects.

The prospect of working in the laboratory of Dr. Weiping Zou initially motivated me to apply to the University of Michigan for graduate studies. Gratefully, I was recruited to his lab where I would have the opportunity to lead projects which were interesting, which contributed to advancements in immuno-oncology and which sought to ultimately improve human health. Throughout the years of working in the Zou Lab, I grew in many ways: intellectually, scientifically, emotionally, and socially. The rigors of our work in the lab continue to humble me and, in this process, I develop as a researcher and evolve as a person. Aside from the science and research practices, I learned a great deal from Weiping regarding leadership – not just how to manage people, but how to manage ideas. Thus, through his mentorship, I benefitted greatly on multiple levels, and this motivated me to always strive to improve myself and my work. Importantly, he gave me the opportunity to not just conduct research but to present my work and network. Weiping encouraged me to present my thesis work at the annual American Association of Immunologists (AAI) meeting in Washington DC and at the European Macrophage and Dendritic cell Society (EMDS) meeting in Ghent, Belgium. At both meetings, I had the valuable opportunity to share and discuss my work with diverse groups of researchers including those who are pioneers in the field. I would also like to acknowledge Ilona “Inka” Kryczek who co-led the Zou Lab. The combined mentorship of Weiping and Inka was essential for my success, my progress and my continued motivation in the lab throughout my PhD work. Inka mentored me on

a day-to-day basis, providing her expert knowledge to help me through various technical challenges and biological quandaries. Moreover, I admire her intuition in immunology, her encyclopedic knowledge in the field and her lack of hesitation to criticize scientific studies when she notices conceptual or methodological limitations. Through the combined mentorship of Weiping and Inka, it has become second-nature for me to remain critical of new and old scientific findings alike. I would like to thank and acknowledge the Zou Lab members – Linda Vatan, Shuang Wei, Wojciech Szeliga, Sara Grove, Jiajia Zhou, Weichao Wang, Peng Liao, Karolina Okla, Jiali Yu, Houjun Xia, Gaopeng Li, Heng Lin, Hongjuan Zhang and Jing Li – who always showed me kindness and from whom I learned a great deal about both science and life. Side-by-side, we worked together each day and learned from each other. Moreover, during my time in the lab, we as a group together endured several major world events including the 2020 coronavirus pandemic, the killing of George Floyd, the rise in anti-Asian violence, the War in Ukraine, the War in Gaza and more. During this transformative time in history, we worked together and supported each other. Having endured this, I believe that our bonds grew stronger. I also need to thank my Thesis Committee members: Yongqing Li, Arul Chinnaiyan and Maria Castro including Inka and Weiping. They were consistent in their support of my work. They were critical when they needed to be but also reminded me of the good progress that I would make along the way. I am deeply grateful for their input and our conversations. I must especially thank Dr. Yongqing Li, who studies PADs in his laboratory and who supplied us with the necessary mice and reagents needed to carry out my experiments. Without his help, none of our discoveries would have been possible.

Most importantly, I must acknowledge my family. With a heavy heart, I acknowledge my father, the late Dr. Michael Claude Pitter MD. He was a chemical engineer and an OB/GYN

who, later in his career, went on to focus on robot-assisted minimally invasive surgery. He was a pioneer in that he was among the first physicians to apply robotic surgery to gynecologic disorders. He also trained physicians around the world on several techniques in robotic surgery. My father and I were very close. He introduced me to several important touchstones of life including the need to know and understand history, to question authority, and to enrich my knowledge on multiple topics including art, science and history. He passed away due to the development of an aggressive prostate cancer shortly before I started my PhD studies. Interestingly, he also lost his father in his early years as a medical student. Given this experience of losing my father, I needed to channel or repurpose my grief towards my academic progress. Thus, my work in the lab became highly personal, since we were investigating a disease that afflicted my father: cancer. Further, I need to thank and acknowledge my mother and sister. Following the loss of my father, my mother, sister and I became increasingly closer. The years following his passing were quite challenging as we dealt with managing grief and living apart. They supported me in several ways as I engaged in my thesis work. Their support was essential for my success throughout the PhD. I owe this accomplishment to them. I am as proud of them as they are of me. I also would like to acknowledge my extended family including my cousins (including Bert and Jasmine) and my maternal grandmother in Belize.

Finally, I acknowledge friends that I have made along my journey. First, I want to acknowledge two of my good college friends: Joshua “Josh” Levkowitz and Phillipe Chatelain. Josh and I traveled extensively during our college years to multiple places in Central America including Belize and Guatemala, and various parts of Ethiopia, including Addis Ababa, Lalibela and other places. These experiences expanded my world view bestowing upon me a global awareness which nurtured my developing scientific mind. Moreover, his continued friendship

has been essential throughout my PhD experience. Next, I acknowledge my good friend Phillipe Chatelain. In college, we started a collaborative music project which evolved into a literary magazine. This was an exciting project in which we could fully exercise our creativity. We initiated this magazine towards the end of my college years and continued to contribute to it throughout my post-baccalaureate years. As I began to develop as a scientist, I started to integrate science more into my writing, which further enhanced my motivation and determination to pursue a future in science.

Finally, I want to thank the entire Molecular and Cellular Pathology (MCP) department including faculty and students. Among the faculty, I want to extend a special thanks to the MCP program directors Drs. Zaneta Nikolovska-Coleska, Jean-François Rual and Simon Hogan. During most of my time as a PhD student, Zaneta was our program director, and I deeply appreciated her guidance and concern for our careers. I would like to acknowledge those in my cohort with whom I entered MCP: Sahiti Marella, Jessica McNaulty Teitel and Alec Monovich. These three individuals including the rest of MCP students were like members of a family. Our MCP family was a tiny community in the macrocosm that is the University of Michigan. Finally, I acknowledge those outside of my cohort who became close friends Will Stith, Mohamed Mire, Jamar Washington, Harihar Mohan, Amelia Grant-Alfieri and Phoenix Williams. I value greatly the time spent with these people and look forward to knowing them in the years to come.

Table of Contents

List of Figures

Abstract

Arginine deimination – also known as citrullination – is an understudied post-translational modification which continues to garner interest across biomedical research fields since the mechanism has been implicated in the progression of multiple diseases. While citrullination has been shown to control processes in pluripotent stem cells and cancer cells, studies on the regulatory roles of citrullination in immune cell subsets are limited. A large body of work has accumulated over the decades describing the process by which aberrant histone citrullination in neutrophils drives a number of autoimmune diseases – most notably rheumatoid arthritis – however the disease-associated processes regulated by citrullination in mononuclear immune cells have yet to be comprehensively studied. A family of peptidyl arginine deiminases (PADs) citrullinate protein targets catalyzing the conversion of arginine residues into peptidylcitrulline changing protein charge from positive to neutral and as a consequence altering protein folding and function. The five PAD isozyme family members including PAD1-4 and 6, modify a wide range of protein targets, however only PAD2 and PAD4 have been shown to translocate into the nucleus and therefore may have more access to controlling fundamental functions of the cell via the citrullination of both cytoplasmic and nuclear proteins alike. In this body of work, we begin by surveying the current knowledge on PAD2 and PAD4-mediated citrullination in immune cell subsets including neutrophils, T-cells and macrophages. To substantiate our understanding on the range of consequences from protein citrullination, we will briefly discuss the outcomes of citrullination in cancer cells and stem cells. Importantly, we will present our original findings demonstrating a key role of PAD4 in macrophages and a preliminary understanding of an important role for PAD2 in lymphocytes. In macrophages, we discovered that PAD4 citrullinates transcription factor signal transducer and activator of transcription 1 (STAT1) facilitating the inhibitory interaction between STAT1 and the protein inhibitor of activated STAT1 (PIAS1), negatively regulating STAT1 binding to DNA and, consequently, restraining key downstream pathways. We observed that MHC-II–mediated antigen presentation was selectively restrained and that this had a major impact on tumor growth *in vivo* and the response to immunotherapy in mice and in humans. In this dissertation, more focus will be placed on the study of PAD4 activity in macrophages. These studies provide novel as well as useful mechanistic insights into how citrullination may be clinically targeted.

Through this work, we aim to elucidate the significance of citrullination in the regulation of immune cell functions for the purpose of suggesting means of targeting immune cell citrullination for the enhancement of anti-tumor immunity.

Chapter 1: Introduction

Section 1: Cancer and anti-tumor immunity via T-cells and macrophages: discoveries, advancements, and challenges

Within the past few decades, the role of the immune system in driving cancer outcomes has become more of a central concern when devising the treatment strategies against a diversity of cancers and pathologies[1]. A multitude of discoveries dating back to the late 19th century demonstrating the role of the immune system in antagonizing tumor growth coalesced over time to give birth to and to shape the field of cancer immunology[2]. Famously, Douglas Hanahan and Robert Weinberg revised their *Hallmarks of Cancer* to include the tumor's ability to avoid immune destruction among other newly understood phenomena occurring in tumor biology[3]. Studies in cancer immunology interrogate how particular cellular systems and components of the tumor microenvironment (TME) contribute to promoting or antagonizing tumor immunity, or tumor cell death due to the immune system. The TME consists of tumor cells, immune cells and other subsets including stroma, non-cancerous epithelial cells and fibroblasts[4]. Each component plays a variety of shared or mutually exclusive roles towards tumor growth or control. Modern clinical cancer immunotherapy has been developed to potentiate T-cell–mediated anti-tumor immunity as a means to circumvent the immunosuppressive functions of tumor cells and antigen-presentation cells[5]. The development and use of immune checkpoint blockade (ICB) therapy constitutes a major scientific breakthrough in cancer treatment offering practical strategies in harnessing the immune system against cancer[6,7,8]. Given the complicated nature of cancer and the tumor evasion from immune surveillance, more recent studies have shifted focus to ascertain

whether other cellular components of the TME could be targeted as a means to enhance anti-tumor immunity. Macrophages constitute the most abundant immune cell in the TME and has been shown to wield a strong influence over determining tumor growth[9]. While macrophages can promote tumor growth through the production of anti-inflammatory cytokines, angiogenesis and other means; macrophages can also prevent tumor growth through the production of pro-inflammatory cytokines, phagocytosis and the upregulation of antigen presentation molecules[10]. In response to this, several new research directions have been initiated to elucidate the mechanisms in macrophages which support pro-tumor functions such that they may be manipulated to maximize anti-tumor functions in macrophages. Today and going forward, targeting the crosstalk between T-cells and macrophages or targeting macrophages alone constitutes a complete and comprehensive strategy for enhancing anti-tumor immunity in cancer patients[11].

Several challenges exist in the targeting T-cells and macrophages in cancer treatment. Principally, tumor immunity relies on the functioning of effector T-cells to induce the cell death of the tumor cells[12,13,14,15]. Therefore, activated tumor–specific T-cells are required for tumor immunity. Unfortunately, several obstacles occur in the TME which are sufficient to impairing the anti-tumor T-cell response. The antithesis to T-cell functioning is T-cell dysfunction which can occur due to T-cell ignorance, tolerance, anergy or so-called exhaustion[5]. A variety of components in the TME as well as in the T-cell activation process can induce dysfunction in T-cells including the accumulation of immunosuppressive cytokines and the dampening of the TCR response due to chronic activation[16,17,18]. Tumor cells, tumor–associated macrophages (TAMs), myeloid–derived suppressor cells (MDSCs) and cancer–associated fibroblasts (CAFs) all

contribute to the maintenance of an immunosuppressive TME through the production of anti-inflammatory cytokines and factors including IL10, arginase 1 (ARG1), transforming growth factor beta (TGF-β), vascular endothelial growth factor A (VEGFA) and more[4,19]. Moreover, tumor cells and TAMs have been extensively reported to also compete for vital nutrients such as glucose with $CD8^+$ T-cells in the TME and consequently, metabolically inducing T-cell dysfunction[20,21]. Importantly, the downregulation of co-stimulatory and antigen presentation surface molecules on antigen–presenting cells (APCs) contributes profoundly to the hypofunctionality of effector T-cells[22]. A foundational study found that the downregulation of MHC class II transcription – mediated by the class II transactivator (CIITA) – is a common strategy used by pathogens to circumvent and escape immune surveillance[23]. In cancer, the downregulation of MHC-II on macrophages leads directly to the exacerbation of tumor growth[24]. Through several means, the components of the TME are sufficient to restrain anti-tumor T-cell responses worsening disease outcomes. Beyond ICB therapy, other modes of immunotherapy such as IL-2 treatment and chimeric antigen receptor (CAR) T-cell therapy have shown limited efficacy (characterized by low response rate) and have also shown to induce a toxic cytokine release syndrome or a cytokine storm which worsens patient survival outcomes[25,26,27]. Although effector T-cells play the crucial role in the tumor killing, the effectiveness and survival of tumor–infiltrating T-cells depends on the TME and thus, the TME determines the T-cell function. Given this insight, new strategies have emerged which target other components in the TME which can directly impact T-cell functioning. Together, targeting the potentiation of T-cells alone as a treatment strategy may be insufficient for durable cancer treatment going forward.

As aforementioned, it has been reported that TAMs are the most abundant immune cell in the TME[9,28,29,30]. Therefore, macrophage functions play a crucial role in determining the course

of tumor growth or regression. On the one hand, macrophages came promote tumor growth through the production of immunosuppressive cytokines, the promotion of angiogenesis and downregulation of antigen presentation molecules[31,32,33,34,35]. On the other hand, macrophages can prevent tumor growth through the production of proinflammatory cytokines, phagocytosis and the upregulation of antigen presentation molecules, particularly major histocompatibility class II (MHC-II)[36,37,38]. Because of this plasticity in TAM functions and the strong influence that macrophages have on systemic immunity in TME, several strategies have been developed and implemented which target macrophages as a means to enhance anti-tumor immunity whether T-cell–mediated or directly mediated by macrophages[37,39]. Research elucidating the role of macrophages in cancer dates back to the 19th century[40]. The Nobel Prize in Physiology or Medicine was awarded to Élie Metchnikoff in 1908 for his discovery of the process of phagocytosis mediated by the so-called phagocyte in the 1880s. Despite the long history of the knowledge on macrophages, only recently has there emerged practical modes of treatment which target the protumor functions of macrophages. In 2018, the anti-CSF1R inhibitor was approved for the treatment of tenosynovial giant cell tumors[40,41]. In 2019, the anti-CD47 antibody – which blocks the so-called 'don't eat me' CD47-SIRPα interaction, enabling macrophage phagocytosis of cancer cells as well as anti-tumor T-cell activation – was approved for clinical trials[40,42,43]. Recently, the human chimeric antigen receptor macrophages were developed which were shown to enhance the macrophage–mediated phagocytosis as well as anti-tumor T-cell activity[11]. While these pioneering studies demonstrate the necessity of targeting macrophages – as a means to enhance systemic anti-tumor immunity via the potentiation of innate immune functions as well as the potentiation of anti-tumor T-cell–mediated activity – there still remains a substantial portion of TAM biology that has yet to be elucidated. More studies are needed to elucidate

intrinsic and homeostatic mechanisms in macrophages which program macrophage phenotypes and shape macrophage functions in the TME.

Elucidation of novel mechanisms which may control T-cell and macrophage functions in the TME remains as a priority in the efforts to develop comprehensive, durable and efficacious immunotherapeutic strategies. Post-translational modifications (PTMs) are processes which shape the final protein functions in cells and, thus, may have a strong influence over immune cell phenotypes[44,45,46]. So far, very few studies have begun to characterize the critical role which PTMs have over governing immune cell functions in the TME[47,48,49]. Given the vast diversity of PTMs including methylation, phosphorylation, acylation, acetylation, prenylation, citrullination and more; there still remains a large field of unknown phenomena controlled by PTMs which may impose strong programs over macrophage and T-cell phenotypes during cancer. Here, through our work, we further elucidate the regulatory role of PADs in macrophages and T-cells and show how the citrullination of key targets controls transcriptional programs in these subsets and, consequently, controls their respective anti-tumor functions.

Section 2: Citrullination: development of the field, research tools and mechanistic details

Section 2.1: Introduction

Citrullinated proteins in mammals were first observed in 1958 when *G.E. Rogers et al* discovered that the fibrous protein of the inner root sheaths of rat hair follicles contained citrulline[50]. Although, preceding this finding, *Smith and Young* had observed the occurrence of citrulline integrated into proteins found in the red algae species[51], *Chondris crispus*. The discovery by *G.E. Rogers et al* would nevertheless pave the way for studies on citrullination in mammalian biology and eventually in human health and medicine. Citrullination occurs when

PADs catalyze the hydrolysis of the guanidine group on peptidyl arginine into urea producing peptidylcitrulline with the elimination of the imine group as ammonia (**Figure 1.1**)[52].

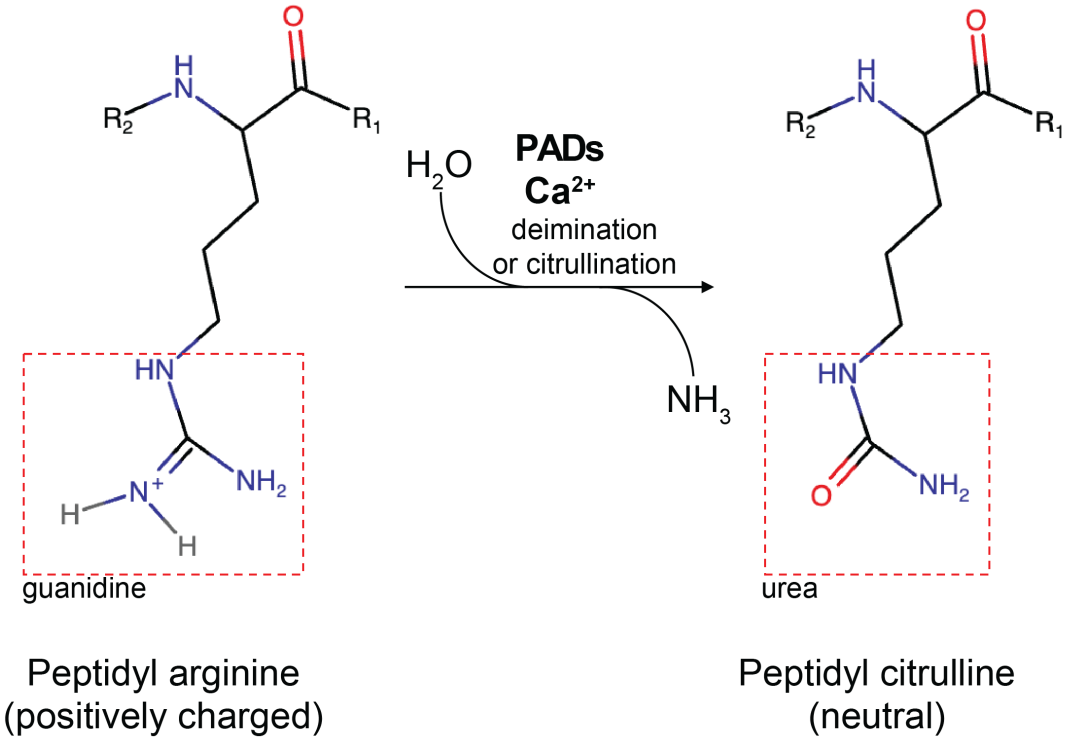

Figure 1.1.0: Citrullination. PADs convert arginine residues on proteins into citrulline via hydrolysis

This molecular event wherein arginine residues are converted into a non-coded amino acid alters the steric conformation of the protein substrate and as a consequence regulates the protein function. Decades following the initial discoveries of citrullinated proteins in the 1950s, further research revealed that several cytoplasmic and nuclear proteins served as substrates to a variety of PAD isozymes[53]. Famously, PADs – PAD2 and PAD4 – citrullinate histones since they can localize into the nucleus altering chromatin structure in the process[54]. Depending on the cell-type and the extracellular conditions, a variety of molecular events occur downstream of histone citrullination including neutrophil extracellular trap (NET) formation, regulation of DNA damage and regulation of transcription via chromatin remodeling. Moreover, a few studies have shown PAD2 or PAD4 regulation of transcription via the citrullination of non-histone targets.

Taken together, the study of citrullination as a critical post-translational modification has emerged because of the important consequences of citrullination in controlling fundamental cellular systems, functions and phenotype.

Here, we will survey a comprehensive body of studies which all together provide useful insights on the phenomenon of citrullination in mammalian biology and its significance in human health. We will place emphasis on the activity of nuclear PADs – PAD2 and PAD4 – as a means to shed light on their potential functions in immune cell subsets.

Section 2.2: Mechanistic insights of citrullination in immune cells

Calcium ion dependence for the induction of PAD citrullination

The dependency on metal ions for the activation of enzymes has long been observed[55]. The enzymatic activation of PADs requires calcium ion (Ca^{2+}) binding to key residues on the PAD protein. The Ca^{2+} binding sites on PAD4 have been well characterized. Studies examining the crystal structures of Ca^{2+}-free PAD4 and Ca^{2+}-bound PAD4 have revealed that PAD4 possesses five calcium ion binding sites[56]. Five distinct Ca^{2+} ions designated as Ca1, Ca2, Ca3, Ca4 and Ca5 were found to bind to nonredundant motifs on PAD4. Ca1 and Ca2 are positioned adjacent to the active site cleft. The molecular location of Ca1 and Ca2 are conserved throughout the PAD family except in PAD6. Ca3-Ca5 are positioned in the N-terminal domain, the same domain which contains the canonical nuclear localization sequence (NLS) enabling PAD4 to translocate into the nucleus. Arita *et al*[56] demonstrated that the binding of Ca3-5 to the particular residues on the N-terminal domain serves to stabilize the N-terminal structure. Thus, the calcium binding required for PAD4 enzymatic activity has been thoroughly described. Preceding these findings regarding PAD4, Takahara *et al* determined that out of a group of metal ions including Mg^{2+},

Mn^{2+}, Co^{2+}, Ni^{2+}, Cu^{2+}, Zn^{2+} and more, only Ca^{2+} ion binding could support PAD2 enzymatic activity in rabbit skeletal muscle tissues[57]. Taken together, Ca^{2+} ion binding to key distinct sites on the PAD2 and PAD4 proteins constitutes a necessary component for deiminase activity or citrullination.

Ca^{2+} influx in immune cell signaling: physiological conditions for inducing PAD activity

Immune cell signal transduction triggered by extracellular ligand–receptor binding often promotes intracellular Ca^{2+} ion influx activating PAD activity. Here, we will survey key signaling pathways which drive Ca^{2+} ion influx which may involve or are known to involve PADs. Studying these mechanisms provide useful prospective insights into the context in which PADs may likely be active informing future research directions.

Neutrophils

As aforementioned, there exists an abundance of studies on citrullination in neutrophils and, therefore, several mechanistic insights on the activation of citrullination can be gained through the examination of neutrophils. The most well-known consequence of citrullination in neutrophils is the production of neutrophil extracellular traps (NETs) leading to a neutrophil– or granulocytic–specific type of cell death called *NETosis*[58]. Classically, lipopolysaccharide (LPS) – a toll-like receptor 4 (TLR4) agonist – has been used as a tool to induce PAD4 citrullination of histones in neutrophils via eliciting Ca^{2+} ion influx[58]. Other TLR agonists such as those for TLR2 have also been shown to induce NET formation via Ca^{2+} influx[59]. TLR4 and TLR2 signal transduction share the MyD88 pathway through to NFκB and AP-1 transcription[60]. Downstream of TLR2 and TLR4 signaling, Ca^{2+} ions are released from the endoplasmic reticulum activating

reactive oxygen species (ROS) which – due to positive feedback – elicits more Ca^{2+} release[61]. Intracellular calcium binds to PAD2 or PAD4 activating nuclear translocation and, consequently, the citrullination of nuclear targets. Several varieties of ligands could serve as TLR2 and/or TLR4 agonists including pathogen-associated molecular patterns (PAMPs) present on microorganisms; damage-associated molecular patterns (DAMPs) which could be generated in the tumor microenvironment[62,63]; and other lysates of various origins. While PAD2 and PAD4 are both induced by TLR signaling, it has been shown that only PAD4 is required for NET formation[64].

Beyond TLR signaling, several proinflammatory cytokines can induce Ca^{2+} ion influx and consequently PAD activity via ROS production[64,65]. It has been reported that TNF-α, IL1-β, and IL8 can induce ROS in neutrophils eliciting Ca^{2+} ion production[65,66]. As neutrophils are common mediators of inflammatory processes, they respond acutely to extracellular stimuli and, consequently, Ca^{2+} ion influx constitutes a central component in the mounting of the innate immune response.

Myeloid cells

While the studies on macrophage PADs are quite limited, few reports do describe distinct inflammatory scenarios involving heightened Ca^{2+} influx in macrophages which consequently will activate PADs.

Similarly, as in neutrophils – albeit lesser known – macrophages can also produce extracellular traps known as macrophage extracellular traps (METs) in a PAD4-dependent manner[67,68]. MET formation occurs in the response to similar stimuli as those that induce PAD4-mediated NETs such as TLR agonists, pro-inflammatory cytokines and H_2O_2.

Ca^{2+} influx in macrophages occurs due to a variety of proinflammatory conditions which brings into consideration a diversity of scenarios in which PADs could be active. Stimuli that activate the NLRP3 inflammasome[69,70,71] or sepsis[72] for example first induce oxidative stress triggering Ca^{2+} influx into the cytoplasm and thereby providing the environment in which PADs can be active. Of course, other common stimuli of macrophages such as type I or type II interferons induce Ca^{2+} influx in macrophages however, the results of which have not been studied[73,74]. Later in this review, we will discuss the signaling triggered by citrullination in these contexts.

T-cells

Although there exist very few studies examining the role of PADs in T-cells, T-cell activation in response to external stimuli requires Ca^{2+} influx[75,76]. Classically, downstream of T-cell receptor (TCR) engagement with antigens transduces signal from the LCK–ZAP70–LAT cascade to PLCγ1 and then to inositol-1,4,5-trisphosphate which elicits the release of Ca^{2+} ions from the endoplasmic reticulum[77]. While this calcium ion release is known to support T-cell activation via promoting nuclear factor of activated T-cells (NFAT) transcription, any T-cell–specific PADs would theoretically be activated as well in the presence of calcium ions. CD3 antibody (anti-CD3 or αCD3) alone has been shown to be sufficient to induce the expression of PAD2 in $CD4^+$ T-cells[49]. In these studies, direct inhibition of calcium and PKC signaling pathways with cyclosporin A and sotrastaurin, respectively, downregulate PAD2 expression in the presence of αCD3. From this work and from very few other studies, it has been established that PAD2 may be the dominant active PAD in T-cells.

As aforementioned, in innate immune cells such neutrophils and other myeloid cells, TLR–MyD88 signaling will elicit Ca^{2+} ion influx driving PAD4 activity. Interestingly, T-cells also express some TLRs and, therefore, TLR agonists can induce Ca^{2+} ion influx in T-cells independent of TCR engagement[78,79]. Consistent with classical TLR–MyD88 signaling, *Lui et al* showed that TLR7 agonist imiquimod can induce PAD2 in T-cells demonstrating the role of PAD2 in TLR7-dependent lupus[80]. Broadly, inflammatory conditions of $CD4^+$ T-cells which occur in autoimmune disorders including rheumatoid arthritis and lupus will induce Ca^{2+} influx and consequently PAD activation.

Here, we sought to survey the current literature describing Ca^{2+} influx in major immune cell subsets to interrogate the conditions in which nuclear immune cell PADs (i.e. PAD2 and PAD4) may be activated for citrullination.

The molecular consequences of citrullination

As aforementioned, citrullination involves the hydrolysis–mediated conversion of arginine residues into citrulline, changing the modified residue charge from positive to neutral, enhancing hydrophobicity and therefore regulating protein folding and function[81]. Crystal structure analysis reveals that Ca^{2+}-bound PAD4 induces a β-turn–like bent conformation on its substrate which includes the target arginine and roughly the five surrounding amino acids before and after the arginine[56]. Although these analyses interrogated the biophysical consequences of histone citrullination, these findings may provide key insights into the consequences of citrullination on protein substrates other than histones. These data may also provide rationales for how PADs can recognize target motifs on substrates. Arita *et al* demonstrates peptide recognition of PAD4 revealing that Ca^{2+}–bound PAD4 in-complex with common substrates histone H3 and H4,

engage specific peptide moieties along the active cleft indicating atomic selectivity in PAD4–substrate binding. Crystal structure analysis has facilitated the examination of peptide recognition of PAD4 targeting histone residues, the most well studied targets of PADs. Although the number of PAD substrates vastly surpasses the amount of PAD–substrate crystal structure studies, these early studies featuring PAD4-histone structures strongly indicate specificity on the part of citrullination. Moreover, these studies reveal the molecular means by which PAD citrullination drives the change in protein structure of the substrate. The citrullination–mediated modification in substrate structure drives the functional consequences of citrullination. Consequences vary depending on the function of the citrullinated substrate.

Section 2.3: Detection of citrullinated proteins: tools enabling PAD research

The detection of citrullination for visual analysis constitutes a critical research tool in the studies of PADs. Measurements on the enzymatic activity of PADs requires some means of detecting protein citrullination. Here, we will survey common methods used in the detection of citrullination.

Color Development Reagent (COLDER)

The so-called COLDER assay constitutes one of the earliest methods to detect protein citrullination. This assay involves the chemical derivatization of the urea group uniquely present on peptidylcitrulline. Particularly, during this reaction, urea undergoes an acid-catalyzed modification with diacetyl monoxime in the presence of thiosemicarbazide, ammonium (III) sulfate, phosphoric and sulfuric acid[82]. Usage of the COLDER method is limited to detecting *in*

vitro citrullination as it would have poor sensitivity to detecting peptidylcitrulline from primary tissue samples which may have low concentrations of protein.

Antibody-based methods

Citrullinated proteins can be detected using commercially available antibodies. The more sensitive antibody–based systems enable detection of peptidylcitrulline in samples with lower protein concentrations. The first citrulline-specific antibody was described by Senshu *et al* in 1992[83]. Their antibody against peptidylcitrulline actually recognized a chemically modified form of citrulline rather than the pure peptidylcitrulline structure. Production of this antibody involved the use of recombinant histones that were deiminated and subsequently derivatized with diacetyl monoxime and antipyrine under acidic conditions. In a separate study, use of this antibody showed efficacy in detecting citrullinated pituitary proteins from rats deiminated *in vitro*[84]. This approach for detecting peptidylcitrulline formed the basis for the commercially available antibodies against peptidylcitrulline.

For the sandwich ELISA system, Moelants *et al.* generated an antibody to a 2,3–butanedione-modified citrulline which can detect as low as 1 nanogram of citrullinated cytokines/proteins with high specificity[85]. This system also proved to be efficacious to detect and quantify the citrullination in granulocytes and peripheral blood mononuclear cells (PBMCs) in response to lipopolysaccharide (LPS).

Nicholas and colleagues developed an antibody so-called F95 against a deca-citrullinated peptide. This antibody was among the first to detect total citrullination in biological samples. Originally, F95 was used to stain human brain samples to show anatomical localization of citrullinated proteins via immunohistochemistry (IHC)[86,87]. Use of F95 and the subsequent

resolution via SDS-PAGE can also reveal all of the citrullinated proteins in a sample distinguished by atomic mass (kDa). The newer generation antibody for detecting total citrullination is the so-called anti-modified (citrulline) antibody which has shown enhanced sensitivity for the detection of citrullinated proteins of all molecular weights.

Given the several studies on the citrullination of histones over the years, there are several antibodies against citrullinated histones commercially available. In particular, several studies have elucidated the importance of the citrullination of histone H3 and, therefore, antibodies have been generated specifically against the arginine residues 2, 8 and 17[88] which have been shown to be citrullinated by PAD2 and PAD4. Western blotting and immunohistochemistry (IHC) antibodies are available to detect citH3R2,7,18. In addition to histone H3, other histone targets have been identified to be substrates of PADs including histone H1, H2A and H4, for which antibodies are commercially available[89,90].

Mass spectrometry

The highest sensitivity detection of the modification of arginine residues into citrulline is achieved by mass spectrometry (mass spec). Mass spec analysis involves the chemical digestion of the proteins reducing them to an array of peptide sequences and the separation of the peptides according to mass and chemical structure via the mass spectrometer[91].

Conducting mass spec for citrullination studies requires the decision to either identify the total set of citrullinated proteins in a complex sample or to determine the site of citrullination on a particular protein. The accurate detection of citrullination via mass spec involves difficulty since the modification of arginine into citrulline, results only in a 0.98 dalton (Da) increase in the

mass of the parent peptide[92]. Commonly, mass spec is conducted to identify the proteins that are citrullinated in the absence of prior knowledge regarding the target substrates of PADs in a sample. Given the reported importance of citrullination and hypercitrullination in the promotion of rheumatoid arthritis (RA), several mass spec studies have been conducted on primary samples from RA patients[93]. The feasibility of identifying both the target citrullinated protein as well as the citrullination sites on the PAD substrates has been demonstrated in the mass spec analysis of synovial fluid from RA patients[92,94,95]. An important technical challenge in performing mass spec to identify citrullinated proteins is posed by the need to decipher citrullination from *deamidation*, another PTM which also results in a 0.98 Da shift[96]. Fortunately, this nonenzymatic PTM only targets asparagine and glutamine while citrullination specifically targets arginine residues. This key distinction enables for the accurate detection of citrullinated proteins in a sample. Sequential window acquisition of all theoretical mass spectra (SWATH-MS), a data–independent acquisition method has also been used for the detection of citrullinated proteins[97]. Mass spec continues to serve as a robust quantitative tool to characterize protein citrullination.

Chemical derivatization of citrulline

Given the ~1 dalton increase in molecular weight between a citrullinated peptide and the parent peptide, some methods are needed to enhance the detection of peptidylcitrulline. As a means to aid the MS-based detection of citrullinated proteins, Holm *et al* demonstrated a method to selectively derivatize the urea group in citrulline with 2,3–butane-dione or in combination with antipyrine[98,99]. These post-hoc modifications result in a gain of 50-200 Da after citrullination enabling the enhanced ability to identify citrullinated versus non-citrullinated proteins. Moreover, this particular method of derivatization was used in the development of antibodies[85].

Phenylglyoxal–based probes

As aforementioned, a critical challenge in the detection of peptidylcitrulline is the low abundance of citrullinated proteins among non-citrullinated proteins in a complex sample. The particular enrichment of citrullinated proteins would greatly enhance the identification of citrullinated proteins using western blotting or mass spec. A promising – and increasingly common – method for the detection of peptidylcitrulline involves the use of chemical probes for citrulline, a concept similar to that of chemical derivatization described above. In acidic environments, phenylglyoxals can be used to cyclize specifically with the urea group present in citrulline[100,101].

Following this logic, Bicker *et al* demonstrated the use of a rhodamine-tagged phenylglyoxal probe in labeling citrullinated proteins in complex mixtures[102]. Newer generations of phenylglyoxals were developed to be conjugated to other compounds as a means to enhance the detection of citrullinated proteins via western blotting or mass spec. Choi *et al* used the 4-bromophenyl glyoxal model to label citrullinated proteins particularly so that the bromine signature could be exploited to identify citrullinated proteins in matrix-assisted laser desorption/ionization (MALDI) mass spec analysis[103]. Tutteren and colleagues conjugated a biotin tag to phenylglyoxal to develop the covalent biotin-PG for a streptavidin pulldown with which investigators may detect citrullinated proteins in primary synovial fluid samples from RA patients[104,105]. This technique enables for the enrichment of citrullinated proteins to be assayed via Western blotting or mass spec, and thus, the biotin-PG model of probes has facilitated the identification of several novel citrullinated proteins. Newer generations of the biotin-PG probe – such as that developed by Lewallen *et al* – achieve a higher resolution of the identification of

citrullinated proteins however cannot reveal the citrullination sites[106]. To detect the citrullination sites of a given protein requires the immunoprecipitation of the protein of interest and then the subsequent performance of mass spec to detect the exact sites of citrullination or deamidation of arginine residues compared to a control sample.

Taken together, the field of citrullination has developed over the years in importance because of its newly understood ubiquity in biological systems, cellular processes and signaling; as well as the growing set of tools available to use in the research studies on PADs.

Section 3: Regulation of disease processes by citrullination

PADs respond to a wide range of inflammatory stimuli indicating that they likely serve key functions in disease states. As aforementioned, citrullination constitutes an important modification on protein substrates which is sufficient to fundamentally alter protein folding and therefore function. The molecular consequences of citrullination are sufficient to trigger key mechanisms which can regulate cellular functions. As a means to further introduce the context within which we characterized a new role for PAD4 in this dissertation, we aim now to survey the current knowledge of the processes regulated by PADs in homeostatic and disease states. Although the focus of this dissertation is placed on the role of PADs in mononuclear immune cells – macrophages in large part – we learn from previous studies on PADs in both immune and non-immune cells to gain valuable insights onto the range of the functional mechanisms involving PADs. The majority of the studies on PADs report the consequences histone citrullination, however other lesser–known roles of PADs have been reported. Here, we will survey the literature to ascertain the range of nuclear PAD enzymatic activity in both immune and non-immune.

Section 3.1: The regulation of cellular processes by citrullination: lessons from immune and non-immune cells

As aforementioned, in this thesis work, we aim to describe how citrullination regulates key processes in non-neutrophil immune cells, particularly macrophages and lymphocytes. As a means to familiarize readers with some common mechanistic features of protein citrullination, we deem it critical to briefly introduce the well–studied mechanistic consequences of citrullination observed in neutrophils, other immune and non-immune cellular systems. Insights from these studies will provide a key foundation for understanding how citrullination could regulate mononuclear immune cell processes.

Citrullination in pluripotent stem cells

Although PAD citrullination of histones has largely been described in the context of the production of extracellular traps, histone citrullination can also serve as the catalysts for the regulation of homestatic cellular processes. Fundamentally, histone citrullination decondenses or opens chromatin[89,107]. As we will discuss later, NET formation involves the decondensation of chromatin to the extent that the chromatin is completely unraveled and released from the cell. However, histone citrullination does not always result in the NET formation and can play other roles in the regulation of transcription via chromatin remodeling. A landmark study conducted by Christophorou *et al* showed that the citrullination of histone linker H1 and histone H3 resulted in the opening of chromatin at the promoter regions of key pluripotent genes enabling the DNA binding of transcription factors such as Nanog, Sox2, Tcf7, Oct4 and others, which are required for the maintenance of pluripotency phenotypes in progenitor cells[90]. In particular, PAD4 has been identified as the isozyme required for histone citrullination–mediated maintenance of

pluripotency in progenitor cells[108]. In another study, it was shown that in hematopoietic stems cells, PAD4 controls and maintains quiescence particularly in lineage$^-$ Sca-1$^+$ c-Kit$^+$ (LSK) cells in the murine bone marrow[109]. This work shows that the PAD4–mediated citrullination of histone H3 at the promoter of *c-myc* controls c-myc expression. Here, Nakashima *et al* observed that the loss of PAD4 in LSK cells resulted in increased proliferation *in vivo* demonstrating the PAD4 serves as a key regulator in hematopoietic stem cells. Related to pluripotency, PAD4 has also been shown to control differentiation. Song *et al* showed that the PAD4 regulation of the SOX4–mediated PU.1 expression and signaling was required for the all-trans retinoic acid (ATRA)–induced differentiation of acute promyelocytic leukemia cells[110]. Given the central role that PAD4 plays in the control stemness and differentiation in pluripotent cells, other studies have emerged focused on the pro- or anti-tumorigenic role of PAD4 in cancer cells.

Citrullination in cancer cells

As reasoned above, key insights gained regarding the citrullination in non-immune cells can shed light on and be applied to our understanding of the mechanism in immune cells. There is a rich body of literature describing the role of citrullination in cancer cells providing insights on the wide range of possible targets that can be exploited to thwart tumor cell growth. Reports have shown that in cancer cells – across different cancer types – citrullination plays a role in regulating cancer cell phenotypes such as proliferative capacity, stemness, resistance to apoptosis and more[109,111,112]. Many of these processes which regulate *tumor* cell persistence rely on mechanisms controlled by citrullination mediated by nuclear PADs, particularly PAD4. Such mechanisms involve both histone and non-histone targets.

A large portion of the early PAD studies investigated the role of PAD4 in cancer cells which led to the elucidation of the key molecular mechanisms enabling nuclear PADs to control cancer cell functions and phenotypes through transcriptional regulation. A pioneering and ground–breaking study led by Cuthbert *et al* showed that the citrullination of histones directly antagonized arginine methylation on histones controlling transcription as a result[113]. The methylation of arginine residues on histone H3 had already been associated with active transcription[114,115]. Then, through the work of Cuthbert *et al*, PAD4 became newly defined as the major nuclear PAD which served as repressor. They demonstrated that PAD4 citrullination in the *VEGF-A* promoter repressed E2 hormone signaling–dependent transcriptional activation of *VEGF-A*, a critical event in breast cancer cells. Importantly, in breast cancer cells, they found that PAD4 citrullination of histone H3 in the *pS2* promoter (known to be methylated during activation in response to estrogen) repressed activation of this gene due to antagonizing arginine methylation in the genomic region. This work was shortly followed by another study showing that the citrullination of histone H4 – directly removing methyl groups – in estrogen–responsive genes in breast cancer cells represses estrogen–induced transcription[116]. More work on breast cancer done in the laboratory of David Allis at the Rockefeller Institute (who was involved in the previously mentioned study) showed that PAD4 citrullinates glycogen synthase kinase-3 beta (GSK3β) activating TGF-β signaling and inducing epithelial-to-mesenchymal transition (EMT) in breast cancer cells[117]. Reasonably, GSK3β – a nuclear protein – would be susceptible to citrullination by PAD4 since this particular PAD isozyme can translocate into the nucleus. While GSK3β governs key transcription factors involved in tumor progression, the PAD4–citrullination of GSK3β facilitates the localization of this protein in the nucleus therefore regulates GSK3β–mediated transcription. In this case, the loss of PAD4 results in the reduction of nuclear GSK3β

protein levels, the enhancement of TGF-β signaling and the advanced invasiveness of breast carcinoma. By these means, PAD4 citrullination is sufficient to regulate EMT in cancer cells. These insights may inform other consequences of PAD4 regulation of GSK3β nuclear accumulation. Multiple papers continued to characterize the role of PAD4 in breast cancer cells specifically. A recent study showed that PADs were overexpressed in ER– breast cancers[118]. Beyond breast cancer, several other roles for PADs in cancers have been reported.

PAD4 has been shown to regulate EMT and other related processes via the citrullination of a variety of targets. One study showed that the citrullination of extracellular matrix protein collogen type I promotes cellular adhesion and induces the expression of epithelial markers demonstrating a role for citrullination in facilitating mesenchymal-to-epithelial transition in the process of metastasis[119]. In another study regarding breast cancer cells, PAD4 was shown to physically interact and citrullinate Elk-1 at the *c-Fos* promoter[120]. Upon citrullination, Elk-1 – a member of the large ETS oncogene transcription factor family – is then able to be phosphorylated by ERK2. The phosphorylation of Elk-1 facilitates the physical interaction with acetyltransferase p300 which results in the acetylation of histone H4 and thereby activating *c-Fos*. Thus, aside from histone citrullination, PAD4 often serves as a necessary co-factor in a sequence of protein-protein interactions and signal transduction events, citrullinating key proteins for the propagation of transcription in response to signals or stimuli. Contrary to the previously described roles of PAD4 in cancer cells, PAD4–mediated citrullination has also been shown to inhibit tumor growth. Tanikawa *et al* characterized a novel role for PAD4 showing that in response to DNA damage, PAD4 citrullinates the histone chaperone protein nucleophosmin (NPM1) facilitating its translocation from the nucleoli to the nucleoplasm; and – consequently – facilitating DNA repair[89,121,122]. In this context, PAD4 was classified as a tumor suppressor since

the loss of PAD4 resulted in apoptosis resistance in cancer cells. Thus, the p53–PAD4 network – reported by Tanikawa *et al* in multiple studies[89,121] – plays a critical role in DNA damage repair processes in cancer cells and therefore in the prevention of tumor growth. Together, we show here what has been reported in the literature regarding PAD4 activity in cancer cells and how this has shed critical light on the range of molecular mechanisms controlled by PADs.

Section 3.2: Pathological PAD4–mediated NET formation

As previously discussed, the most well-known report of citrullination in immune cells is that which occurs in neutrophils. Here, we will only briefly discuss citrullination in neutrophils since there already exists a great abundance of studies on citrullination in neutrophils[123,124,]. The most important phenomenon in neutrophils that involves citrullination is the production of the neutrophil extracellular traps or NETs[125,126]. Classically, the PAD4–mediated citrullination of histone H3 decondenses chromatin to the extent which induces a form of cell death in neutrophils so-called NETosis[127,128]. In normal conditions, NET formation serves to trap microorganisms as an innate immune defense mechanism[129,130,131,132]. The majority of the studies investigating the pathological role of PAD–mediated histone citrullination and NETosis are those which center on rheumatoid arthritis (RA) pathogenesis[133]. The first piece of evidence suggesting the role of PADs in RA dates back to 1998 when Schellekens *et al* discovered that citrulline is an essential component of the autoantigens which are recognized by the autoantibodies in the sera of RA patients[134]. It became established knowledge that citrullinated histone H3 (H3-cit) as well as other citrullinated nuclear proteins expelled along the NETs of neutrophils served directly as autoantigens driving RA pathogenesis[92,104,135,136]. Thus, H3-cit has served as a key clinical biomarker in the treatment of RA.

Moreover, several reports have shown that various factors in the TME promote NET formation and that NETs can promote tumor growth and metastasis. It was shown by Albrengues *et al* that NETs produced during inflammation can awaken dormant cancer cells in mice[137]. In another study, Yang *et al* showed that the NET-DNA released by inflammatory neutrophils promotes metastasis via binding CCDC25, a tumor transmembrane protein, and consequently, enhancing cell motility[138]. Other studies have followed to further elucidate the role of NETs in promoting tumor growth.

Section 3.3: PAD citrullination of transcription factors

Few studies have shown that immune cell PADs can citrullinate non-histone targets. In neutrophils, while extracellular stimuli such TLR agonists can induce PAD citrullination of histones, PADs can also be induced to citrullinate key transcription factors involved in the inflammatory response. Sun *et al* showed that in response to TLR activation, PAD4 citrullinates the p65 subunit of transcription factor NF-κB promoting its nuclear transport and subsequent binding to DNA enabling the expression of IL-1β and TNFα[139]. In another study by the same group, they demonstrated that PAD2 citrullinates T-cell RORγt and GATA3 transcription factors controlling their DNA binding and therefore regulating the balance between Th2 and Th17 polarization of $CD4^+$ T-cells during autoimmune disease[49]. These seminal studies were among the first to show that PADs can citrullinate transcription factors and that this PTM regulates transcriptional activity in immune cells.

Section 4: Clinical relevance of PAD citrullination

As we discussed above, citrullination mediated by nuclear PADs (PAD4 or PAD2) serves as a crucial mechanism to trigger a variety of cellular processes during the immune response. Our initial interest to investigate PADs stemmed from preliminary knowledge gained from the literature that PADs were involved in a number of diseases including cancer. An ultimate aim of the research investigation reported in this dissertation is to provide insights regarding how our knowledge of PADs can be exploited to improve health outcomes, particularly in cancer. In this section, we will survey the studies in which PADs are clinically targeted.

Section 4.1: Current pre-clinical and clinical therapeutics targeting citrullination

Given the novelty of the field investigating PAD regulation of immune cells in disease, there exists only a limited body of studies investigating the efficacy of therapies targeting PADs. As aforementioned, the pathological role of PAD4–mediated histone citrullination in autoimmune diseases such as rheumatoid arthritis (RA) or lupus[80] has been thoroughly studied and therefore treatment strategies targeting PAD4 have been conceived. Early observations of NETs in the circulating and in the synovial fluid neutrophils initiated the focus on neutrophils and later PADs in disease processes of RA. Research tools such as pharmacological inhibitors targeting PAD4 or PAD2 specifically or all PADs are commercially available for *in vitro* and *in vivo* use. Firstly, there have been multiple preclinical studies demonstrating the efficacy of PAD4 inhibitors in ameliorating the effects of RA[133,140]. PAD4 citrullination of histones in neutrophils decondenses chromatin facilitating the formation of extracellular traps composed of chromatin and citrullinated histones. Citrullinated histones serve as autoantigens stimulating the inflammatory response and the worsening of RA[141]. Furthermore, other citrullinated proteins may serve as

autoantigens driving the disease[136]. Therefore, in multiple studies, PAD4 inhibitors as well as antibodies have been demonstrated to inhibit NET formation and consequently to antagonize disease progression[142,143]. Thus far, the detection of PAD4 and NETs continues to serve as a diagnostic biomarker of RA[133] however, clinical trials in which patients are treated with PAD4 inhibitors have yet to be initiated.

As aforementioned, the emerging critical role of PAD4 in promoting cancer has begun to crystallize with the studies examining PAD4 activity in cancer cells and in neutrophils alike. PAD4–specific inhibitors have been used to show that inhibiting PAD4 in tumor cells reduces tumors growth[144,145]. More recently, pharmacologically targeting PAD4 in neutrophils as a cancer treatment has been investigated. Deng *et al* demonstrated that the novel PAD4 inhibitor JBI-589 successfully blocked neutrophil CXCR2–mediated chemotaxis and, consequently, reduced primary tumor size as well as metastasis[146]. Other studies have followed to demonstrate optimized strategies to target neutrophil PAD4 in the TME[147].

Section 5: Contributions of this Thesis Work

Our studies contribute to advancements in multiple fields. We elucidate that (1) PAD4 citrullinates STAT1 in TAMs regulating STAT1 transcriptional signaling, an unreported phenomenon – and (2) that this mechanism could be exploited as a therapeutic target to enhance anti-tumor immunity. Firstly, this thesis work features among the very first studies investigating PAD4 enzymatic activity in tumor-associated macrophages. Most reports on PAD4 activity focuses on citrullination in neutrophils or in cancer cells. Thus, we augment the field of studies on PADs and we provide new and potentially useful insights into how TAMs may be reprogrammed to better support T-cell killing of tumor cells. And importantly, through our work,

we shed greater light on the STAT1-PIAS1 interaction by showing for the first time that PAD4 is required for the maintenance of this interaction.

Secondly, we introduce a novel modality of targeting macrophages for the maintenance of antitumor immune. Targeting post-translational modifications (PTMs) as a means to reprogram macrophage or T-cell functions to better support anti-tumor immunity is an under-investigated treatment approach. Given the ubiquity and necessity of PTMs that occur along signal transduction pathways, targeting PTMs constitutes a potentially promising treatment strategy. Through our work, we demonstrated that both the genetic deletion and the pharmacological inhibition of PAD4 citrullination significantly reduced tumor growth. Furthermore, PAD4 deletion or inhibition synergized with immune checkpoint blockade (ICB) therapy, suggesting that targeting PAD4 could serve as a durable efficacious target. Having demonstrated that PAD4 is required for the STAT1-PIAS1 interaction – the interaction which regulates STAT1 DNA binding macrophages – we reasoned that inhibiting PAD4 as a means to disrupt this interaction would drive enhanced STAT1 signaling in macrophages including IFNγ signaling and antigen presentation. Importantly, in our work, we observed that the loss of PAD4 not only enhanced MHC-II in macrophages, but enhanced MHC-II expression on the classically MHC-II^{low} anti-inflammatory macrophages. The MHC-II^{low} anti-inflammatory or immunosuppressive macrophages have been shown to accommodate pre-metastatic niches and support tumor growth[148]. Therefore, we show that PAD4–deficiency reprograms these macrophages to better support T-cell activation and tumor immunity. As aforementioned, the concept of targeting macrophages – in particular – for the purpose of enhancing anti-tumor immunity has recently emerged as a reasonable strategy. Decades of research has revealed that macrophages possess a variety of functions sufficient to promote and sustain tumor growth[40]. Therefore, through our

work, we aim to make an insightful contribute to the field of immunotherapy which may further inform advancements in cancer treatment.

Chapter 2: PAD4 Restrains MHC-II Functions in TAMs Controlling Tumor Immunity

Abstract

Tumor-associated macrophages (TAMs) shape tumor immunity and therapeutic efficacy. However, it is poorly understood if and how post-translational modifications (PTMs) intrinsically affect the phenotype and function of TAMs. Here, we found that peptidylarginine deiminase 4 (PAD4) manifested the highest expression among common PTM enzymes in TAMs. Genetic and pharmacological inhibition of PAD4 in macrophages prevented tumor progression in tumor–bearing mouse models, accompanied by an increase in macrophage MHC-II function and T-cell effector function.

Background: Tumor associated macrophages (TAMs) shape tumor immunity and therapeutic efficacy. Therefore, targeting TAMs has become a key strategy as a means to enhance immunotherapy and tumor clearance. The study of intrinsic regulatory molecular mechanisms in macrophages brings important awareness to the means by which macrophage functions contribute to or affect tumor growth in the TME. Post-translational modifications (PTMs) play crucial and diverse roles in the programming of cellular functions, however, it is poorly understood whether and how they intrinsically affect the phenotype and function of TAMs. Peptidylarginine deiminase 4 (PAD4) has been shown to play a role in tumor progression in cancer cells and neutrophils. Here, we advance the understanding of the role of PAD4 in mononuclear immune cells by showing that PAD4 was among the most highly expressed PTM

enzymes enriched in both human and mouse TAMs and that PAD4 expression was negatively correlated MHC-II functions and tumor immunity.

Methods and Materials: Several methods were used for the study and characterization of a role of PAD4 in TAMs. Bioinformatic analyses will be discussed in a later chapter. ELISPOT assays were used as a means to detect mouse IFNγ production by primary tumor antigen–specific T-cells enriched from *Padi4*$^{fl/fl}$ and *Padi4*$^{fl/fl}$ *LysM*^{cre} mouse tumors and then stimulated with dead MC38 tumors cells. Flow cytometry was performed as a means to determine the cytokine production in activated T-cells harvested from tumors; or tumor-draining lymph nodes (TDLNs) or T-cells from OT-II transgenic mice.

Results: PAD4 is among the most highly expressed post-translational modification enzyme in TAMs compared to other enzymes. The loss of PAD4 in the macrophages of tumor–bearing mice resulted in enhanced anti-tumor immunity and reduced tumor growth or metastasis. The loss of PAD4 enhanced MHC-II expression and MHC-II–mediated antigen presentation.

Summary: PAD4 citrullination restrains STAT1 signaling and consequently MHC-II function on macrophages abrogating tumor immunity in multiple mouse models.

Background

Macrophages constitute the most abundant immune cell in the TME and pose a strong influence over whether the tumor continues to grow or regresses[9,29,36]. While T-cell–based immunotherapies have shown considerable promise, the efficacy of boosting T-cell effector activity depends highly on macrophage functions[149,150]. Macrophages or TAMs in the TME can promote tumor growth through the production of immunosuppressive cytokines, the promotion of angiogenesis and the down regulation of antigen presentation surface molecules[9]. On the other

hand, macrophages can produce proinflammatory cytokines, perform phagocytosis and upregulate antigen presentation molecules, better supporting anti-tumor T-cell activation and contributing to tumor cell death[9]. Due to this crucial role which macrophages play in the TME, several novel strategies have emerged which target macrophages as a means to enhance either macrophage– or T-cell–mediated anti-tumor immunity. Historically, the different strategies of targeting macrophages in pre-clinical cancer research as well as in the clinic involve either the elimination of macrophages, the blocking of macrophage recruitment and the reprogramming of macrophages into a proinflammatory phenotype enabling enhanced macrophage–mediated anti-tumor immunity or enhanced macrophage facilities to better support T-cell–mediated anti-tumor immunity[40,151]. Indeed, PD-L1 blockade would antagonize much of the immunosuppressive effect of TAMs as TAMs express high levels of PD-L1[152]. Moreover, the efficacy of other macrophage–targeted therapies including anti-CSF1 receptor antibodies and inhibitors, anti-CD40 antibodies and anti-CD47/SIRPα antibodies has been examined in preclinical studies, and have reached early phase clinical trials[153,154,155]. Although these recent novel strategies provide valuable insights on targeting macrophages in cancer treatment, there still remains several poorly understood aspects of macrophage biology including crucial, homeostatic intrinsic mechanisms which may control the pro-tumor functions in TAMs.

Post-translational modifications (PTMs) determine the final structure and function of proteins[156,157]. Moreover, signal transduction pathways utilize PTMs as a means to translate environmental signals into molecular changes which affect several different kinds of cellular functions[158]. Despite the ubiquity and fundamental importance of PTMs in governing cellular functions, the means by which PTMs control TAM functions in the TME is poorly studied. Peptidyl arginine deiminase 4 (PAD4) has been shown to contribute substantially to the

development of cancers in cancer cells and in neutrophils. In cancer cells, PAD4 citrullinates histones and some key nuclear proteins[89,117] as a means to enhance cancer cell stemness. In neutrophils, PAD4 citrullination of histones decondenses chromatin to form the neutrophil extracellular traps (NETs) which have been shown to 'awaken' dormant tumor cells[137] as well as to promote metastasis[138]. Since the tumor–promoting role of PAD4 in neutrophils has been repeatedly reported, some studies have been gone further to show that the pharmacological inhibition of PAD4–mediated NET formation significantly enhanced antitumor immunity[146]. Given the known role of PAD4 in different contexts to promote cancer and also given the strong influence of macrophages on tumor development and anti-tumor immunity, we sought to investigate whether PAD4 served any protumor roles in TAMs in the TME.

Materials and Methods

The study of how PAD4 enzymatic activity impacts macrophage phenotypes requires a comprehensive coalescence of several different methods.

Cell lines

B16F10 (CRL-6475) and Py8119 (CRL-3278) were purchased from the American Type Culture Collection (ATCC, Manassas, VA). Use of the MC38 cells were previously reported[152]. MC38, B16F10 and Py8119 cells were maintained in RPMI-1640 Medium (HyClone SH30255, GE Healthcare, Chicago, IL) supplemented with 10% fetal bovine serum. All cell lines were tested for *Mycoplasma* contamination by MycoAlert Mycoplasma Detection Kit and confirmed negative for *Mycoplasma*. All cells were cultured at 37ºC under a humidified atmosphere containing 5% CO_2.

Animal models

Padi4$^{fl/fl}$ mice, *LysM*^{cre} mice, *Cd4*^{cre} mice, and wild type C57BL/6J mice were purchased from the Jackson Laboratory. *Padi4*$^{-/-}$ mice were generated in house (Yongqing Li). *Padi4*$^{fl/fl}$ mice were crossed with *LysM*^{cre} mice to generate both wild-type *Padi4*$^{+/+}$ *LysM*^{cre} mice and *Padi4*$^{fl/fl}$ *LysM*^{cre} mice, which are deficient in their macrophage expression of *Padi4*. Respectively, these mice are referred to as *Padi4*$^{fl/fl}$ (*LysM*^{Cre}+) and *Padi4*$^{fl/fl}$ *LysM*^{cre} (*LysM*^{Cre}–). *Padi4*$^{fl/fl}$ mice were crossed with *Cd4*^{cre} mice to generate both wild-type *Padi4*$^{+/+}$ *Cd4*^{cre} and *Padi4*$^{fl/fl}$ *Cd4*^{cre} mice, which are deficient in their CD4^{+} and CD8^{+} T-cell expression of *Padi4*. As above, these mice are referred to as *Padi4*$^{fl/fl}$ (*Cd4*^{Cre}+) and *Padi4*$^{fl/fl}$ *Cd4*^{cre} (*Cd4*^{Cre}–). Mice were bred in the specific-pathogen-free animal facility (~22 °C with ~40% humidity) on a 12 h dark/12 h light cycle at the University of Michigan. All procedures were approved by the Institutional Animal Care and Use Committees (IACUC) and the Unit for Laboratory Animal Medicine (ULAM) at the University of Michigan.

Murine colon carcinoma (MC38) cells (3 x 10^6) were injected subcutaneously into the left flanks of age- and sex-matched *Padi4*$^{-/-}$ or C57BL/6J mice (8-10 weeks); *Padi4*$^{+/+}$ *Cd4*^{cre} or *Padi4*$^{fl/fl}$ *Cd4*^{cre} mice (8-10 weeks) and *Padi4*$^{+/+}$ *LysM*^{cre} or *Padi4*$^{fl/fl}$ *LysM*^{cre} mice (8-10 weeks). Py8119 breast adenocarcinoma cells (2 x 10^4) were injected subcutaneously into the left flanks of age-matched, female *Padi4*$^{+/+}$ *LysM*^{cre} or *Padi4*$^{fl/fl}$ *LysM*^{cre} mice (8-10 weeks). Tumor monitoring began 7 days after inoculation and continued every 3 days until endpoint. Tumor length, width and height was measured with calipers fitted with a Vernier scale. Tumor volume was calculated as previously described[159]. B16F10 murine melanoma (2 x 10^5) was injected intravenously into the tail vein of age- and sex-matched *Padi4*$^{+/+}$ *LysM*^{cre} or *Padi4*$^{fl/fl}$ *LysM*^{cre} mice (8-10 weeks).

Human samples

Primary ascites fluid was collected from patients with ovarian cancer at the University of Michigan and used as an agonist to induce PAD4 expression in HL60 cells or in primary human monocytes. The study for which we acquired the patient ascites fluid was approved by the Institutional Review Boards of the University of Michigan (IRB: HUM00054493). Human monocytes were positively enriched from blood buffy coats (Carter BloodCare) using the EasySep^{TM} Human Monocyte Isolation Kit (STEMCELL Technologies). Monocytes were differentiated into macrophages following overnight stimulation with 1 μg/mL LPS and 10ng/mL IFNγ. Patient mononuclear cells from primary patient ovarian tumors (Cooperative Human Tissue Network) were isolated from the tumor mass following processing into a single-cell suspension and then submitting to Ficoll density gradient centrifugation. Mononuclear cells were then cultured in RPMI-1640 medium supplemented with 10% fetal bovine serum. TAMs were then identified via fluorescent staining as $CD45^{+}CD14^{+}$ mononuclear cells and analyzed via FACS. All human samples in our studies were collected with informed consent from each individual donor.

Magnetic-activated cell sorting (MACS) of peritoneal macrophages

Mice were euthanized via a CO_2 overdose and peritoneal lavage was harvested in MACS buffer on ice. 10-15 mL of peritoneal lavage per mouse was collected after multiple washes of the peritoneal cavity. Cell suspensions were centrifuged and resuspended to be incubated with the primary PE–anti–Tim-4 antibody (clone RMT4-54, BD Biosciences) diluted (1:10) in MACS buffer at 4ºC for 10 minutes in the dark. Cells were washed and centrifuged. The supernatant was aspirated completely and the pellet was resuspended in 80μL of MACS buffer prior to adding and mixing 20μL of anti–PE microbeads (Miltenyi Biotec) for a 15-minute incubation at 4ºC in the

dark. Cells were washed, centrifuged and resuspended in MACS buffer. The PE positive cells were sorted by passing them through LS columns (Miltenyi) according to the manufacturer's instructions. Enriched macrophages were cultured in Dulbecco's Modified Eagle Medium (DMEM) supplemented with 10% fetal bovine serum.

Isolation of primary T-cells from OT-II transgenic mice

Mice were euthanized via a CO_2 overdose and spleens were removed. Primary splenocytes were isolated in the process described above. Lymphocytes also served as a source for T-cells. Lymph nodes were removed from the euthanized mice and smashed with a 1 mL syringe plunger and washed through a 70μM strainer over a 50 μL conical tube to collect 35 mL of a single-cell suspension containing splenocytes and/or lymphocytes. T-cells were isolated from the splenocyte and/or lymphocyte single–cell suspensions using EasySep^{TM} Mouse CD3^{+} T-cell Isolation Kit (STEMCELL Technologies).

In vitro antigen presentation–mediated OT-II T-cell activation assay

OT-II cells from the OT-II transgenic mice were isolated as described above. T-cells were either cultured alone, co-cultured with *Padi4*$^{+/+}$ or *Padi4*$^{-/-}$ macrophages, or cultured with macrophages supplemented with 50 μg/mL soluble OVA protein in RPMI-1640 medium supplemented with 10% fetal bovine serum in a 96-well plate. After a 3-day incubation period in 37ºC under a humidified atmosphere containing 5% CO_2, cells were harvested and T-cell activation was assessed via fluorescent staining and FACS analysis. To assess macrophage–mediated antigen presentation of OVA to OT-II T-cells when cultured with OVA^{+} MC38 cells, tumor cells were first osmotically loaded with 10mg/mL OVA and then irradiated with ultra violet (UV) light in 10 mm dishes as

previously described[159]. 2 x 10^5 T-cells from OT-II transgenic mice were culture alone, or co-cultured only with 1 x 10^4 peritoneal macrophages, or with macrophages and 1 x 10^5 dead tumor cells in flat 96 well plates. After 4 days, cells were collected and analyzed for cytokine production in OT-II T-cells.

Flow cytometry analysis

Single-cell suspensions were prepared from fresh mouse peritoneal lavage, lungs, spleen, lymph nodes, and tumor tissues. For surface staining alone, single cell suspensions were washed with PBS, pelleted via centrifugation and then resuspended in 50 µL of MACS buffer. Fluorescent antibodies were added and a 20-minute incubation followed at room temperature protected from light. For intracellular cytokine staining, lymphocytes were incubated in culture medium containing phorbol 12-myristate-13-acetate (5ng ml^{-1}; Sigma-Aldrich), ionomycin (500 ng ml^{-1}; Sigma-Aldrich), brefeldin A (1:1000; BD Biosciences) and monensin (1:1000; BD Biosciences) at 37°C for 4 h. Antibodies (0.6 µg) were added for 20-minute for surface staining. The cells were then washed and resuspended in 1 mL freshly prepared Fix/Perm solution (BD Biosciences) at 4°C overnight. After being washed with Perm/Wash buffer (BD Biosciences), the cells were staining with 0.6 µg antibodies against intracellular proteins from 30-minute, washed and fixed in 4% formaldehyde (Sigma-Aldrich). All samples were read on an LSR II cytometer and analyzed with FACS DIVA software v. 8.0 (BD Biosciences).

Gating strategies for flow cytometry analysis

Assessing key features of T-cell or macrophage activation requires detection of anti-tumor cytokines from effector subsets or the expression of surface proteins involved in the immune

response. To measure T-cell activity in the tumor or tumor–draining lymph nodes (TDLNs) of subcutaneous tumor–bearing wild-type, *Padi2*$^{-/-}$, *Padi4*$^{-/-}$ or *Padi4*$^{fl/fl}$ *LysM*^{cre} mice, we gated for CD45^{+}CD90^{+}CD3^{+}CD4^{+} or CD8^{+} subsets and detected IL-2, IFNγ and TNFα production (**Figure 2.1A-B**). Further, we assessed exhaustion of the tumor–infiltrated T-cells in the *Padi4*$^{fl/fl}$ vs the *Padi4*$^{fl/fl}$ *LysM*^{cre} MC38–bearing mice via staining for CD4^{+} and CD8^{+}KRLG1^{+}Lag-3^{+} subsets

(**Figure 2.1C**). To measure T-cell activation in the lung metastases of *Padi4*$^{fl/fl}$ vs *Padi4*$^{fl/fl}$ *LysM*^{cre} mice inoculated intravenously with B16F10 melanoma, we gated for

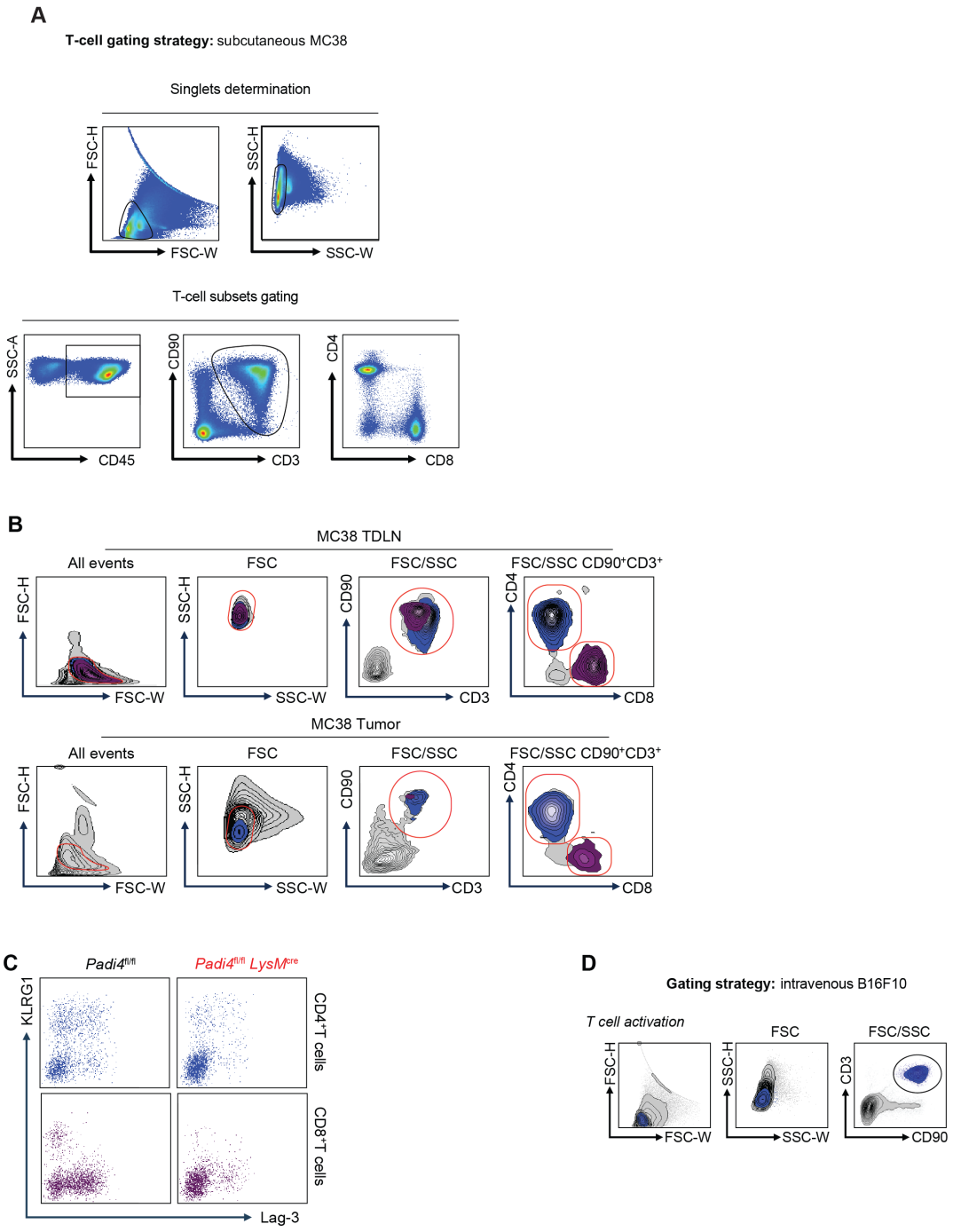

Figure 2.1.0: Gating strategies to detect T-cell activation in the tumor and the TDLNs. (A) Gating strategy to detect CD4$^+$ and CD8$^+$ T-cells in the subcutanous tumors and TDLNs of MC38 tumor–bearing wild-type and Padi4$^{-/-}$ mice. (B) Gating strategy to detect CD4$^+$ and CD8$^+$ T-cells in the subcutanous tumors and TDLNs of MC38 tumor–bearing *Padi4*$^{fl/fl}$ and *Padi4*$^{fl/fl}$ *LysM*^{cre} mice. (C) Gating strategy to assess T-cell exhaustion in CD4$^+$ and CD8$^+$ T-cells from the subcutanous tumors of MC38 tumor–bearing

Padi4$^{fl/fl}$ and *Padi4*$^{fl/fl}$ *LysM*^{cre} mice. (D) Gating strategy to detect T-cells in the lung metastases of the B16F10–bearing *Padi4*$^{fl/fl}$ and *Padi4*$^{fl/fl}$ *LysM*^{cre} mice.

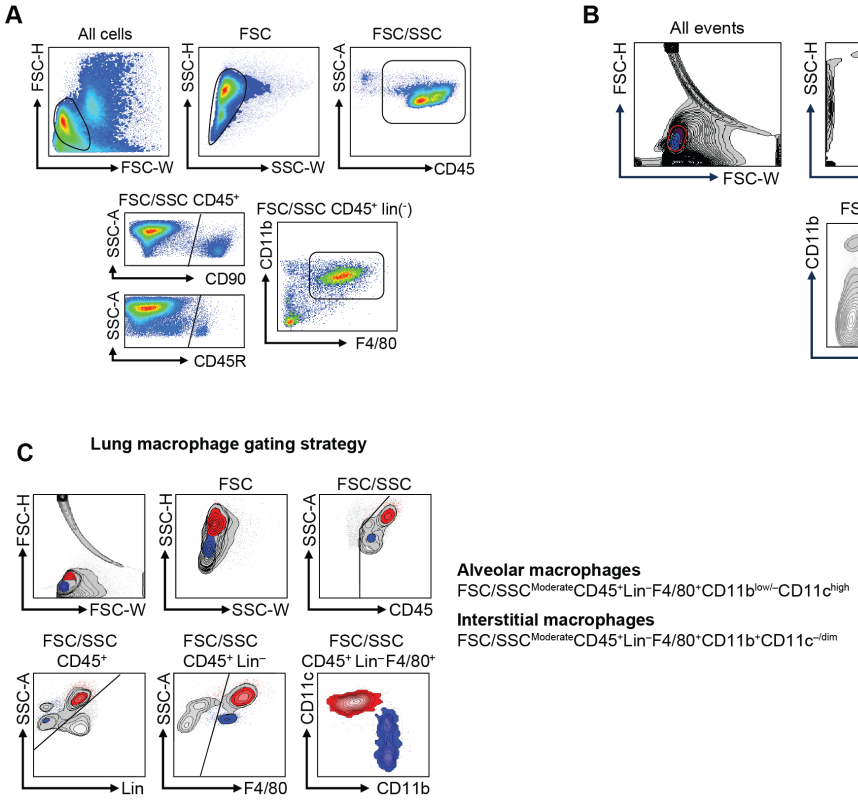

Figure 2.2.0: Gating strategies to detect and assess macrophage populations and functions. (A) Gating strategy to identify macrophages across tissues or in tumors ex vivo. (B) Gating strategy to identify tissue–resident and non-tissue–resident (Lyve1^{+} and Lyve1^{-}, respectively) macrophages in subcutaneous tumors. (C) Gating strategy to identify tissue–resident and non-tissue–resident (alveolar and interstitial, respectively) macrophages in the lung metastasis of B16F10–bearing mice.

CD45^{+}CD90^{+}CD3^{+}subsets and detected IFNγ, TNFα and granzyme B production (**Figure 2.1D**). In our assessment of differences in macrophage phenotype between healthy or tumor–bearing wild-type vs *Padi4*$^{-/-}$ or vs *Padi4*$^{fl/fl}$ *LysM*^{cre} mice, we gated for the CD45^{+}CD90^{-}B220^{-}CD3^{-} CD11b^{+}F4/80^{+} subsets in the peritoneal lavage, lung tissues or the tumor (**Figure 2.2A**). Next, to assess macrophage phenotypes in tissue–resident vs non-tissue–resident macrophages in the subcutaneous tumors, we gated for CD45^{+}CD90^{-}B220^{-}CD3^{-}CD11b^{+}F4/80^{+}Lyve1^{+} subset to

detect tissue–resident macrophages and the $CD45^{+}CD90^{-}B220^{-}CD3^{-}CD11b^{+}F4/80^{+}Lyve1^{-}$ subset to detect non-tissue–resident macrophages (**Figure 2.2B**). To detect tissue–resident vs non-tissue–resident subsets in the lung metastasis of B16F10–bearing mice, we gated for alveolar macrophages ($FSC/SSC^{Moderate}CD45^{+}Lin^{-}F4/80^{+}CD11b^{low/-}CD11c^{high}$) and interstitial macrophages ($FSC/SSC^{Moderate}CD45^{+}Lin^{-}F4/80^{+}CD11b^{+}CD11c^{-/dim}$), respectively (**Figure 2.2C**).

Immunoblotting

Protein was extracted from the cells with RIPA buffer supplemented with 100X protease inhibitor (Thermo) and resolved on SDS-PAGE gels, then transferred to nitrocellulose or PVDF membranes. The primary antibodies against mouse PADI4 (1:1000, Abcam, ab214810), STAT1 (1:1000, CST, 9172), phosphor-STAT1 (Tyr107) (1:1000, CST, 9167) and β-actin (1:1000, CST, 3700) were used. Peroxidase-conjugated secondary antibody (Vector Laboratories) was used and the antigen-antibody reaction was visualized using an enhanced chemiluminescence assay (ECL, BioRad).

Quantitative PCR analysis

Total RNA was isolated from cells by column purification (Direct-zol RNA Miniprep kit; Zymo Research) with DNase treatment. Complementary DNA (cDNA) was synthesized using a High-Capacity cDNA Reverse Transcription Kit (Thermo Fisher Scientific) with poly-dT or random hexamer primers. Quantitative PCR was performed on cDNA using Fast SYBR Green Master Mix (Thermo Fisher Scientific) on a QuantStudio 3 Real-Time PCR System (Thermo Fisher Scientific). Gene expression was quantified using the following primers:

mouse *H2-Aa* forward: GGAGGTGAAGACGACATTGAGG

mouse *H2-Aa* reverse: CTCAGGAAGCATCCAGACAGTC

mouse *Cd74* forward: GCTGGATGAAGCAGTGGCTCTT

mouse *Cd74* reverse: GATGTGGCTGACTTCTTCCTGG

mouse *Ciita* forward: ACCTTCGTCAGACTGGCGTTGA

mouse *Ciita* reverse: GCCATTGTATCACTCAAGGAGGC

mouse *Stat1* forward: GCCTCTCATTGTCACCGAAGAAC

mouse *Stat1* reverse: TGGCTGACGTTGGAGATCACCA

mouse Gbp2 forward: ACCAAGGGCATCTGGATGTG

mouse Gbp2 reverse: TAGCGGAATCGTCTACCCCA

mouse β-actin forward: AGATCAAGATCATTGCTCCTCCT

mouse β-actin reverse: ACGCAGCTCAGTAACAGTCC

.

Bioinformatic analysis

Bulk and single-cell RNA-seq counts were obtained from the Gene Expression Omnibus database with the accession numbers GSE117970, GSE212643, GSE193814, GSE157673, GSE146771, GSE121521, GSE165905, GSE1552 and GSE169246. In our analysis of bulk RNA sequencing data, raw counts were processed and normalized using Limma-Voom tools. Quality control measures were performed and log counts per million were generated prior to assessing gene expression levels between groups. Differential expression analysis was performed using the EdgeR package. Single-cell RNA-seq data was processed and analyzed using the Seurat (v. 4.3.0.1) workflow[160]. Immune cell subsets were determined based on the annotations of the clusters computed during the Seurat workflow. Comparisons of TAM gene expression between TNBC patient Responders and Nonresponders to ICB therapy were achieved by applying single-cell

RNA-seq data integration tools provided by Seurat. tSNE plots were generated using the RunTSNE package with Seurat object inputs. Gene set enrichment analysis (GSEA) was performed using the gseGO package. Prediction of functional relationship between PAD4 expression and transcription factor STAT1 in macrophages was performed by analyzing the *Padi4*^{high} macrophage gene set with binding analysis for regulation of transcription (BART)[161].

Quantification and statistical analysis

No statistical methods were used to predetermine sample size. Statistical significance was calculated between two separate groups (i.e. wild-type versus knockout or control versus treatment) by an unpaired two-tailed Student's T-test. Statistical significance was calculated between two groups of the same cellular source (i.e. primary patient ovarian cancer TAMs treated with IFNg subjected to treatment with DMSO or GSK484) by a paired two-tailed Student's T-test. The Mann-Whitney *U*-test was applied for comparisons between two separate groups of continuous outcomes. It has been shown that nonparametric tests are suitable for epigenetic data.[162,163,164] One-Way analysis of variance (ANOVA) was applied to determine statistical difference between multiple (3 or more) experimental groups. Cell-based experiments were performed with at least 3 biological and 3 technical replicates unless otherwise stated. All FACS analysis was performed on at least 3 biological replicates. Animal experiments were performed with C57BL/6 mice including *Padi4*$^{+/+}$, *Padi4*$^{-/-}$, *Padi4*$^{fl/fl}$, *Padi4*$^{fl/fl}$ *LysM*^{cre} and *Padi4*$^{fl/fl}$ *Cd4*^{cre} mice. Wild-type vs *Padi4*–deficient mice were sex and age-matched during tumor inoculation. At least 5-10 mice were used for each group. Statistical analysis for animal or cell–based experiments was performed using GraphPad Prism9. Statistical analysis within the bioinformatic data was performed using RStudio.

Results

PAD4 is an abundant post-translational-modification enzyme in TAMs

Post-translational modifications (PTMs) drive the final conformations and functions of proteins[165,166]. However, it is poorly understood if and how PTMs control TAM functions. To address this question, we analyzed multiple RNA-sequencing datasets to assess the expression levels and patterns of major PTM enzymes, including methyltransferases, kinases, ubiquitin enzymes, acyltransferases, acetyltransferases, deacetylases, and peptidylarginine deiminases, in the TAMs of both human and mouse cancers. In patients with breast cancer[9], differential expression (DE) analysis revealed that PAD4 was among the most highly expressed PTM enzyme among major PTM enzymes in TAMs as compared to normal macrophages (**Figure 2.3A**). Similar results were obtained in the TAMs of breast cancer–bearing mice[167] whereby *Padi4* was among the most significantly enriched PTM enzyme transcripts TAMs compared to other PTM enzyme transcripts (**Figure 2.3B)**. Moreover, within TAM subsets reported to exhibit enhanced tumor–promoting features[168,169], CSF1R^{high} TAMs sorted from colorectal cancer (CRC) patient tissues and Tim-4^{high} TAMs sorted from ovarian cancer–bearing mice featured significantly more highly enriched expression of PAD4 transcript compared to in CSF1R^{low} or Tim4^{low} TAMs (**Figure 2.3C-D**). Evidently, compared to several other PTM enzyme genes, PAD4 was particularly more highly enriched. Comparing *PADI4* (or *Padi4*) mRNA expression in normal macrophages versus TAMs in both breast cancer patients and tumor-bearing mice revealed that PAD4 transcript levels were significantly higher in TAMs versus in normal macrophages (**Figure 2.3E**).

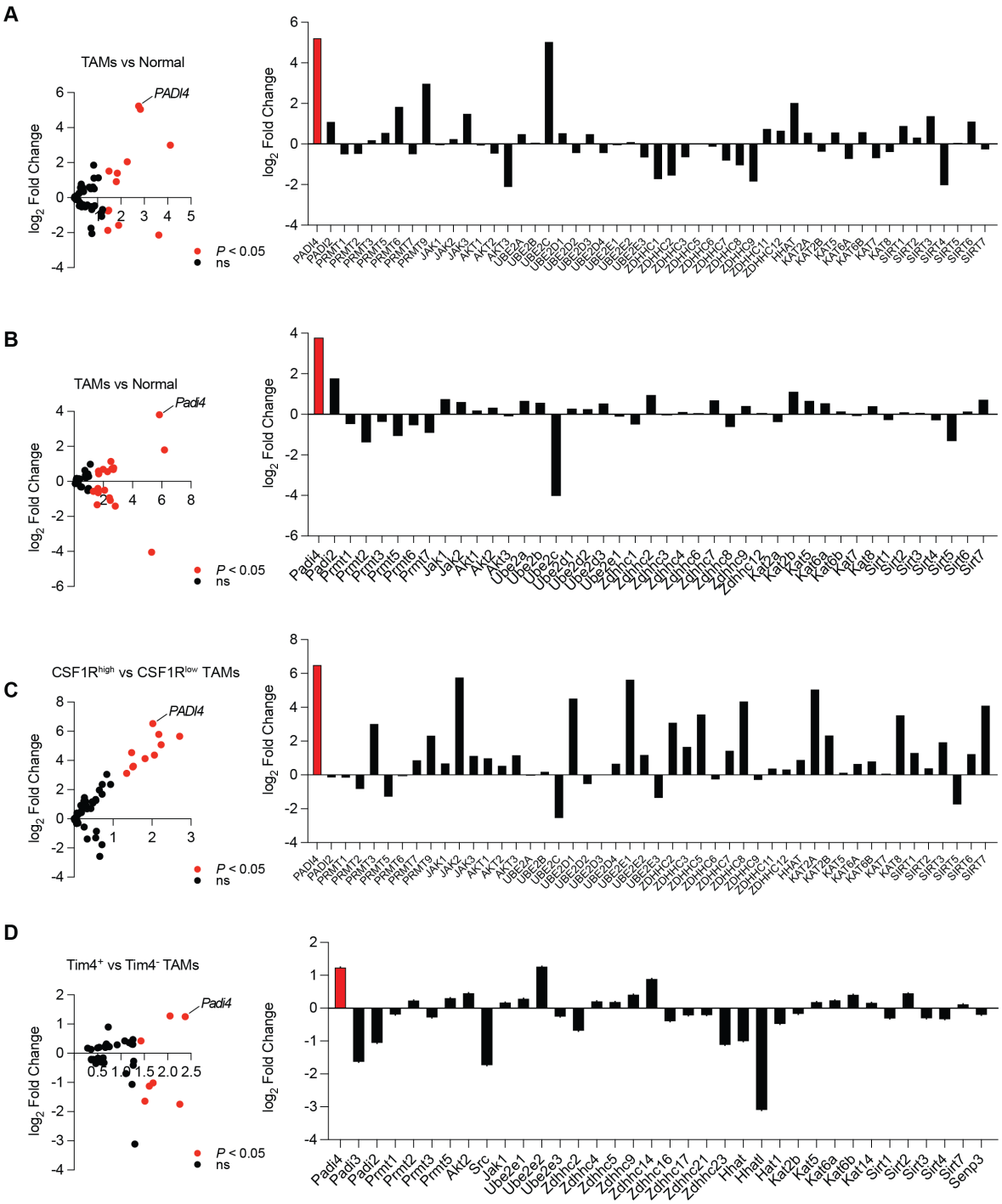

Figure 2.3.0: PAD4 is an abundant post-translational modification enzyme in TAMs. (A) Differential expression analysis of PTM enzymes in TAMs vs normal macrophages from breast cancer patients (GSE117970). (B) Differential expression analysis of PTM enzymes in TAMs vs normal macrophages from breast tumor–bearing mice (GSE212643). (C) Differential expression analysis of PTM enzymes in $CSF1R^{high}$ versus $CSF1R^{low}$ TAMs sorted from CRC patients (GSE193814). (D) Differential expression analysis of PTM enzymes in Tim-4^{high} versus Tim-4^{low} TAMs sorted from the peritoneal metastasis of ID8 tumor–bearing mice (GSE157673).

While we observed that PAD4 was among the most active PTM enzymes in TAMs, we sought to confirm whether PAD4 expression was restricted to macrophages compared to other mononuclear immune cells. We analyzed a publicly available single-cell RNA-sequencing dataset featuring the $CD45^+$ cells from mouse peritoneal lavage (GSE121521)[170]. T-distributed neighbor embedding (t-SNE)–mediated visualization revealed that *Padi4* was largely exclusively expressed in macrophages compared to T-cells, B-cells, and dendritic cells (DCs) (**Figure 2.3F**). The immune cell subset with the highest proportion and expression of *Padi4* was that of the macrophages (**Figure 2.3G-H**). Consistent with these mouse peritoneal lavage data, in the blood of CRC patients, *PADI4* was predominantly expressed in macrophages (**Figure 2.3I-J**). In addition to the PAD4 expression in macrophages, we show that in triple negative breast cancer (TNBC) patients, that the expression of PAD4 was associated with an immunosuppressive macrophage profile (**Figure 2.3K**). Further, we sought to demonstrate that PAD4 induction was associated with tumor–promoting conditions. To first ascertain the transcriptional landscape for $Padi4^{high}$ versus $Padi4^{low}$ TAMs in tumor–bearing mice, we performed bulk RNA-sequencing on mouse TAMs and examined a pro-inflammatory IFNγ–associated macrophage profile. We observed that in the $Padi4^{high}$ TAMs, the expression of key genes along the IFNγ–MHC-II signaling pathway were downregulated suggesting that `PAD4 may impede anti-tumor functions in macrophages (**Figure 2.3L**). As aforementioned, *Padi4* transcriptional expression occurred more significantly in the Tim-4^{high} TAMs from ovarian tumor–bearing mice. We validated that PAD4 protein expression occurred more significantly in the Tim-4^{high} mouse TAMs (**Figure 2.3M**). Next, we sought to demonstrate that tumor–associated factors can induce PAD4 in macrophages, providing evidence that the TME promotes PAD4 expression and function. Among the several diverse factors within the TME are toll-like receptor (TLR) agonists, including tumor lysates or DAMPs[65,66,171] and all

trans retinoic acid (ATRA)[172]. Further, retinoic acid has been shown to regulate intratumoral monocyte differentiation to form tumor–promoting macrophages[172]. Treating HL60 (human myeloid leukemia cell line) with LPS or ATRA resulted in the induction of PAD4 protein (**Figure 2.3N**). Next, we treated HL60 cells with primary ascites fluid harvested from ovarian cancer patients to observe whether this would induce PAD4, providing evidence that the TME induces PAD4 activity. Patient ovarian cancer ascites fluid induced PAD4 in HL60 cells (**Figure 2.3O**) and in primary human blood monocytes enriched from the buffy coats of two donors (**Figure 2.3P**). Finally, we examined whether some specific factors –including IL-6, VEGF and GM-CSF – known to be present in ascites fluid[173,174,175] could directly induce PAD4 in HL60 cells. Treating HL60 cells with each of these factors induced PAD4 (**Figure 2.3Q**). Taken together, we demonstrate that among the mononuclear immune cells, macrophages – particularly the immunosuppressive TAMs – exhibit enhanced expression of PAD4 transcript and proteins in mice and in humans.

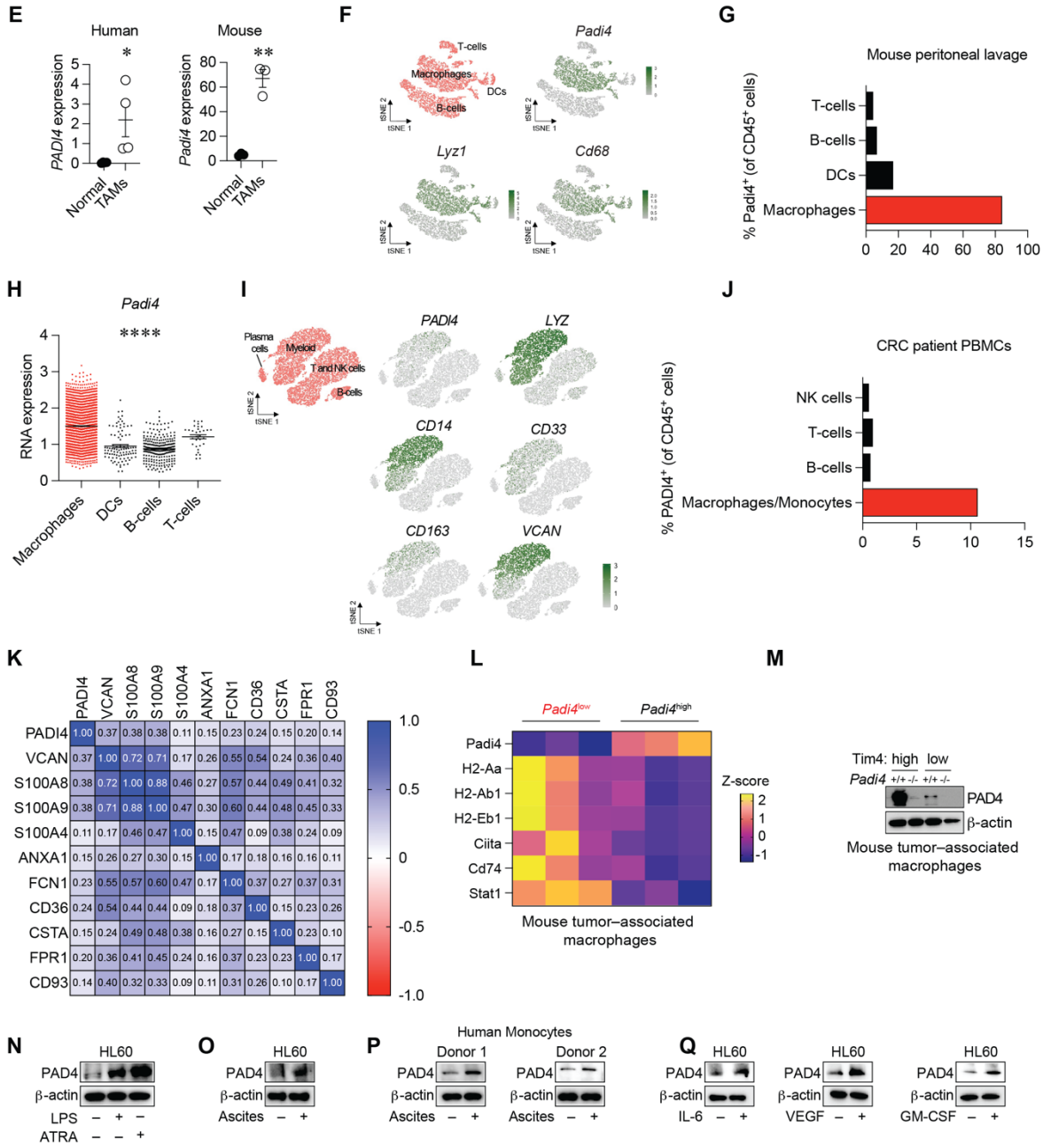

Figure 2.3.1: PAD4 is an abundant post-translational modification enzyme in TAMs. (E) Human *PADI4* and mouse *Padi4* mRNA expression in normal breast macrophages versus in breast cancer TAMs examined in bulk RNA-seq datasets (GSE117970, n=4; and GSE212643, n=3; respectively). (F) tSNE plots generated from scRNA-seq data (GSE121521) showing distribution of macrophage–associated genes across peritoneal lavage subsets from mice. (G) Proportion of *Padi4*$^{+}$ cells in each immune cell subset of the mouse peritoneal lavage (GSE121521).(H) Expression levels of *Padi4* across immune cell subsets of the mouse peritoneal lavage (GSE121521).(I) tSNE plots generated from scRNA-seq data (GSE146771) showing the distribution of macrophage/monocyte-associated genes across the PBMC subsets of CRC patients. (J) Proportion of *PADI4*$^{+}$ cells in each immune cell subset of peripheral blood mononuclear cells from patients with colorectal cancer patient PBMCs (GSE146771). (K) Correlation matrix featuring *PADI4* and immunosuppressive macrophage genes. (L) Heatmap representation of bulk RNAseq data showing the STAT1/MHC-II gene expression profile in *Padi4*^{low} and *Padi4*^{high} mouse TAMs. (M) Protein expression of PAD4 in mouse Tim-4^{high} versus Tim-4^{low} TAMs. (N) PAD4 protein induced by LPS or ATRA. (O) PAD4 protein expression in HL60 cells cultured with ascites fluid. (P) PAD4 protein expression in primary human blood monocytes cultured with ascites fluid from patients with primary ovarian cancer (n = 2 donors). (Q) PAD4 protein expression in HL60 cells cultured with with IL-6, VEGF or GM-

CSF. Data are shown as mean ± S.E.M. (E and H). Unpaired two-tailed Student's T-test (E). One-Way ANOVA test (H). *p < 0.05; **p < 0.01; ****p < 0.0001. scRNA-seq, single-cell RNA-sequencing; ns, not significant

PAD4 in macrophages restrains anti-tumor immunity

While we observed that PAD4 was particularly highly expressed in immunosuppressive TAMs compared to normal macrophages and that tumor–promoting factors activated PAD4 in myeloid cells, we then asked whether PAD4 in macrophages posed an effect on tumor growth and tumor immune responses. We inoculated subcutaneously MC38 cells, a murine colon adenocarcinoma cell line, into wild-type (*Padi4*$^{+/+}$) and total-body *Padi4* knockout (*Padi4*$^{-/-}$) mice. We found that *Padi4*$^{-/-}$ mice developed smaller tumors compared to *Padi4*$^{+/+}$ mice as shown by tumor volume and weight (**Figure 2.4A-C**). Importantly, effector T-cell functions were enhanced in the *Padi4*$^{-/-}$ mouse tumors indicating enhanced anti-tumor immunity associated with the reduced tumor growth (**Figure 2.4D-E**). We next sought to determine whether the T-cell phenotype observed in the *Padi4*$^{-/-}$ tumor-bearing mice was attributed to the loss of PAD4 activity in T-cells or macrophages. To specifically examine a role of PAD4 in T-cells and macrophages, we bred *Padi4*$^{fl/fl}$ mice with *Cd4*^{cre} and *LysM*^{cre} mice to generate two conditional knock-out mouse strains: *Padi4*$^{fl/fl}$*Cd4*^{cre} and *Padi4*$^{fl/fl}$*LysM*^{cre} mice (**Figure 2.4F).** We first asked whether specific loss of PAD4 in T-cells could alter anti-tumor immunity in tumor–bearing mice. When we inoculated MC38 cells subcutaneously into *Padi4*$^{fl/fl}$ mice and *Padi4*$^{fl/fl}$ *Cd4*^{cre} mice, we observed no difference in tumor volume and weight (**Figure 2.4G**). Interestingly, when we inoculated MC38 cells into *Padi4*$^{fl/fl}$ vs *Padi4*$^{fl/fl}$ *LysM*^{cre} mice, we observed that the *Padi4*$^{fl/fl}$ *LysM*^{cre} mice developed smaller tumors compared to the wild-type *Padi4*$^{fl/fl}$ counterparts (**Figure 2.4H**). The tumor–infiltrating T-cells from the *Padi4*$^{fl/fl}$ *LysM*^{cre} mouse tumor were more highly activated indicated by higher levels of IFNγ^+ and IFNγ^+TNFα^+CD4$^+$ and CD8$^+$ T-cells (**Figure 2.4I-L**). The TDLNs

of the MC38–bearing *Padi4*$^{fl/fl}$ *LysM*^{cre} mice also harbored higher proportions of IFNγ^{+}CD8^{+} and TNFα^{+}CD4^{+} and CD8^{+} T-cells (**Figure 2.4M-P**). The tumor–infiltrated CD4^{+} and the CD8^{+} T-cells of the *Padi4*$^{fl/fl}$ *LysM*^{cre} mice also exhibited less exhaustion or dysfunction compared to those from the wild-type counterparts indicated by levels of Lag-3 and KLRG1 (**Figure 2.4Q**). Moreover, we assessed whether the tumor-infiltrated T-cells were activated in a tumor-specific manner. We performed an ELISpot assay to measure MC38 antigen–specific murine IFNγ production. We harvested and enriched T-cells from the tumors of *Padi4*$^{fl/fl}$ mice and *Padi4*$^{fl/fl}$ *LysM*^{cre} mice and then plated them in a mouse IFNγ ELISpot either alone or stimulated by dead UV–irradiated MC38 cells to then find that the T-cells from the *Padi4*$^{fl/fl}$ *LysM*^{cre} mice produced higher amounts of IFNγ upon induction by dead MC38 cell lysates compared to those of the wild-type counterparts (**Figure 2.4R**). Thus, the specific loss of PAD4 in macrophages enhances tumor-antigen–specific T-cell–mediated anti-tumor immunity. To further substantiate this conclusion, we inoculated subcutaneously Py8119 cells, a mouse breast cancer cell line, into *Padi4*$^{fl/fl}$ mice and *Padi4*$^{fl/fl}$ *LysM*^{cre} mice. Again, the *Padi4*$^{fl/fl}$ *LysM*^{cre} mice developed smaller tumors compared to their wild-type counterparts (**Figure 2.4S-U**).

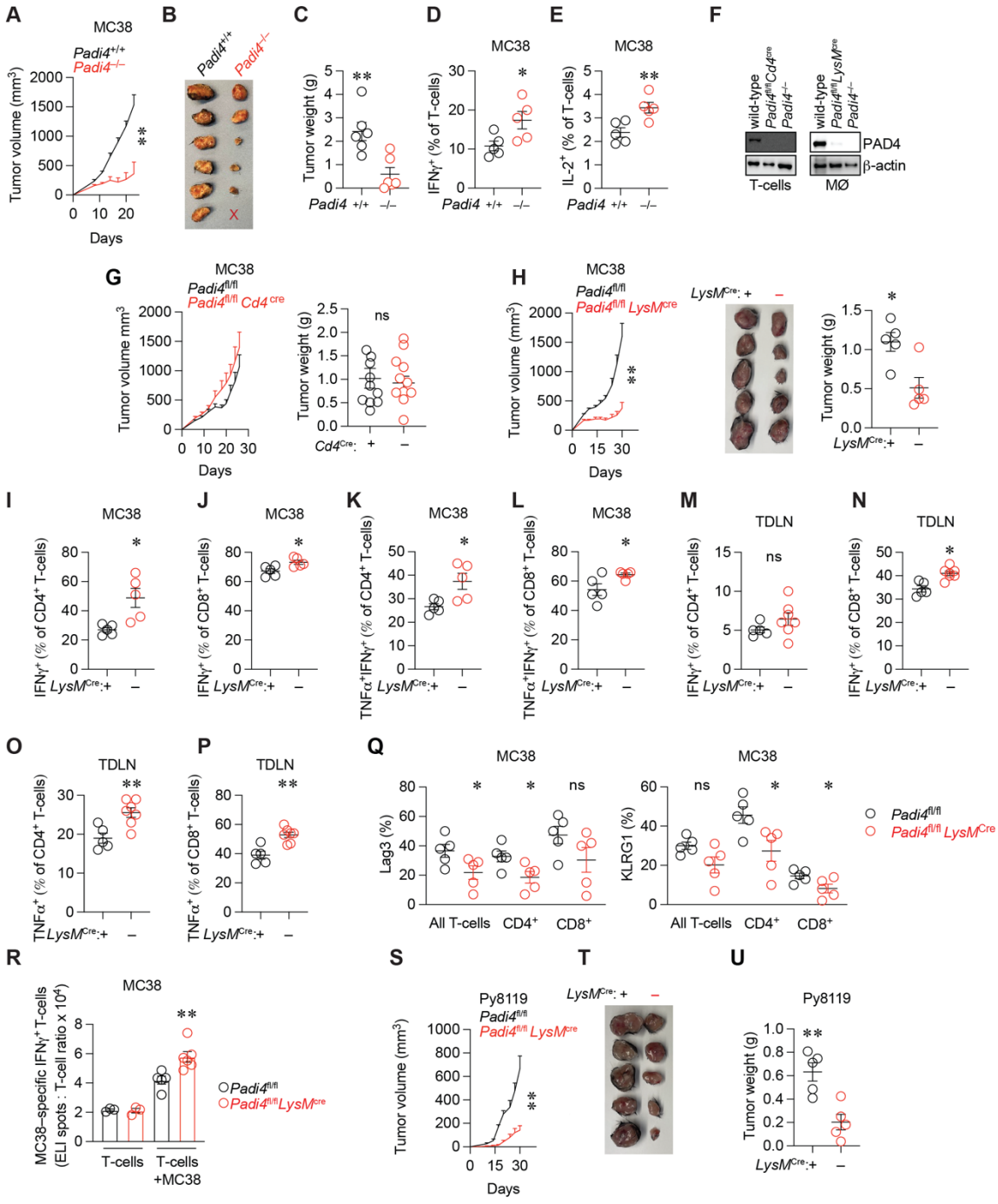

Figure 2.4.0: PAD4 in macrophages restrains anti-tumor immunity. (A) Growth kinetics of subcutaneous MC38 murine colorectal cancer in Padi4$^{+/+}$ and Padi4$^{-/-}$ mice (n = 6). (B) At endpoint, MC38 tumors from Padi4$^{+/+}$ and Padi4$^{-/-}$ mice were excised (n = 6).(C) Weight of the tumors excised from Padi4$^{+/+}$ and Padi4$^{-/-}$ MC38–bearing mice. (D and E) Percentages of IFNγ^{+} (D) and IL-2^{+} (E) T-cells from MC38 tumor-bearing Padi4$^{+/+}$ and Padi4$^{-/-}$ mice (n = 5). (F) PAD4 protein expression in the enriched T-cells from wild-type, *Padi4*$^{fl/fl}$ *Cd4*^{cre}, and *Padi4*$^{-/-}$ mice and in the enriched peritoneal macrophages from wild-type, *Padi4*$^{fl/fl}$ *LysM*^{cre}, and *Padi4*$^{-/-}$ mice. (G) *Padi4*$^{fl/fl}$ and *Padi4*$^{fl/fl}$ *Cd4*^{cre} mice were inoculated subcutaneously with MC38 colon adenocarcinoma cells. (H) Growth kinetics of subcutaneous MC38 murine colorectal cancer in *Padi4*$^{fl/fl}$ and *Padi4*$^{fl/fl}$ LysM^{cre} mice (n = 5) (left). At endpoint, MC38 tumors from *Padi4*$^{fl/fl}$ and *Padi4*$^{fl/fl}$ *LysM*^{cre} mice were excised (n = 5) (center). Weight of the tumors excised from *Padi4*$^{fl/fl}$ and *Padi4*$^{fl/fl}$ *LysM*^{cre} MC38–bearing mice (n=5) (right). (I and J) Percentages of IFNγ^{+}CD4^{+} (I) and IFNγ^{+}CD8^{+} (J) T-cells from MC38 tumors of *Padi4*$^{fl/fl}$ and *Padi4*$^{fl/fl}$ *LysM*^{cre} mice (n = 5). (K and L) Percentages of TNFα^{+}IFNγ^{+}CD4^{+} (K) and

TNFα$^+$IFNγ$^+$CD8+ (L) T-cells from MC38 tumors of *Padi4*$^{fl/fl}$ and *Padi4*$^{fl/fl}$ *LysM*^{cre} mice (n = 5). (M and N) Percentages of IFNγ$^+$CD4$^+$ (M) and IFNγ$^+$CD8$^+$ (N) T-cells in the TDLNs of MC38 tumor–bearing *Padi4*$^{fl/fl}$ and *Padi4*$^{fl/fl}$ *LysM*^{cre} mice (n = 5). (O and P) Percentages of TNFα$^+$CD4$^+$ (O) and TNFα$^+$CD8$^+$ (P) T-cells in the TDLNs of MC38 tumor–bearing *Padi4*$^{fl/fl}$ and *Padi4*$^{fl/fl}$ *LysM*^{cre} mice (n = 5). (Q) Percentages of Lag3$^+$ and KLRG1$^+$ CD4$^+$ and CD8$^+$ T-cells from the MC38 tumors of tumor–bearing mice. Data are shown as mean ± S.E.M. (A,C-E,G-S, and U). Unpaired two-tailed Student's T-test. *$p < 0.05$; **$p < 0.01$.

We then sought to determine whether the loss of PAD4 in macrophages would enhance anti-tumor immunity in metastasis conditions. We inoculated intravenously B16F10 – a murine melanoma cell line – into *Padi4*$^{fl/fl}$ mice and *Padi4*$^{fl/fl}$ *LysM*^{cre} mice. We observed less lung tumor nodules in the *Padi4*$^{fl/fl}$ *LysM*^{cre} mice compared to wild-type counterparts (**Figure 2.4V-W**). Further, we assessed the T-cell activation phenotype in B16F10 lung metastatic nodules in the wild-type mice and the *Padi4*$^{fl/fl}$ *LysM*^{cre}. We observed higher levels of IFNγ$^+$, TNFα$^+$ and granzyme B$^+$ T-cells in the lung metastasis of the *Padi4*$^{fl/fl}$ *LysM*^{cre} mice as compared to that of the wild type mice (**Figure 2.4X-Z**). Taken together, the loss of PAD4 in macrophages results in enhanced anti-tumor immunity indicated by enhanced tumor T-cell activation and reduced tumor growth and metastatic burden.

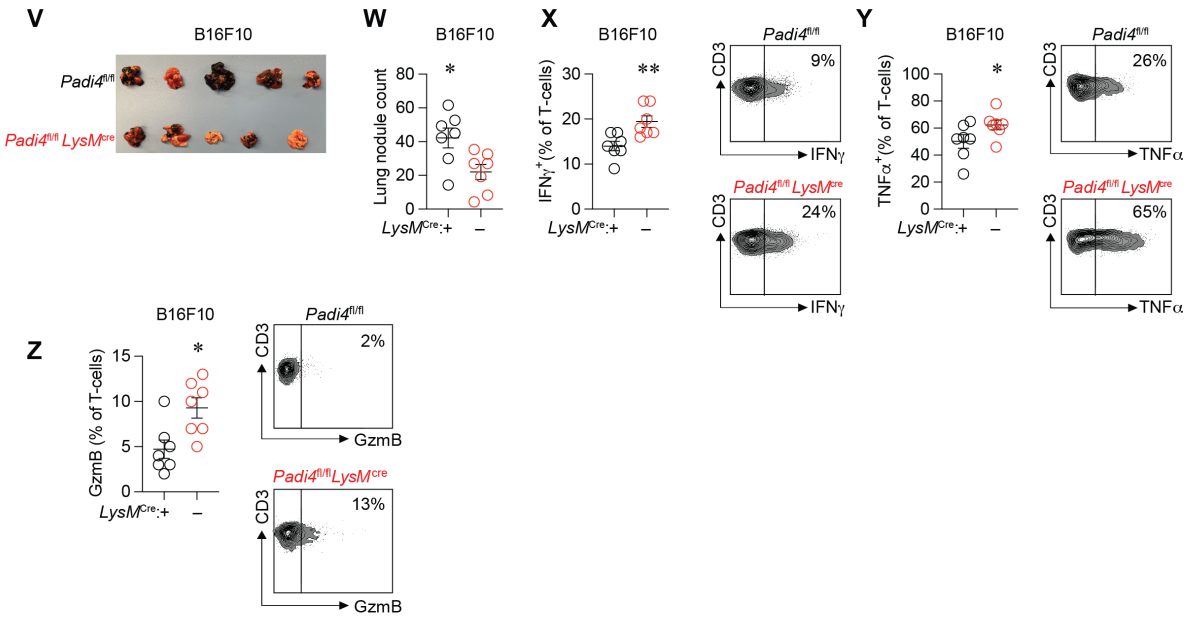

Figure 2.4.1: PAD4 in macrophages restrains anti-tumor immunity. (R) Mouse IFNγ ELISpot assay measuring IFNγ production in tumor–infiltrating T-cells from *Padi4*$^{fl/fl}$ and *Padi4*$^{fl/fl}$ *LysM*^{cre} MC38–bearing mice following stimulation with dead UV–irradiated MC38 tumor cells (n= 5-6). (S) Growth kinetics of subcutaneous Py8119 murine breast cancer in *Padi4*$^{fl/fl}$ and *Padi4*$^{fl/fl}$ *LysM*^{cre} mice (n = 5). (T) At endpoint, Py8119 tumors from *Padi4*$^{fl/fl}$ and *Padi4*$^{fl/fl}$ *LysM*^{cre} mice were excised (n = 5). (U) Weight of the tumors excised from *Padi4*$^{fl/fl}$ and *Padi4*$^{fl/fl}$ *LysM*^{cre} Py8119–bearing mice. (V) Harvested lungs from *Padi4*$^{fl/fl}$ and *Padi4*$^{fl/fl}$ *LysM*^{cre} mice intravenously inoculated with B16F10. (W) Lung nodule counts on the metastatic lungs excised from *Padi4*$^{fl/fl}$ and *Padi4*$^{fl/fl}$ *LysM*^{cre} mice intravenously inoculated with B16F10 (n = 7). (X-Z) Percentages of (X) IFNγ$^+$, (Y) TNFα$^+$ and (Z) granzyme B$^+$ tumor-infiltrated T-cells from the lung metastasis of B16F10-bearing Padi4$^{fl/fl}$ and Padi4$^{fl/fl}$ LysM^{cre} mice (n = 7). Data are shown as mean ± S.E.M. (W-Z). Unpaired two-tailed Student's T-test. *p < 0.05; **p < 0.01.

PAD4 restrains MHC-II machinery in macrophages

We next assessed the mechanism by which PAD4 negatively regulates TAM-mediated anti-tumor immunity. First, we examined the immune phenotype of peritoneal macrophages from wild-type and *Padi4*$^{-/-}$ mice, assessing the expression of key surface proteins involved in the immune response including CD80, CD86, MHC-I and MHC-II. Interestingly, there was no difference in MHC-I, CD80, and CD86 expression between *Padi4*$^{-/-}$ and *Padi4*$^{+/+}$ macrophages – only MHC-II protein expression differed significantly between *Padi4*$^{-/-}$ and *Padi4*$^{+/+}$ macrophages (**Figure 2.5A**). Indeed, across tissues – in the peritoneum and in the lungs (and in liver, colon, and lymph nodes; data not shown) – MHC-II expression was enhanced on the *Padi4*$^{-/-}$ macrophages (**Figure**

2.5B-D). Moreover, in response to IFNγ treatment over time, MHC-II and not MHC-I or PDL1 was enhanced during induction in the PAD4-deficient macrophages compared to the wild-type counterparts (**Figure 2.5E**). In these assessments of MHC-II expression, we measured surface MHC-II; however, when we measure intracellular MHC-II, we observed the same phenomenon of higher MHC-II expression in the *Padi4*$^{-/-}$ macrophages (**Figure 2.5F**). We then asked whether the expression of MHC-II was controlled on the protein level or on the transcriptional level. When we harvested primary macrophages from wild-type and *Padi4*$^{-/-}$ mice, we assessed the expression of MHC-II–coding genes as well as the IFNγ signaling gene pathway. We found that the *Padi4*–deficient macrophages expressed significantly higher levels of MHC-II–coding genes, including *H2-Aa*, *Ciita*, and *Cd74* as well as IFN-signaling genes such as *Stat1* and *Gbp2* (**Figure 2.5G**). To validate these findings, we analyzed a publicly available single cell RNA-sequencing dataset featuring mouse peritoneal immune cells[170]. Based on *Padi4* expression, we divided macrophages into two groups: high *Padi4* (*Padi4*^{high}) and low *Padi4* (*Padi4*^{low}) expressing cells (**Figure 2.5H**). Consistently, we found higher expression levels of genes which directly code for MHC-II – such as *H2-Aa*, *H2-Ab1,* and *Ciita* – as well as genes which code for the several co-factors involved in the transcriptional regulation of MHC-II machinery in *Padi4*^{low} macrophages as compared to the *Padi4*^{high} macrophages (**Figure 2.5I**). Interestingly, we observed no difference in the MHC-II levels on wild-type versus *Padi4*$^{-/-}$ dendritic cells (DCs) as MHC-II is constitutively expressed on mature DCs, unlike macrophages which exhibit multifaceted roles in immune response and homeostasis, and which require induction for the upregulation of MHC-II (**Figure 2.5J**)[176].

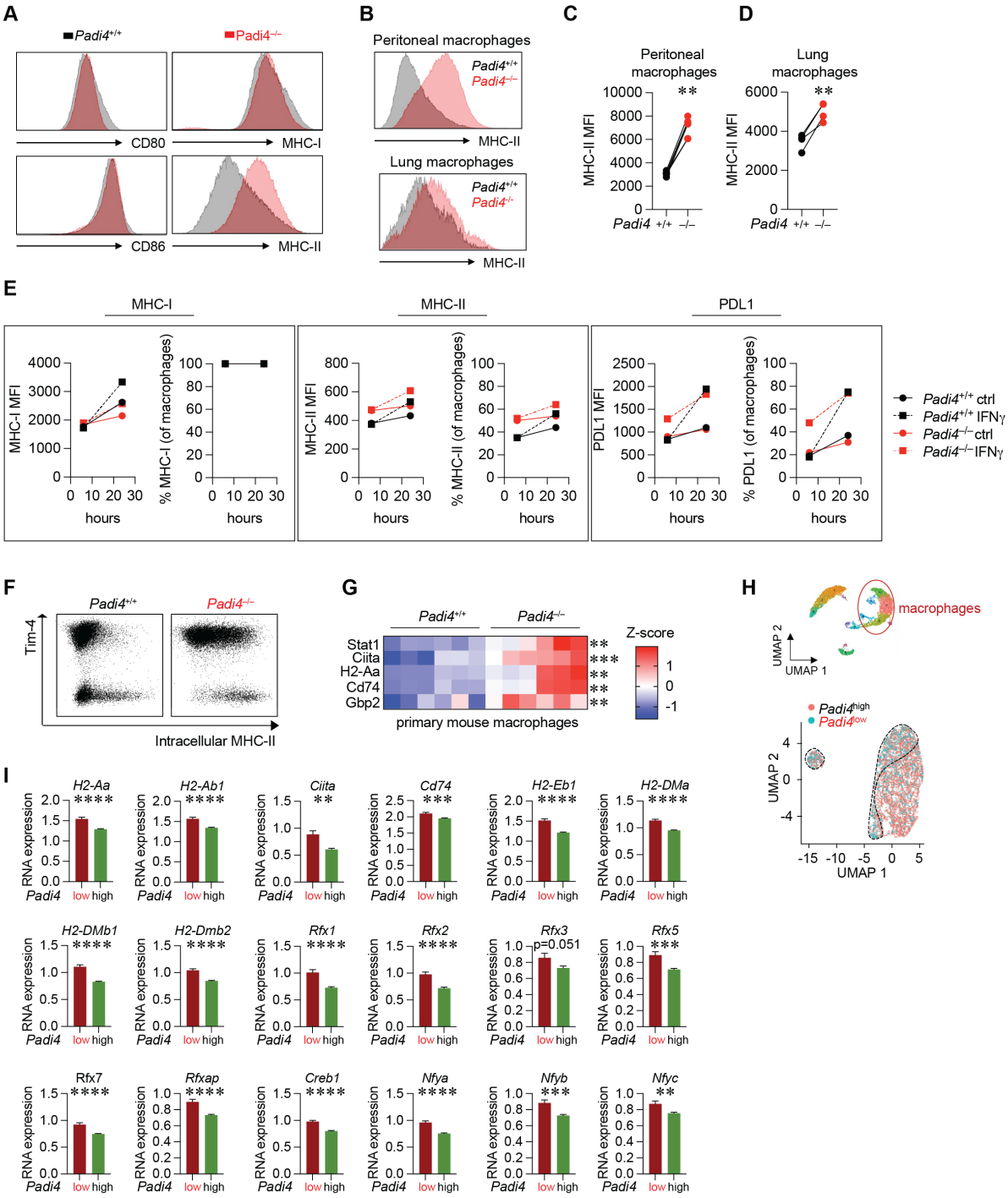

Figure 2.5.0: PAD4 restrains MHC-II machinery in macrophages. (A) The basic surface immune phenotype of Padi4$^{+/+}$ and Padi4$^{-/-}$ peritoneal macrophages. (B) Representative histogram quantifying MHC-II protein expression in peritoneal and lung macrophages from *Padi4*$^{+/+}$ and *Padi4*$^{-/-}$ mice. (C) Mean fluorescence intensity (MFI) of MHC-II expression on unchallenged primary peritoneal macrophages harvested from *Padi4*$^{+/+}$ and *Padi4*$^{-/-}$ mice. Representative of nine independent experiments. (D) Mean fluorescence intensity (MFI) of MHC-II expression on unchallenged primary lung macrophages harvested from *Padi4*$^{+/+}$ and *Padi4*$^{-/-}$ mice. Representative of four independent experiments. (E) MFI of MHC-I, MHC-II and PDL1 expression at 6 hours and 24 hours with or without IFNγ stimulation. (F) Dotplot of intracellular MHC-II expression in *Padi4*$^{+/+}$ and *Padi4*$^{-/-}$ peritoneal macrophages. (G) Quantitative polymerase chain reaction (qPCR) results showing MHC-II–coding and IFNγ–responsive gene expression in the peritoneal macrophages from healthy *Padi4*$^{+/+}$ and *Padi4*$^{-/-}$ mice (n = 6/group, qPCR normalized to β-actin

expression). (H) UMAP projection of single-cell RNAseq data featuring the immune cells from murine peritoneal lavage (GSE121521) and UMAP projection of murine peritoneal macrophages indicating high and low expression of *Padi4*. Data are shown as mean ± S.E.M. (C-D, G, and I). Unpaired two-tailed Student's T-test. *p < 0.05; **p < 0.01; ***p < 0.001; ****p < 0.0001.

While we demonstrate that the loss of PAD4 enhances MHC-II expression on the transcriptional level and consequently on the protein level, we then sought to show that PAD4–deficiency results in enhanced MHC-II function. We performed an *in vitro* antigen presentation assay in which we co-cultured *Padi4*$^{+/+}$ or *Padi4*$^{-/-}$ macrophages with T-cells from OT-II transgenic mice which can only be activated as a result of antigen presentation by MHC-II. We also supplemented the culture system with soluble ovalbumin (sOVA) protein which is processed and then presented to T-cells as peptides by the macrophages. We observed that the T-cells cultured with the *Padi4*$^{-/-}$ macrophages and the sOVA were significantly more activated than those cultured with the *Padi4*$^{+/+}$ macrophages indicated by enhanced IFNγ, IL-2 and TNFα production, demonstrating enhanced antigen presentation achieved by the *Padi4*$^{-/-}$ macrophages (**Figure 2.5K**). Further, we sought to demonstrate that PAD4–deficient macrophages could activate OT-II T-cells via the presentation of tumor–associated antigens. We osmotically loaded OVA protein onto MC38 cells as previously described[159] and then killed tumor cells via UV-irradiation so that we could prime macrophages with OVA^{+} tumor lysates to then be presented to OT-II T-cells, activating them. Similarly, as when the macrophage–OT-II T-cell culture system was supplemented was sOVA (**Figure 2.5K**), co-culturing *Padi4*$^{-/-}$ macrophages with OT-II T-cells and dead OVA^{+} MC38 cells resulted in the enhanced T-cell activation indicated by higher proportions of IFNγ^{+} and IL-2^{+} T-cells compared to the culture system with the wild-type macrophages (**Figure 2.5L**).

We extended our analysis to TAMs in mice bearing multiple tumor types. As before, we observed that the loss of PAD4 resulted in enhanced MHC-II expression in the TAMs of mice

bearing subcutaneous MC38, subcutaneous Py8119, and B16F10 lung metastasis (**Figure 2.5M**). Moreover, we examined tissue–resident and non-tissue–resident macrophage subsets in each of the tumor models and we observed that while total PAD4–deficient macrophages expressed enhanced MHC-II, the loss of PAD4 tended to affect the tissue–resident macrophages more than the non-tissue–resident subsets (**Figure 2.5M**). These results suggest that PAD4 negatively regulates MHC-II–mediated antigen presentation and T-cell activation; and therefore, *in vivo*, impedes anti-tumor immunity via the restraint of MHC-II transcriptional expression and function.

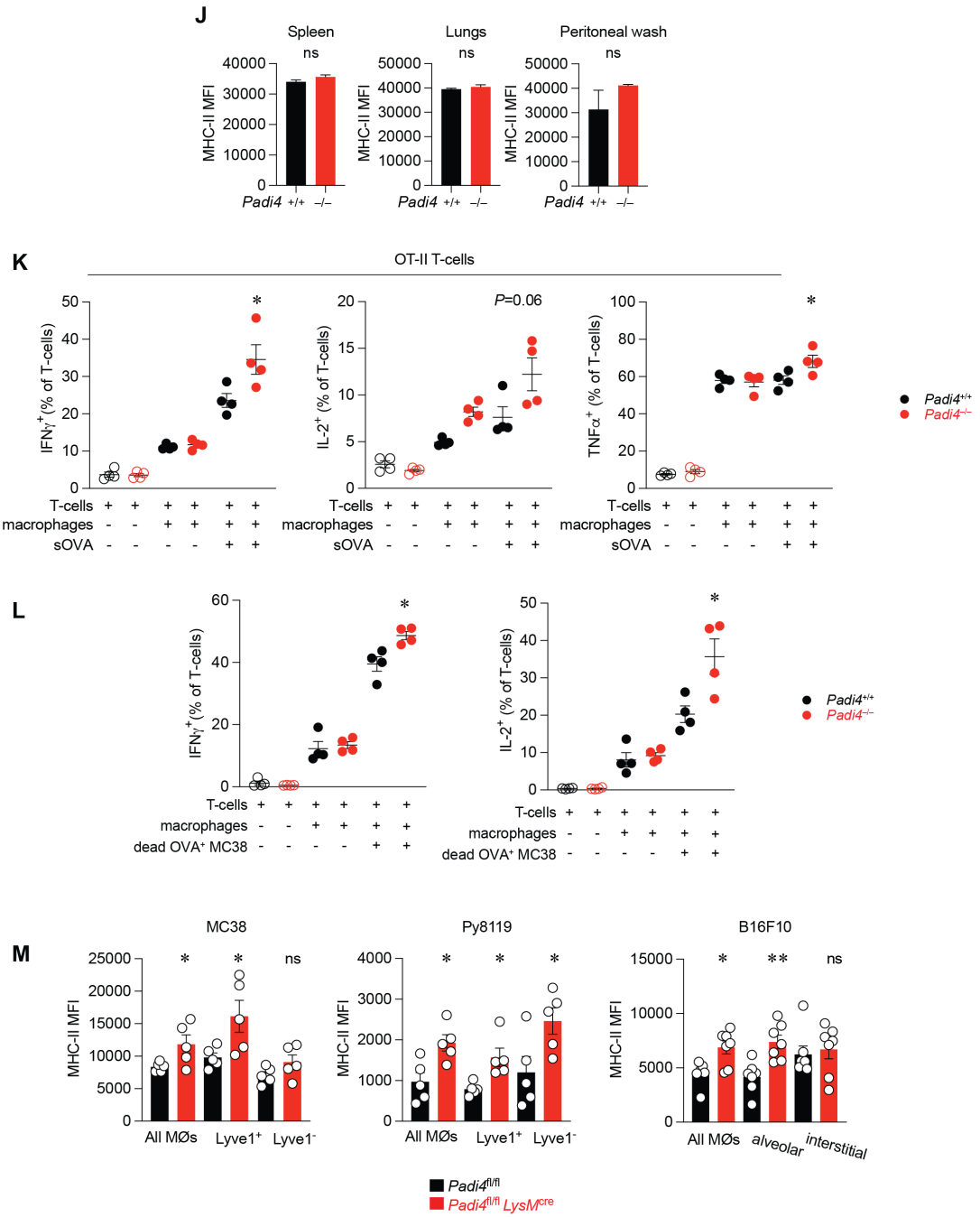

Figure 2.5.1: PAD4 restrains MHC-II machinery in macrophages. (I) Assessment of MHC-II–coding gene expression in *Padi4*^{low} versus *Padi4*^{high} macrophages from single-cell RNAseq data. (J) MFI of MHC-II expression on DCs from the spleen, lungs, and peritoneal lavage of *Padi4*$^{+/+}$ and *Padi4*$^{-/-}$. (K) Percentages of IFNγ^{+}, IL-2^{+} and TNFα^{+} OT-II T-cells cultured alone, with *Padi4*$^{+/+}$ and *Padi4*$^{-/-}$ macrophages in the presence or absence of sOVA (n = 4). (L) Percentages of IFNγ^{+} and IL-2^{+} OT-II T-cells cultured alone, with *Padi4*$^{+/+}$ and *Padi4*$^{-/-}$ macrophages in the presence or absence of 10^5 UV–irradiated OVA^{+}MC38 cells (n = 4). (M) FACS analysis showing the mean fluorescence intensity (MFI) of MHC-II in Lyve1^{+} and Lyve1^{-} tumor macrophages from MC38 tumor bearing *Padi4*$^{fl/fl}$ versus *Padi4*$^{fl/fl}$ *LysM*^{cre} mice (n = 5) (left). FACS analysis showing the MFI of MHC-II in Lyve1^{+} and Lyve1^{-} tumor macrophages from Py8119 tumor bearing *Padi4*$^{fl/fl}$ versus *Padi4*$^{fl/fl}$ *LysM*^{cre} mice (n = 5) (center). FACS analysis showing the MFI of MHC-II in alveolar and interstitial lung tumor macrophages from B16F10–bearing *Padi4*$^{fl/fl}$ versus *Padi4*$^{fl/fl}$ *LysM*^{cre} mice (n = 7) (right). Data are shown as mean ± S.E.M. (J-M). Unpaired two-tailed Student's T-test. *p < 0.05; **p < 0.01

Broadly, we observed that in macrophages, PAD4 restrained STAT1 signaling affecting MHC-II expression downstream. Returning to the single cell RNA-sequencing dataset discussed previously which featured the immune cells in the mouse peritoneal lavage[170], we performed gene set enrichment analysis (GSEA) on the *Padi4*^{high} macrophages. This revealed that while the most positively enriched pathways included peptidyl-arginine modification (GO:0018195), protein citrullination (GO:0018101), and protein-arginine deiminase activity (GO: 0004668); several of the downregulated pathways, including antigen processing and presentation of exogenous peptide antigen via MHC class II (GO:0019886), MHC class II protein complex (GO:0042613), and IFNγ signaling genes (GO:0071346) (**Figure 2.5N**). When we analyzed a human single-cell RNA-sequencing dataset featuring human PBMCs, we observed similar results with human blood monocytes as in the mouse data (**Figure 2.5O**). These results suggest that PAD4 in macrophages restrains IFNγ/STAT1 signaling in macrophages affecting MHC-II–mediated antigen presentation as a consequence. The TAMs enriched from the ascites of ID8 murine ovarian cancer–bearing PAD4-deficient mice expressed markedly higher STAT1 protein compared to the wild-type counterparts (**Figure 2.5P**).

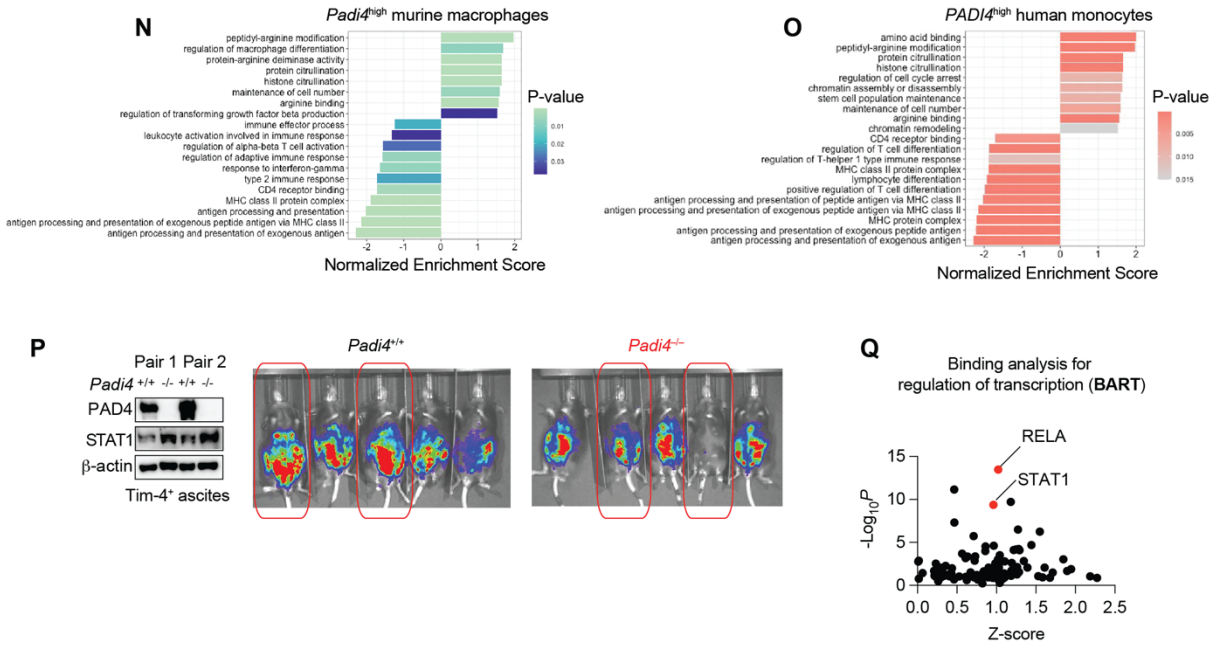

Figure 2.5.2: PAD4 restrains MHC-II machinery in macrophages. (N) Gene set enrichment analysis (GSEA) of *Padi4*^{high} mouse peritoneal macrophages from single-cell RNA-sequencing data of murine peritoneal lavage (GSE121521). (O) Gene set enrichment analysis (GSEA) of *PADI4*^{high} human blood monocytes from single-cell RNA-sequencing data of human PBMCs (GSE169246). (P) Western blot showing PAD4 and STAT1 expression in TAMs enriched from the ascites of two pairs of ID8 ovarian cancer–bearing *Padi4*$^{+/+}$ vs *Padi4*$^{-/-}$ mice. (Q) Transcription factor enrichment analysis or BART conducted on *Padi4*^{high} mouse peritoneal macrophages from single-cell RNA sequencing data of murine peritoneal lavage (GSE121521).

We sought to determine how PAD4 enzymatic activity might regulate STAT1 transcriptional activity. Since in response to IFNγ signaling, STAT1 binds to various promoter regions in the class II transactivator (*CIITA*) gene to control MHC-II expression, we asked whether PAD4 might directly regulate STAT1 protein. PADs have been shown to regulate transcription factor activity via direct citrullination[49,139]. We hypothesized that PAD4 may directly citrullinate STAT1, thereby regulating STAT1 transcriptional activity and consequently MHC-II expression. To begin to test this hypothesis, we performed the binding analysis for regulation of transcription (BART)[161] on the *Padi4*^{high} mouse peritoneal macrophages[170]. The BART analysis revealed that STAT1 was one of the most enriched transcription factors which correlated with high expression of PAD4 in mouse macrophages (**Figure 2.5Q**). It has also been shown that PAD4 directly

citrullinates RELA[139], regulating nuclear import and DNA binding suggesting that STAT1 could be a target of PAD4 citrullination. This observation prompted us to explore a potential regulatory relationship between PAD4 and STAT1.

Discussion

Here, we show that the loss of PAD4 in macrophages results in enhanced anti-tumor immunity, providing a rationale as to how PAD4 expression may be supporting the pro-tumor phenotype in TAMs. Analysis of multiple bulk and single-cell RNA-sequencing datasets revealed that *PADI4* (or *Padi4*) transcription was enhanced in TAMs compared to in normal macrophages in both patients with cancer and tumor–bearing mice. We elucidate that PAD4 restrains MHC-II expression and function, and that this was associated limited and insufficient anti-tumor immunity. Multiple studies established that enhanced MHC-II expression on TAMs plays a major role in determining tumor growth outcomes[177,178]. We demonstrate that the loss of PAD4 in TAMs enhanced anti-tumor immunity via its control over MHC-II function, abrogating tumor growth in the process. We next sought to identify the mechanism through which PAD4 enzymatic activity could achieve the negative regulation of MHC-II–mediated antigen presentation.

Chapter 3: The Citrullination of STAT1 Facilitates the STAT1-PIAS1 Interaction Restraining *CIITA* Transcription

Abstract

While we showed that PAD4 negatively regulates the expression and function of MHC-II on macrophages – restraining T-cell–mediated antitumor immunity as a result – the underlying mechanism still needs to be elucidated. Through the analysis of single-cell RNA-sequencing datasets and further validation via *ex vivo* experiments, we observed that the loss of PAD4 enhanced STAT1/IFNγ signaling strongly affecting MHC-II in particular. We reasoned that PAD4 may be directly regulating STAT1 transcriptional activity since it has been shown that PADs can directly regulate transcription factor functions via citrullination. Here, we discovered that PAD4 citrullinates STAT1 at arginine 121 (R121), thereby promoting the interaction between STAT1 and protein inhibitor of activated STAT1 (PIAS1) which restrains STAT1 DNA binding via physical interaction. The loss of PAD4 completely abolished this interaction, ablating the inhibitory role of PIAS1 in the expression of MHC-II machinery in macrophages and enhancing T-cell activation. Mechanistically, the citrullination of STAT1 inhibited arginine methylation on STAT1 and this modulated the STAT1-PIAS1 interaction. Importantly, PAD4 deficiency resulted in enhanced STAT1 binding to multiple promoters in the *CIITA* gene locus promoting MHC-II transcription. Thus, the PAD4-STAT1-PIAS1 axis is a previously unknown intrinsic immune restriction mechanism in macrophages controlling antigen presentation and may serve as a cancer immunotherapy target.

Background: Targeting macrophages as a means to enhance anti-tumor immunity is an essential strategy in cancer treatment given the high abundance and functional plasticity of macrophages in the TME. However, given the complexities of the regulatory mechanisms within the different macrophage subsets, determining the critical targets within macrophages – which would have a durable anti-tumor effect – poses a difficult challenge. Post-translational modifications (PTMs) set the final structure and therefore function of proteins. Discovery and characterization of PTMs which control macrophage functions in the TME provides important insights which may be exploited for strategies in targeting macrophages to enhance antitumor immunity. Importantly, PTMs can serve as practical and efficacious drug targets.

Materials and Methods: To detect the citrullination of STAT1, protein lysates were labeled with a citrulline–specific probe conjugated to biotin, enriched via streptavidin pulled down, subjected to SDS page and then probed with anti-STAT1 antibody. Co-immunoprecipitation (Co-IP) was used to detect the PAD4–STAT1 physical interaction, mono-methylarginine and the STAT1-PIAS1 physical interactions. Chromatin immunoprecipitation (ChIP) PCR was performed to detect STAT1 binding to *CIITA* gene promoter regions.

Results: PAD4 citrullinates transcription factor STAT1 facilitating the physically inhibitory STAT1-PIAS1 interaction which restrains STAT1 binding to multiple promoter regions of the *CIITA* gene and, as a result, limits MHC-II transcriptional expression on macrophages. PAD4 control of the STAT1-PIAS1 interaction is achieved through the citrullination of STAT1, involving the inhibition of arginine methylation on STAT1.

Summary: The citrullination of STAT1 facilitates the inhibitory STAT1-PIAS1 interaction serving as an intrinsic inhibitory mechanism in macrophages

Background

Targeting macrophages in combination with immune check blockade as a therapeutic strategy may constitute an efficacious and comprehensive approach to cancer treatment. As we discussed previously, macrophages compose the majority of the immune cell population in the TME[9], having a strong, governing effect on tumor growth progression. Various macrophage functions may be and have been exploited as a means to reprogram macrophages to better serve anti-tumor immunity. Post-translational modifications (PTMs) expand the diversity of a protein's structure and therefore protein functions. However, the way in which PTMs control macrophage functions is severely understudied. Nuclear PADs have been shown to directly regulate transcription factor function via citrullination[49,139]. The genetic regulation of MHC-II in response to IFNγ requires that STAT1 binds to *CIITA* promoters resulting in the transcription and then translation CIITA which then binds to MHC-II promoters resulting in MHC-II expression[179]. Studies on PIAS1 have established that the physical interaction between PIAS1 and STAT1 results in reduced STAT1 DNA binding and therefore reduced STAT1 transcriptional signaling[180]. Interestingly, PIAS1–mediated inhibition of STAT1 selectively restrains only specific pathways downstream of STAT1. In this part of our study, we sought to determine the mechanism by which PAD4 regulates STAT1 transcriptional activity sufficient to control MHC-II transcriptional expression.

Methods and materials

The study of how PAD4 enzymatic activity impacts macrophage phenotypes requires a comprehensive coalescence of several different methods.

Cell lines

HL60 cells (CCL-240) and HEK293T cells (CRL-3216) were purchased from the American Type Culture Collection (ATCC, Manassas, VA). HEK293T were maintained in RPMI-1640 Medium (HyClone SH30255, GE Healthcare, Chicago, IL) supplemented with 10% fetal bovine serum. HL60 cells were maintained in Iscove's modified Dulbecco's medium (IMDM) supplemented with 20% fetal bovine serum. All cell lines were tested for *Mycoplasma* contamination by MycoAlert Mycoplasma Detection Kit and confirmed negative for *Mycoplasma*. All cells were cultured at 37ºC under a humidified atmosphere containing 5% CO_2.

Animal models

Wild type C57BL/6J (*Padi4*$^{+/+}$) mice were purchased from the Jackson Laboratory. *Padi4*$^{-/-}$ mice were generated in house (Yongqing Li). Mice were bred in the specific-pathogen-free animal facility (~22 °C with ~40% humidity) on a 12 h dark/12 h light cycle at the University of Michigan. All procedures were approved by the Institutional Animal Care and Use Committees (IACUC) and the Unit for Laboratory Animal Medicine (ULAM) at the University of Michigan.

Magnetic-activated cell sorting (MACS) of peritoneal macrophages

Mice were euthanized via a CO_2 overdose and peritoneal lavage was harvested in MACS buffer on ice. 10-15 mL of peritoneal lavage per mouse was collected after multiple washes of the peritoneal cavity. Cell suspensions were centrifuged and resuspended to be incubated with the primary PE–anti–Tim-4 antibody (clone RMT4-54, BD Biosciences) diluted (1:10) in MACS buffer at 4ºC for 10 minutes in the dark. Cells were washed and centrifuged. The supernatant was aspirated completely and the pellet was resuspended in 80µL of MACS buffer prior to adding and

mixing 20μL of anti–PE microbeads (Miltenyi Biotec) for a 15-minute incubation at 4ºC in the dark. Cells were washed, centrifuged and resuspended in MACS buffer. The PE positive cells were sorted by passing them through LS columns (Miltenyi) according to the manufacturer's instructions. Enriched macrophages were cultured in Dulbecco's Modified Eagle Medium (DMEM) supplemented with 10% fetal bovine serum.

Generation of mouse bone marrow–derived macrophages

Mice were euthanized via a CO_2 overdose and the tibias and femurs were removed and scraped to isolate the bones only. Marrow was flushed out of the bones into a petri dish with DMEM supplemented with 10% fetal bovine serum and 100X penicillin-streptomycin. Bone marrow cells were plated at $5x10^6$ per well in 6 well plates and then treated with 10 ng/mL M-CSF. On Day 3 after plating, half of the volume of media per well was removed and replaced with fresh media. Cells were treated again with 10 ng/mL M-CSF. On Day 6, cells were treated with 2μg/mL LPS and/or 10 ng/mL IFNγ to complete maturation.

Isolation of primary mouse splenocytes

Mice were euthanized via a CO_2 overdose and spleens were removed. Spleens were mashed with a 1 mL syringe plunger and washed through a 70μM strainer over a 50 μL conical tube to collect 35 mL of a single-cell suspension. To isolate splenocytes from the granulocytes and other splenic tissue cells, we remove the latter subsets via density gradient centrifuge by overlaying the 35 mL of single-cell suspension on top of 15 mL of 100% Ficoll. After centrifugation, with a reduced-speed starting and ending, the enriched layer of splenocytes was visible. The layer was removed and washed. Cells were quantified prior to experimentation.

Detection of citrullination

Cells were lysed with 0.2% SDS and further disrupted with sonication. Protein lysates were then incubated with phenylglyoxal-biotin (PG-biotin) (0.1mM) in a buffer containing 50mM HEPES and 20% trichloroacetic acid at 37°C for 30-minutes as previously described[181]. Biotin-PG-labeled citrullinated proteins were then captured with streptavidin-agarose beads (Thermo Fisher) overnight at 4°C. The captured proteins were subjected to Western blotting.

In vitro citrullination assay

Recombinant human PAD4 (Sigma-Aldrich) were incubated with recombinant human STAT1 (Abcam) in a buffer containing 100mM HEPES, 2mM $CaCl_2$ and water at 37ºC.

Identification of citrullination site by LC-Tandem MS

In-gel digestion

The protein samples were processed and analyzed at the Mass Spectrometry Facility of the Department of Pathology at the University of Michigan. Gel slice corresponding human STAT1 was destained with 30% methanol for 4 h. Upon reduction (10 mM DTT) and alklylation (65 mM 2-Chloroacetamide) of the cysteines, proteins were digested overnight with 500 ng of sequencing grade, modified trypsin (Promega) at 37° C. Peptides were extracted by incubating the gel with 150 µL of 50% acetonitrile/0.1% TFA for 30 min at room temperature. A second extraction with 150 µL of 100% acetonitrile/0.1% TFA was also performed. Both extracts were combined and dried in a vacufuge (Eppendorf).

Mass spectrometry

Resulting peptides were dissolved in 9 µL of 0.1% formic acid/2% acetonitrile solution. Two µLs of the resulting peptide solution were resolved on a nano-capillary reverse phase column (Acclaim PepMap C18, 2 micron, 50 cm, ThermoScientific) using a 0.1% formic acid/acetonitrile gradient at 300 nL/min over a period of 90 minutes (2-25% acetonitrile in 35 min; 25-50% acetonitrile in 20 min followed by a 90% acetonitrile wash for 5 min and a further 30 min re-equilibration with 2% acetonitrile). Eluent was directly introduced into *Q Exactive HF* mass spectrometer (Thermo Scientific, San Jose CA) using an EasySpray source. MS1 scans were acquired at 60K resolution (AGC target=$3x10^6$; max IT=50 ms). Data-dependent collision induced dissociation MS/MS spectra were acquired on 20 most abundant ions following each MS1 scan (NCE ~28%; AGC target $1x10^5$; max IT 45 ms).

Database Search

Proteins were identified by searching the data against the UniProt human protein database (20315 entries; downloaded on 01/05/2023) using Proteome Discoverer (v2.4, Thermo Scientific). Search parameters included MS1 mass tolerance of 10 ppm and fragment tolerance of 0.05 Da; two missed cleavages were allowed; carbamidomethylation of cysteine (+57.012 Da) was considered fixed modification and oxidation of methionine (+15.994 Da), deamidation of arginine, asparagine and glutamine (+0.984 Da), were considered as potential modifications. False discovery rate (FDR) was determined using Percolator and proteins/peptides with an FDR of ≤1% were retained for further analysis.

Flow cytometry analysis

Single-cell suspensions were prepared from fresh mouse peritoneal lavage, lungs, spleen, lymph nodes, and tumor tissues. For surface staining alone, single cell suspensions were washed with PBS, pelleted via centrifugation and then resuspended in 50 μL of MACS buffer. Fluorescent antibodies were added and a 20-minute incubation followed at room temperature protected from light. For intracellular cytokine staining, lymphocytes were incubated in culture medium containing phorbol 12-myristate-13-acetate (5ng ml^{-1}; Sigma-Aldrich), ionomycin (500 ng ml^{-1}; Sigma-Aldrich), brefeldin A (1:1000; BD Biosciences) and monensin (1:1000; BD Biosciences) at 37°C for 4 h. Antibodies (0.6 μg) were added for 20-minute for surface staining. The cells were then washed and resuspended in 1 mL freshly prepared Fix/Perm solution (BD Biosciences) at 4°C overnight. After being washed with Perm/Wash buffer (BD Biosciences), the cells were staining with 0.6 μg antibodies against intracellular proteins from 30-minute, washed and fixed in 4% formaldehyde (Sigma-Aldrich). All samples were read on an LSR II cytometer and analyzed with FACS DIVA software v. 8.0 (BD Biosciences).

Immunoblotting

Protein was extracted from the cells with RIPA buffer supplemented with 100X protease inhibitor (Thermo) and resolved on SDS-PAGE gels, then transferred to nitrocellulose or PVDF membranes. The primary antibodies against mouse PADI4 (1:1000, Abcam, ab214810), STAT1 (1:1000, CST, 9172), PIAS1 (1:1000, CST, 3350), β-actin (1:1000, CST, 3700), MHC-II (1:1000, Abcam, ab55152 or ab180779), CIITA (1:500, Abcam, ab70060), HLA-DR (1:1000, Abcam, ab118347) and Mono-methyl arginine (1:5, Abcam, ab414) were used. Peroxidase-conjugated secondary

antibody (Vector Laboratories) was used and the antigen-antibody reaction was visualized using an enhanced chemiluminescence assay (ECL, BioRad).

Co-immunoprecipitation (Co-IP)

The cells were prepared in IP lysis buffer with 100X protease inhibitor (Thermo Fisher Scientific) and further disrupted by repeated passage through a 21-gauge needle and sonication. Lysates were then centrifuged for 15 minutes at 12,000rpm and 4°C. Next, for preclearance, the supernatants were incubated with Protein A/G plus-agarose (SCBT) and with the IgG isotype control antibody for 30 minutes in rotation at 4°C. Samples were then incubated with indicated antibodies (2µg/sample) overnight at 4°C followed by a 4-hour incubation with Protein A/G plus-agarose at 4°C.

Chromatin immunoprecipitation (ChIP) quantitative PCR analysis

ChIP assay was performed according to the SimpleChIP® Enzymatic Chromatin IP Kit (CST, 9003). In brief, cells were fixed with formaldehyde and lysed, and chromatin was fragmented by partial digestion with Micrococcal Nuclease to obtain chromatin fragments of 1 to 5 nucleosomes. ChIP was performed using antibodies against STAT1 (CST, 9172) and IgG control (CST, 2729), and ChIP-Grade Protein G Magnetic Beads. After reversal of protein–DNA cross-links, the DNA was purified using DNA purification spin columns, ChIP–enriched chromatin was used for real-time PCR. Relative expression levels were normalized to input. Immunoprecipitation of STAT1 on the *Ciita* (mouse) or *CIITA* (human) gene was quantified using the following primers: mouse *promoter I* (forward: CTGCACCGGAATGAGGAAAC; reverse: AGCCTTGCAGCATCCAAAAC); mouse *peak A* (forward:

GGTGGTGACATCGCTGTATGAC; reverse: TCTCCTCCACACAGGCTTGAG); mouse *exon 2* (forward: AGAGGGCAGCTACCTGGAACTC; reverse: GCCAGGTCCATCTGGTCATAG); human *promoter IV* (forward: TCACGGTTGGACTGAGTTGG; reverse: CCTGAGTTGCAGGGAGCTTG). STAT1 DNA binding was quantified using the Fold enrichment method (also known as signal over background). ChIP signals are divided by the non-antibody signals, representing the ChIP signal as the fold increase in signal relative to the background signal. The cycle threshold (CT) value detected from the mock IgG sample is subtracted from the CT value detected from the antibody sample to compute the ΔΔCT value. Fold enrichment is calculated by computing the $2^{-(\Delta\Delta CT)}$ value from the antibody samples.

Generation of mutant plasmids

STAT1 mutant plasmids were generated to form a single nucleotide mutation converting R121 into K121 in the STAT1 protein. The Site–Directed Mutagenesis® Kit (200523) was used to generate the PCR product containing the STAT1-R121K mutant sequence. The mutant PCR product was then transformed using XL-1 Blue super compentant cells and then selected for kanamycin resistance on agar. Plasmids were then purified using the QIAprep® Spin Miniprep Kit (QIAGEN). The mutant plasmids used for the overexpression of human mutant STAT1 (forward: CGCCCAGAAATTTAATCAGGCTCAGTCGGGGAA; reverse: TTAAATTTCTGGGCGTTTTCCAGAATTTTCCT) were generated.

Transfection of HEK-293T cells

Transfection of HEK-293T cells with the mutant STAT1R121K plasmid was performed using the Lipofectamine 2000 (ThermoFisher) kit. HEK 293T cells were seeded at $1x10^6$ cells per well in a

6-well plate. After 24 hours, the Lipofectamine® reagent and the mutant STAT1R121K plasmid were diluted separately in Opti-MEM® Medium. The diluted Lipofectamine® reagent and the diluted mutant STAT1 plasmid were then applied to the cultured cells to be transfected. Cells were analyzed 1-3 days later. All transfections were conducted at a ratio of 1μg plasmid: 2μL transfection reagent.

Bioinformatic analysis

Bulk and single-cell RNA-seq counts were obtained from the Gene Expression Omnibus database with the accession numbers GSE117970, GSE212643, GSE193814, GSE157673, GSE146771, GSE147580, GSE121521, GSE165905, and GSE169246. In our analysis of bulk RNA sequencing data, raw counts were processed and normalized using Limma-Voom tools. Quality control measures were performed and log counts per million were generated prior to assessing gene expression levels between groups. Differential expression analysis was performed using the EdgeR package. Single-cell RNA-seq data was processed and analyzed using the Seurat (v. 4.3.0.1) workflow[160] as previously described[182]. Immune cell subsets were determined based on the annotations of the clusters computed during the Seurat workflow. tSNE plots were generated using the RunTSNE package with Seurat object inputs. Gene set enrichment analysis (GSEA) was performed using the gseGO package. Microarray data were RMA normalized. Prediction of functional relationship between PAD4 expression and transcription factor STAT1 in macrophages was performed by analyzing the $Padi4^{high}$ macrophage gene set with binding analysis for regulation of transcription (BART)[161]. ProteinProspector v.6.4.9[183], was used to determine the theoretical mass-to-charge ratio (m/z) of each amino acid within the noncitrullinated versus the citrullinated ILENAQRNQAQS peptide of interest.

Quantification and statistical analysis

No statistical methods were used to predetermine sample size. Statistical significance was calculated between two separate groups (i.e. wild-type versus knockout or control versus treatment) by an unpaired two-tailed Student's T-test. Statistical significance was calculated between two groups of the same cellular source (i.e. primary patient ovarian cancer TAMs treated with IFNg subjected to treatment with DMSO or GSK484) by a paired two-tailed Student's T-test. The Mann-Whitney *U*-test was applied for comparisons between two separate groups of continuous outcomes. It has been shown that nonparametric tests are suitable for epigenetic data[162,163,164]. One-Way analysis of variance (ANOVA) was applied to determine statistical difference between multiple (3 or more) experimental groups. Cell-based experiments were performed with at least 3 biological and 3 technical replicates unless otherwise stated. All FACS analysis was performed on at least 3 biological replicates. Statistical analysis for animal or cell–based experiments was performed using GraphPad Prism9. Statistical analysis within the bioinformatic data was performed using RStudio.

Results

PAD4 citrullinates STAT1 in the N-terminal domain

We next tested if PAD4 mediated the citrullination of STAT1. We labeled citrullinated proteins using a biotin–conjugated phenylglyoxal (PG)–based chemical probe which specifically modifies

peptidylcitrulline under acidic conditions enabling the visualization of citrullinated proteins following the capture with streptavidin slurry and immunoblotting[102]. Initially, we observed that the citrullination of STAT1 could be induced by lipopolysaccharide (LPS) and IFNγ in both mouse and human cells (**Figure 3.1A**). We then sought to determine whether PAD4 specifically citrullinated STAT1. We enriched peritoneal macrophages from wild-type and *Padi4*$^{-/-}$ mice and performed co-immunoprecipitation (co-IP) experiments to demonstrate whether PAD4 physically interacted with STAT1. Results showed that in macrophages enriched from *Padi4*$^{+/+}$ mice, PAD4 physically interacts with STAT1 (**Figure 3.1B**). Next, we sought to demonstrate that PAD4 specifically citrullinates STAT1. We enriched macrophages from *Padi4*$^{-/-}$ and *Padi4*$^{+/+}$ mice, lysed cells, labeled citrullinated proteins, pulled them down and probed for STAT1 via Western blot. While we had already demonstrated that STAT1 could be citrullinated in response to LPS and IFNγ, this revealed that STAT1 citrullination was mediated specifically by PAD4 in macrophages, since the loss of PAD4 in *Padi4*$^{-/-}$ mice results in the loss of STAT1 citrullination (**Figure 3.1C**). Previously, we showed that LPS and IFNγ induced citrullination on STAT1 however, in the absence of PAD4 in the *Padi4*$^{-/-}$ cells, LPS and IFNγ failed to induce STAT1 citrullination (**Figure 3.1D**). In HL60 cells, we observed that the specific pharmacological inhibition of PAD4 resulted in the reduction of STAT1 citrullination, indicating that PAD4 citrullination of STAT1 occurs in human tissue as well as in mouse (**Figure 3.1E**). To further validate that STAT1 is a substrate of PAD4 citrullination, we performed an *in vitro* citrullination assay in which we incubated recombinant human PAD4 and STAT1 proteins in the presence of calcium ions. In the presence of PAD4, STAT1 citrullination accumulates over time (**Figure 3.1F**).

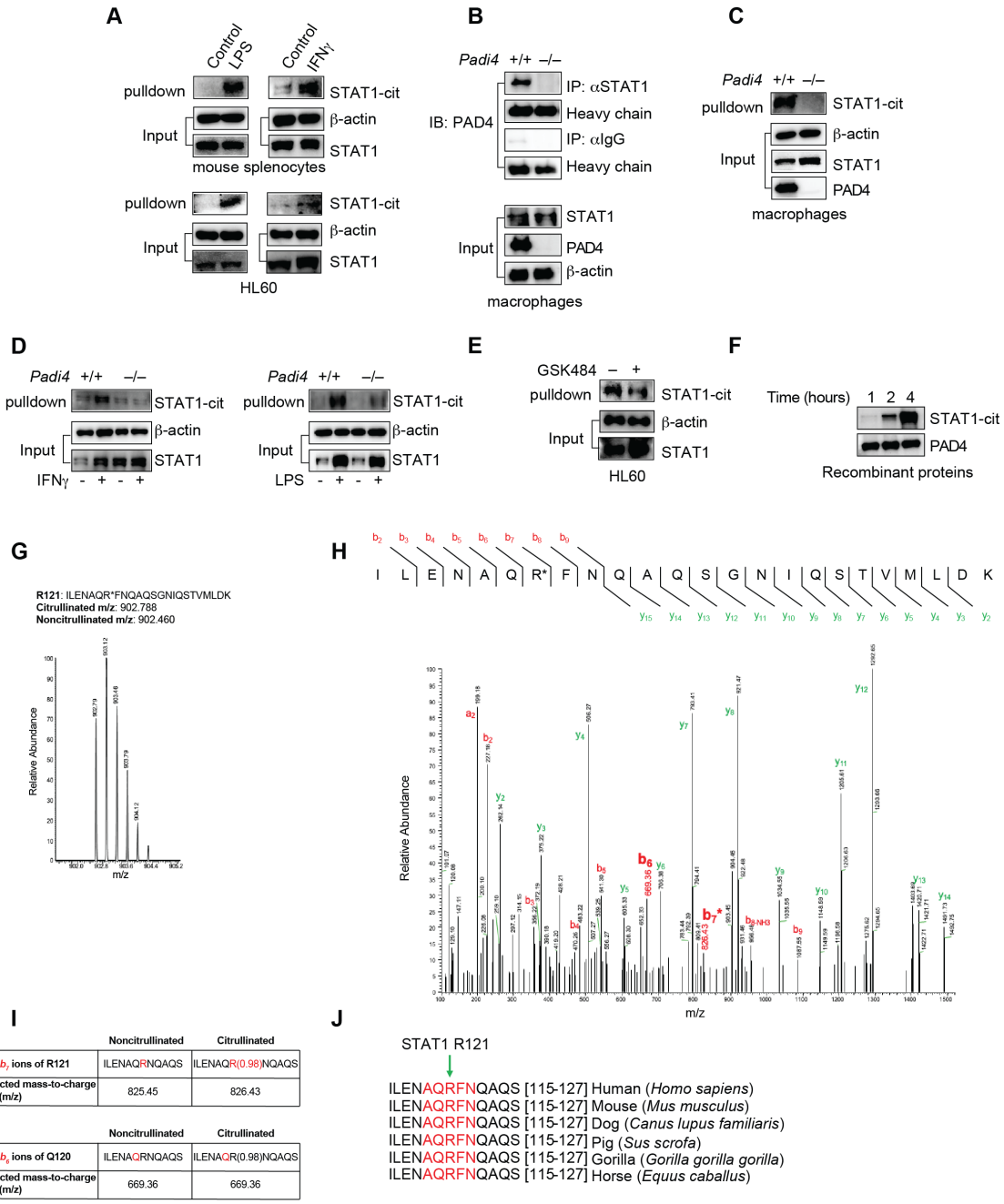

	Noncitrullinated	Citrullinated
b_7 ions of R121	ILENAQRNQAQS	ILENAQR(0.98)NQAQS
Predicted mass-to-charge ratio (m/z)	825.45	826.43

	Noncitrullinated	Citrullinated
b_6 ions of Q120	ILENAQRNQAQS	ILENAQR(0.98)NQAQS
Predicted mass-to-charge ratio (m/z)	669.36	669.36

Figure 3.1.0: PAD4 citrullinates STAT1 in the N-terminal domain. (A) Treatment of wild-type mouse splenocytes with 1 μg/mL LPS (top left) or 10 ng/mL IFNγ (top right) for 30 minutes. Treatment of HL60 cells with 1 μg/mL LPS (bottom left) or 10 ng/mL IFNγ (bottom right) for 30 minutes. (B) Tim-4$^+$ peritoneal macrophages from *Padi4*$^{+/+}$ and *Padi4*$^{-/-}$ mice were stimulated with 10ng/mL IFNγ ex vivo for 1hr. Whole-cell lysates from *Padi4*$^{+/+}$ versus *Padi4*$^{-/-}$ Tim-4$^+$ macrophages were subjected to immunoprecipitation with anti-STAT1 or control IgG. The immunoprecipitant was probed with anti-PAD4. (C) *Padi4*$^{+/+}$ and *Padi4*$^{-/-}$ primary mouse Tim-4$^+$–enriched peritoneal macrophages were stimulated with 10ng/mL IFNγ ex vivo for 1hr. STAT1 citrullination was detected via streptavidin pulldown of citrulline–labeled proteins and probed with anti-STAT1. (D) 10ng/mL IFNγ or 1 μg/mL LPS stimulation of *Padi4*$^{+/+}$ and *Padi4*$^{-/-}$ splenocytes for 1hr followed by the detection of citrullinated STAT1. (E) Treatment of HL60 cells with 10 ng/mL IFNγ and 10 μM GSK484 or DMSO followed by the detection of citrullinated STAT1. (F) The *in vitro* citrullination assay performed with recombinant human PAD4 (0.5μg) and recombinant human STAT1 (0.5μg) proteins supplemented with 2 mM $CaCl_2$ and HEPES. (G) High-resolution precursor ion (MS1) isotopic envelopes of the R121 peptide of citrullinated STAT1. (H) MS2 fragmentation spectra originating from the same precursor ion. Observed *b*- and *y*- ions are indicated.

Presence of unmodified b_6 and modified b_7 ions suggest that R121 is citrullinated. The resulting m/z of 826.43 due to the modified b_7 ions is indicated in red. (I) ProteinProspector results revealing the predicted mass-to-charge ratio at the noncitrullinated versus the citrullinated R121 in the ILENAQRNQAQS peptide (top). ProteinProspector results validating unmodified b_6 ions in the noncitrullinated vs the citrullinated ILENAQRNQAQS peptide (bottom). (J) The ILENAQRNQAQS residue containing R121 is evolutionarily conserved across species.

Next, we sought to determine the exact site on STAT1 which is modified sufficient to regulate STAT1 transcriptional activity. We next examined the potential citrullination sites on STAT1. STAT1 includes the N-terminal Domain (N-domain), the "Coiled-Coil" domain, the DNA Binding Domain, the Linker Domain, the SH2 Domain, and the C-terminal Transactivation Domain (TAD)[184]. The N-domain is indispensable in the process of STAT1 transcriptional activity[185,186,187,188]. PTMs on the N-domain regulate STAT1 transcriptional activity[189,190]. Given these insights, we asked whether the citrullination of STAT1 occurred at the N-domain which is located within the first 136 amino acids of STAT1[184]. To test this possibility, we incubated recombinant human STAT1 with recombinant human PAD4 protein and then performed mass spectrometry (MS). We found that arginine 121 (R121) was the only residue citrullinated in the N-domain (**Figure 3.1G-H**). Firstly, the citrullinated form of the peptide ILENAQRNQAQS, containing R121, was identified (**Figure 3.1G-H**). Interrogation of the high-resolution MS1 spectra confirmed the presence of the 0.98-dalton (Da) heavier citrullinated species for this peptide (**Figure 3.1G**). The lack of the corresponding monoisotopic peak for the non-citrullinated peptide within the isotopic envelope (indicated by the m/z of the far-left peak) indicated that citrullination occurred within this peptide (**Figure 3.1G**). Generation of the high-resolution MS2 fragmentation spectra localized the site of citrullination to R121. Observation of unmodified ions up to y_{14} demonstrated that the Asn and Gln were not *deamidated*, a non-enzymatic modification which can also produce a 0.98-Da shift (**Figure 3.1H**). The presence of the unmodified b_6 and the modified b_7 ions further validated the citrullinated site, R121 (**Figure 3.1H-I**). In addition, we used the

Protein Prospector software[183] to predict the m/z values at the b_6 and b_7 ions corresponding to Q120 and R121, respectively, of the ILENAQRNQAQS peptide. The results generated by the software matched our experimental results. Experimentally, through MS, the modified b_7 ions (which correspond to R121) held an m/z of 826.43 because of citrullination (**Figure 3.1H**). When comparing the m/z of R121 in the ILENAQRNQAQS peptide with and without citrullination using Protein Prospector, the results showed that citrullination induced a shift in m/z from 825.45 to 826.43 which precisely matched our experimental results (**Figure 3.1H-I**). As aforementioned the b_6 ions were not modified, therefore, with or without citrullination, Q120 sustained the same m/z value (**Figure 3.1H-I**). This peptide residue sequence containing R121 – "AQRFN" – is evolutionarily conserved across species (**Figure 3.1J**). Together, PAD4 directly citrullinates STAT1 at R121 in the N-domain.

STAT1 citrullination facilitates the STAT1-PIAS1 interaction and MHC-II reduction

We next sought to determine the consequences of STAT1 citrullination on STAT1 transcriptional activity; and how this controls the genetic regulation of MHC-II transcriptional expression. We observed previously that the loss of PAD4 enhanced STAT1 signaling and – as a consequence – enhanced MHC-II expression and function (**Figure 2.3**). Hence, we hypothesized that STAT1 citrullination resulted in the inhibition of STAT1 transcriptional activity. PIAS1 (protein inhibitor of activated STAT1) physically interacts with STAT1 and, consequently, antagonizes STAT1 DNA binding in the nucleus, thereby resulting in the inhibition of STAT1 transcriptional activity[191,192,193]. Among the PAD family members, PAD4 is the only isozyme to contain the canonical nuclear localization signal (NLS). Thus, we examined the relationship between PAD4 and the STAT1-PIAS1 interaction. To achieve this, we generated bone marrow–derived *Padi4*$^{+/+}$ and *Padi4*$^{-/-}$

macrophages and performed a co-immunoprecipitation (co-IP) experiment with anti-PIAS1 and probed with anti-STAT1. We detected a potent physical interaction between PIAS1 and STAT1 in *Padi4*$^{+/+}$ macrophages (**Figure 3.2A**). Interestingly, the loss of PAD4 largely reduced STAT1 citrullination and abolished the interaction between STAT1 and PIAS1 (**Figure 3.2A**). We obtained similar results in freshly isolated peritoneal macrophages from *Padi4*$^{+/+}$ and *Padi4*$^{-/-}$ mice (**Figure 3.2B**). The same phenomenon occurred in the human cells. We treated HL-60 cells with LPS or IFNγ, with or without GSK484, a PAD4–specific inhibitor. We detected a potent interaction between STAT1 and PIAS1 in the control conditions, however, treatment with GSK484 reduced this interaction in response to LPS or IFNγ (**Figure 3.2C-D**). Thus, PAD4 is required for the interaction between STAT1-PIAS1.

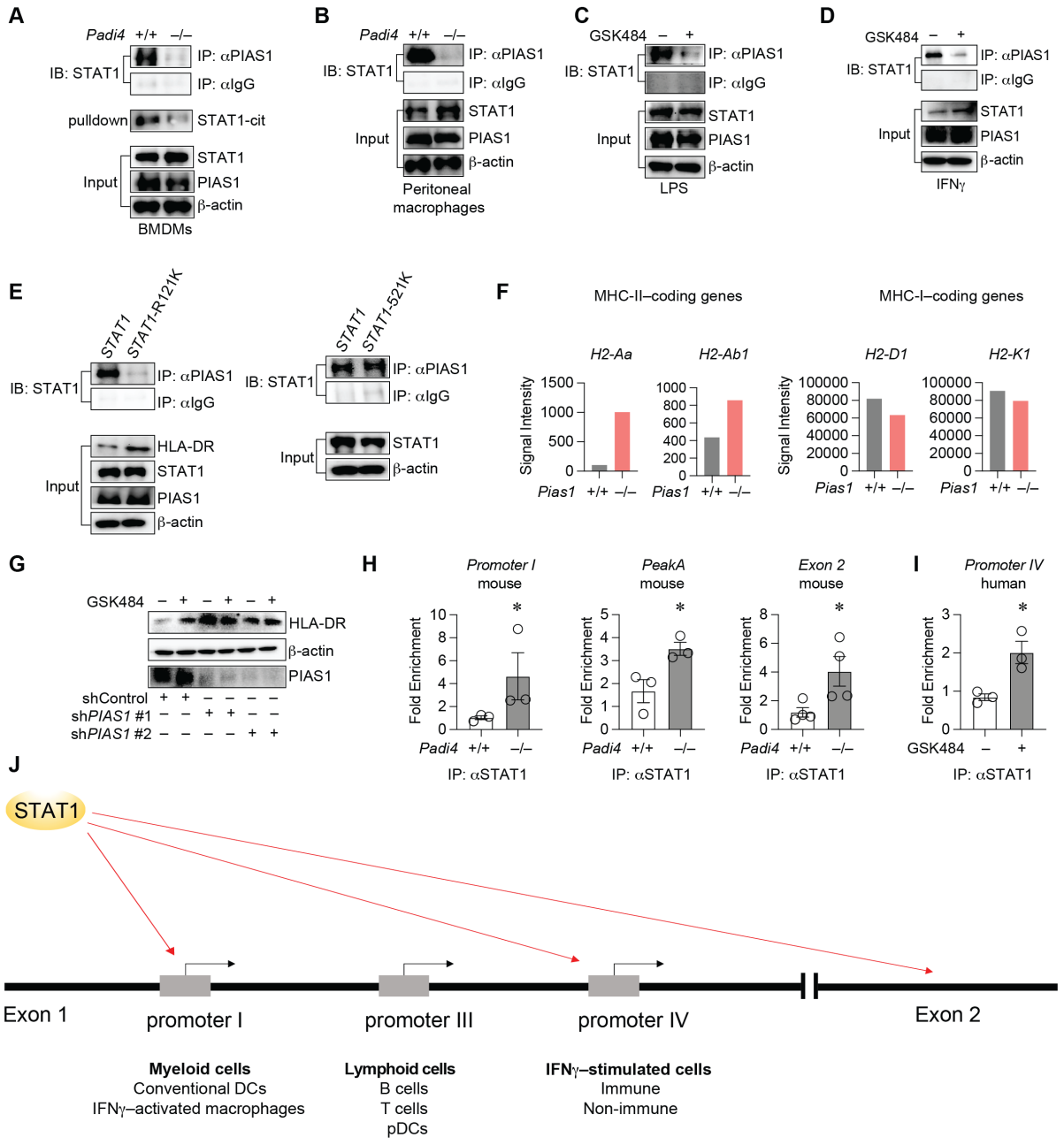

Figure 3.2.0: STAT1 citrullination facilitates the STAT1-PIAS1 interaction and MHC-II reduction. (A) *Padi4*$^{+/+}$ and *Padi4*$^{-/-}$ bone marrow-derived macrophages were generated, and proteins were lysed and processed to detect STAT1 citrullination and for the co-immunoprecipitation with anti-PIAS1. (B) Peritoneal macrophages were harvested from *Padi4*$^{+/+}$ and *Padi4*$^{-/-}$ mice and stimulated with 10 ng/mL IFNγ for 1 hour. Proteins were lysed and processed for the co-immunoprecipitation with anti-PIAS1. (C) HL60 cells were treated with 1 μg/mL LPS for 1hr with or without GSK484 and proteins were lysed and processed for the co-immunoprecipitation with anti-PIAS1. (D) HL60 cells were treated with 10 ng/mL IFNγ for 1hr with or without GSK484 and proteins were lysed and processed for the co-immunoprecipitation with anti-PIAS1. (E) Mutant STAT1 HEK 293T cell lines in which the R121 was converted into K121 (left) and the R521 was converted into K521 (right) were generated. Cells were treated with 10 ng/mL IFNγ for 1hr and proteins were lysed and processed to detect HLA-DR levels (left) and for the co-immunoprecipitation with anti-PIAS1. (F) Microarray data (GSE1552) featuring bone marrow–derived macrophages (BMDMs) from *Pias1*$^{+/+}$ or *Pias1*$^{-/-}$ mice. MHC-I– and MHC-II–coding gene expression were assessed. (G) Wild-type or PIAS1–knockdown (shPIAS1) 293T cells were treated with IFNγ with or without GSK484 for 24 hours. (H) Chromatin immunoprecipitation was performed on DNA extracted from IFNγ–treated *Padi4*$^{+/+}$ and *Padi4*$^{-/-}$ mouse splenocytes. qPCR primers for the detection of STAT1

at multiple IFNγ–responsive genomic regions in the *CIITA* gene were designed. (I) Chromatin immunoprecipitation was performed on DNA extracted from IFNγ–treated human myeloid HL60 cells treated also with DMSO or 10 μM GSK484. qPCR primers for the detection of STAT1 at promoter IV in the *CIITA* gene were designed (n = 3). (J) Graphical schematic showing the STAT1-binding promoter regions in the *Ciita*/*CIITA* gene. Data are shown as mean ± S.E.M. n = 3-4. One-tailed Mann-Whitney U-test. *p <0.05.

Previously, via mass spectrometry, we observed that STAT1 was citrullinated at R121 on the N-terminus (**Figure 3.1G-I**). Therefore, we assessed whether the citrullination of STAT1 at R121 was essential for the STAT1-PIAS1 interaction. We used CRISPR-Cas9 to generate *STAT1*$^{-/-}$ HEK 293T cells. We ectopically expressed in *STAT1*$^{-/-}$ HEK 293T cells a wild-type *STAT1* plasmid or a mutated *STAT1* plasmid whereby R121 was converted to a lysine (K121). We found that the STAT1 R121K mutants failed to interact with PIAS1, indicating that the citrullination of R121 is essential for the interaction between STAT1 and PIAS1 (**Figure 3.2E**). Moreover, we detected an increase in HLA-DR expression in cells expressing R121K mutants as compared to cells expressing wild-type STAT1 demonstrating that the citrullination of R121 controls the STAT1–PIAS1 interaction and consequently regulates HLA-DR expression (**Figure 3.2E**). Via MS, we detected that beyond the N-terminus, R521 of STAT1 were citrullinated; however, mutation of this site did not disrupt the STAT1-PIAS1 interaction indicating that citrullination of R121 is essential for the STAT1-PIAS1 interaction (**Figure 3.2E**). Thus, loss of the STAT1-PIAS1 interaction results in enhanced HLA-DR expression. To corroborate the observation that the STAT1-PIAS1 interaction controls HLA-DR (or MHC-II) transcription, we analyzed a publicly available microarray dataset featuring wild-type (*Pias1*$^{+/+}$) versus *Pias1* knockout (*Pias1*$^{-/-}$) bone marrow–derived macrophages (BMDMs) from mice[194]. We observed higher levels of MHC-II–coding gene (*H2-Aa* and *H2-Ab1*) expression in *Pias1*$^{-/-}$ macrophages compared to *Pias1*$^{+/+}$ macrophages and no difference in the express levels of the MHC-I–coding genes (**Figure 3.2F**). These data provide additional evidence that the STAT1-PIAS1 interaction controls MHC-II

expression in macrophages. To confirm that the modulation of MHC-II via PAD4 citrullination occurs in PIAS1–dependent manner, we showed that HLA-DR cannot be modulated by the inhibition of PAD4 when we knock down *PIAS1* in HEK 293T cells (**Figure 3.2G**). This demonstrates that the citrullination of STAT1 by PAD4 regulates HLA-DR levels but only in a PIAS1–dependent manner.

The physical interaction between STAT1 and PIAS1 regulates STAT1 binding to DNA to mediate the downstream transcriptional regulation[180,194]. Since we aim to elucidate how PAD4 regulates MHC-II in a STAT1 transcription–dependent manner, we performed a chromatin immunoprecipitation (ChIP) to measure the levels of STAT1 binding to the major promoter regions in the *CIITA* gene in response to IFNγ stimulation. The results showed that the loss of PAD4 enhanced STAT1 binding to key promoter regions including *promoter I* and *Exon 2* in mice (**Figure 3.2H, J**). So-called "*Peak A*" or -47kb *Ciita* is a novel enhancer region described by Buxadé *et al.*[195], which exhibits chromosomal looping to physically interact with *promotor I*, supporting the transcription of *Ciita* in response to IFNγ signaling in macrophages (**Figure 3.2K**). Similarly, as with *promoter I* and *Exon 2* of *Ciita*, we observed that the loss of PAD4 significantly enhanced STAT1 binding to *Peak A* in the presence of IFNγ signaling (**Figure 3.2H**). *Promoter IV* of *CIITA* has also been described as a key promoter region for STAT1 binding to the *CIITA* gene in macrophages in response to IFNγ in humans (**Figure 3.2J**). We showed that the specific pharmacological inhibition of PAD4 via GSK484 in IFNγ–treated HL60 cells resulted in enhanced STAT1 binding to *promoter IV* (**Figure 3.2I**). Together we show that the citrullination of STAT1 facilitates the inhibitory physical interaction between STAT1 and PIAS1 which restrains STAT1 binding to *CIITA* – and consequently – restrains MHC-II transcriptional activation.

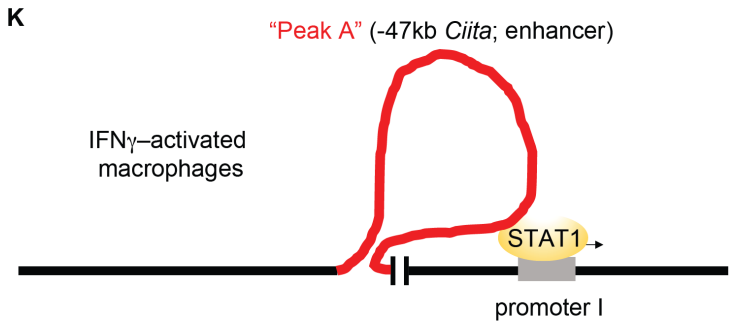

Figure 3.2.1: STAT1 citrullination facilitates the STAT1-PIAS1 interaction and MHC-II reduction. (K) Graphical schematic showing the intrachromosomal looping physical interaction between the *Ciita* enhancer so-called Peak A and promoter I of *Ciita* in complex with STAT1 bound to the promoter.

The citrullination of STAT1 inhibits arginine methylation on STAT1 regulating the STAT1-PIAS1 interaction

We showed that the regulation of STAT1 DNA binding is mediated by the PAD4 citrullination control of the STAT1-PIAS1 interaction. While we demonstrated that the regulation of the STAT1-PIAS1 interaction is PAD4 citrullination–dependent, there are other aspects of the mechanism enabling PAD4 to control this physical interaction. It has been shown that the inhibition of arginine methylation on STAT1 affects the STAT1-PIAS1 interaction and, consequently, STAT1 DNA binding to IFNγ–responsive promoters in the genome[189]. Moreover, multiple reports have established that citrullination inhibits or restrains arginine methylation[113,116]. Together, we demonstrated that the citrullination of STAT1 restrains or inhibits the arginine methylation on STAT1 in mouse and human cells. Firstly, we recapitulate what has been shown already in the literature, that arginine methylation occurs on STAT1 in response to IFNγ or LPS (**Figure 3.3A**). In primary macrophages enriched from mice, we showed that IFNγ stimulation induces the mono-methylation of STAT1 (**Figure 3.3B**). Further, we show that the IFNγ–induced STAT1 methylation can be enhanced when we specifically inhibit PAD4 pharmacologically with GSK484, suggesting

that the PAD4–mediated citrullination of STAT1 restrains arginine methylation on STAT1 (**Figure 3.3C**). Further, upon genetic deletion of PAD4, the loss of PAD4 in primary mouse macrophages, results in the enhancement of STAT1 arginine methylation indicating that the PAD4 citrullination of STAT1 restrains arginine methylation on STAT1 during IFNγ and LPS treatment conditions (**Figure 3.3D-E**). While we demonstrate that STAT1 citrullination restrains arginine methylation on STAT1, when we performed mass spectrometry, we did not observe that PAD4 citrullinated STAT1 at the same arginine residue which was methylated. While it was reported that STAT1 arginine methylation occurred at arginine 31[189,190], we did not detect citrullination at R31 in our mass spectrometry experiments and, therefore, cannot conclude or indicate directly that citrullination inhibits arginine methylation at R31, an event which was reported to regulate the STAT1-PIAS1 interaction[189]. Nevertheless, the specific inhibition of PAD4 via GSK484 synergizes with IFNγ to completely abolish the STAT1-PIAS1 interaction driving enhanced mono-methylation of the arginine on STAT1 (**Figure 3.3F**). Future further studies may elucidate the biochemical (and biophysical) mechanism by which citrullination controls arginine methylation on STAT1, however currently, the biophysical means by which citrullination on STAT1 controls arginine methylation remains elusive. Mass spectrometry results revealed that the citrullination of R121 controls the STAT1-PIAS1 interaction, and not the citrullination of R31. Perhaps, in the 3-dimensional space, the citrullination of R121 physically affects the methylation of R31. Nevertheless, it remains reasonable that the citrullination of STAT1 and the inhibition of arginine methylation on STAT1 by PAD4–mediated citrullination control the STAT1-PIAS1 interaction and, therefore, the transcriptional activity of STAT1. Together, the citrullination of STAT1 inhibits arginine methylation on STAT1 which contributes to the control of the STAT1-PIAS1 interaction.

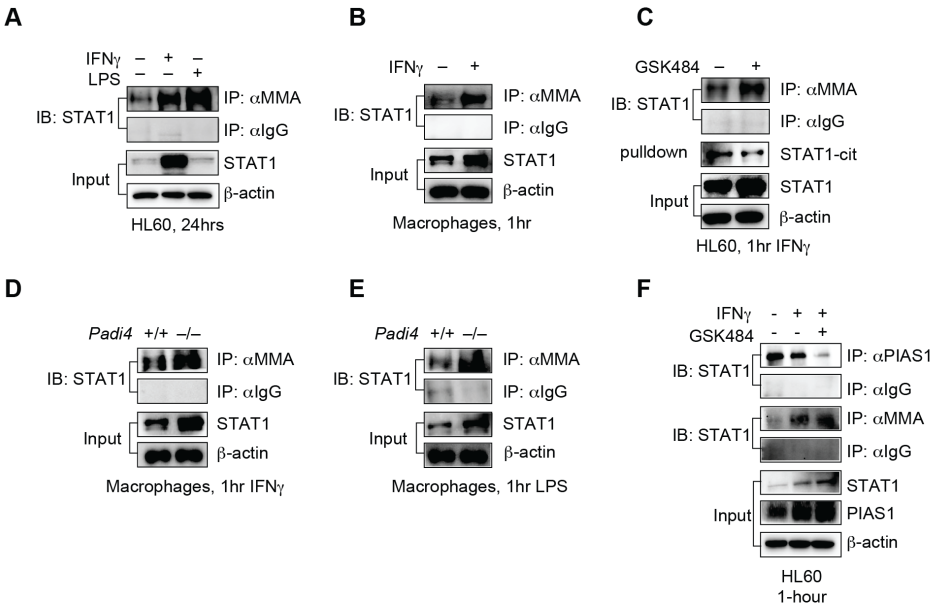

Figure 3.3.0: The citrullination of STAT1 inhibits its arginine methylation regulating the STAT1–PIAS1 interaction. (A) HL60 cells were treated with 10 ng/mL IFNγ or 1 μg/mL LPS for 24hrs and proteins were lysed and processed for the co-immunoprecipitation with anti-mono-methylarginine (MMA). (B) Primary Tim-4^{+} peritoneal macrophages from wild-type mice were stimulated with 10 ng/mL IFNγ ex vivo for 1hr. Whole-cell lysates from were subjected to immunoprecipitation with anti-MMA. (C) HL60 cells were treated with 10 ng/mL IFNγ for 1hr with or without GSK484 and proteins were lysed and processed to detect STAT1 citrullination and for the co-immunoprecipitation with anti-MMA. (D and E) Peritoneal macrophages were harvested from *Padi4*$^{+/+}$ and *Padi4*$^{-/-}$ mice and stimulated with (D) 10 ng/mL IFNγ and (E) 1 μg/mL LPS for 1 hour. Proteins were lysed and processed for the co-immunoprecipitation with anti-MMA. (F) HL60 cells were treated with DMSO or with 10 ng/mL IFNγ for 1hr with or without GSK484 and proteins were lysed and processed for the co-immunoprecipitation wit anti-PIAS1 and anti-MMA.

Discussion

Here, we reveal the mechanism which underlies how PAD4 citrullination controls MHC-II expression and therefore function. In Chapter 2, we demonstrated that PAD4 is among the most highly expressed PTM enzymes in TAMs and that PAD4 negatively regulates MHC-II–mediated antigen presentation. Following these initial observations, we sought to determine the mechanism. As discussed above, previous reports confirm that PTMs occur on STAT1[189,190], that PADs can citrullinate transcription factors[49,139] and that STAT1 binding to *CIITA* promoters is required for

MHC-II expression and function[179]. In our investigations into whether PAD4 can citrullinate STAT1 affecting its transcriptional activity, we observed that the citrullination of STAT1 by PAD4 enforces the physical interaction between STAT1 and PIAS1 and, thus, serves to restrain STAT1 binding to DNA. Further, we demonstrate that the citrullination of STAT1 at R121 was required for the maintenance of the STAT1–PIAS1 interaction. Altogether, with these insights, the role of PAD4 in maintaining low MHC-II expression on TAMs is elucidated. With this knowledge, we then seek to investigate PAD4 activity in human biology and whether PAD4 can be targeted therapeutically to enhance anti-tumor immunity and improve current ICB treatment.

Chapter 4: PAD4 Negatively Correlates with IFNγ Signaling and Impairs Therapeutic Response to ICB

Abstract

The PAD4 regulation of MHC-II transcription in macrophages controls anti-tumor immunity but whether macrophage PAD4 affects the response to ICB therapy in mice or in humans as not been shown. As discussed throughout this dissertation, our study aims to contribute to the growing work elucidating the optimal means by which macrophages can be targeting in the clinical treatment for cancer. Macrophage heterogeneity and plasticity pose challenges for the development of durable strategies to control macrophages to better support anti-tumor immunity. Through our work, we demonstrated that targeting PTMs – citrullination in particular – may constitute a reasonable approach when leveraging macrophage functions to enhance antitumor immunity. Further, we built upon these observations to show that the genetic deletion or the pharmacological inhibition of PAD4 in macrophages synergized with ICB therapy resulting in the significant reduction of tumor growth. Thus, we demonstrate that blocking PAD4 *in vivo* can enhance the response to ICB. Further, we extended our studies on PAD4 into the human context. We demonstrate that in human macrophages, PAD4 is negatively correlated with IFNγ signaling and HLA-DR expression, suggesting that PAD4 could be exploited as an effective macrophage target in human cancer treatment.

Background: Targeting macrophages as a means to enhance anti-tumor immunity has become understood to be an efficacious strategy. Macrophages compose the majority of the immune cells

in the TME[9] and therefore, they wield a powerful influence over the course of tumor development, growth or regression. Therefore, several different approaches have been taken to reprogram macrophages to better support anti-tumor immunity and – consequently – the clinical treatment of cancer.

Methods and materials: Primary ovarian cancer patient tumor tissue from several donors was processed into a single cell suspension and then submitted to Lymphoprep™ density gradient centrifugation for isolation of mononuclear immune cells. This cellular suspension was then stimulated with IFNγ and then treated with GSK484 or DMSO for 24 hours. Human blood monocytes were enriched from buffy coats, stimulated with IFNγ, treated with GSK484 or DMSO and processed cells for detection of STAT1 citrullination and western blotting. A single-cell RNA sequencing dataset featuring the $CD45^+$ cells from TNBC patients was analyzed to assess PAD4 regulation of IFNγ signaling and response to ICB treatment. *Padi4*$^{fl/fl}$ and *Padi4*$^{fl/fl}$ *LysM*^{cre} mice were inoculated with MC38 or Py8119, with or without 100μg PDL1 antibody. Wild-type mice were inoculated with MC38 or Py8119, with or without 100μg PDL1 antibody or 4mg/kg GSK484.

Results: PAD4 was negatively associated with IFNγ signaling and HLA-DR expression in human TAMs; and was associated with poor response to ICB treatment in TNBC patients. Genetic deletion or pharmacological inhibition of PAD4 synergized with PDL1 blockade to significantly reduce tumor growth in mice.

Background

The high infiltration, functional heterogeneity and plasticity of TAMs poses diverse challenges in the process of cancer treatment[9]. For this reason, several novel treatment strategies involve the targeting of macrophages[39]. A general approach in the targeting of macrophages is to reprogram

macrophage functions such that they exhibit more proinflammatory phenotypes enabling better support to anti-tumor T-cells[40]. There is a long history of studies investigating the macrophage functions which promote or prevent tumor growth[40]. Yet, only recently have practical macrophage–focused treatments been developed to be used in patients[41,42,43]. As aforementioned, Klichinsky *et al.* developed the first human chimeric antigen receptor macrophages for cancer immunotherapy[11]. Within a short period of time, a second-generation M1-polarized CAR macrophage with antitumor efficacy has been developed[196]. The development of new CAR macrophage technologies and strategies does not only constitute a novel macrophage-focused therapeutic approach but also demands new discoveries regarding molecular mechanisms which control macrophage functions. Previously unknown or understudied mechanisms which govern effector macrophage functions may be incorporated in the engineering of the CAR macrophages. Not only are there several different macrophage functions which could potentially be exploited, but there exists several targets and modalities which have not been exploited. Echoed throughout this dissertation, post-translational modifications (PTMs) inevitably play essential and fundamental roles governing the functioning of immune cells since PTMs construct the final forms of active proteins[156,157]. Previously, we demonstrated that the loss of PAD4 resulted in enhanced MHC-II and antitumor immunity since PAD4 citrullination promoted the inhibitory interaction between STAT1 and PIAS1, restraining the STAT1-mediated limiting of MHC-II function. Whether this mechanism could be exploited to enhance immunotherapy has not been shown. Further, whether PAD4 activity plays a role in the regulation of human macrophages has also not been shown.

Methods and materials

Animal models

Padi4$^{fl/fl}$ mice, *LysM*^{cre} mice, and wild type C57BL/6J mice were purchased from the Jackson Laboratory. *Padi4*$^{fl/fl}$ mice were crossed with *LysM*^{cre} mice to generate both wild-type *Padi4*$^{+/+}$ *LysM*^{cre} mice and *Padi4*$^{fl/fl}$ *LysM*^{cre} mice, which are deficient in their macrophage expression of *Padi4*. Respectively, these mice are referred to as *Padi4*$^{fl/fl}$ and *Padi4*$^{fl/fl}$ *LysM*^{cre}. Mice were bred in the specific-pathogen-free animal facility (~22 °C with ~40% humidity) on a 12 h dark/12 h light cycle at the University of Michigan. All procedures were approved by the Institutional Animal Care and Use Committees (IACUC) and the Unit for Laboratory Animal Medicine (ULAM) at the University of Michigan.

Murine colon carcinoma (MC38) cells (3 x 10^6) were injected subcutaneously into the left flanks of age-matched male *Padi4*$^{fl/fl}$ or *Padi4*$^{fl/fl}$ *LysM*^{cre} mice (8-10 weeks). Py8119 breast adenocarcinoma cells (2 x 10^4) were injected subcutaneously into the left flanks of age-matched, female *Padi4*$^{fl/fl}$ or *Padi4*$^{fl/fl}$ *LysM*^{cre} mice (8-10 weeks). For the GSK484 *in vivo* studies, male or female C57BL/6J mice (8-10 weeks) were inoculated with MC38 or Py8119 respectively. Tumor monitoring began 7 days after inoculation and continued every 3 days until endpoint. Tumor diameters were measured using calipers fitted with a Vernier scale. Tumor volume was calculated as previously described[8,159].

Anti-PD-L1 and IgG1 isotype antibodies were given intraperitoneally at a dose of 100µg per mouse on day 7 after tumor cell inoculation and then every 3 days for the duration of the experiment. Mice received 3 doses total. GSK484 was administered intraperitoneally at a dose of 4mg/kg per mouse as previously described[197] every day for the duration of the experiment.

Human samples

Patient mononuclear cells from primary patient ovarian tumors (Cooperative Human Tissue Network) were isolated from the tumor mass following processing into a single-cell suspension and then submitting to Ficoll density gradient centrifugation. Mononuclear cells were then cultured in RPMI-1640 medium supplemented with 10% fetal bovine serum. TAMs were then identified via fluorescent staining as $CD45^{+}CD14^{+}$ mononuclear cells and analyzed via FACS. Human monocytes were positively enriched from blood buffy coats (Carter BloodCare) using the EasySep™ Human Monocyte Isolation Kit (STEMCELL Technologies). Monocytes were differentiated into macrophages following overnight stimulation with 1 μg/mL LPS and 10ng/mL IFNγ. All human samples in our studies were collected with informed consent from each individual donor.

Detection of citrullination

Cells were lysed with 0.2% SDS and further disrupted with sonication. Protein lysates were then incubated with phenylglyoxal-biotin (PG-biotin) (0.1mM) in a buffer containing 50mM HEPES and 20% trichloroacetic acid at 37°C for 30-minutes as previously described[198]. Biotin-PG-labeled citrullinated proteins were then captured with streptavidin-agarose beads (Thermo Fisher) overnight at 4°C. The captured proteins were subjected to Western blotting.

Bioinformatic analysis

Single-cell RNA-seq counts were obtained from the Gene Expression Omnibus database with the accession number GSE169246. Single-cell RNA-seq data was processed and analyzed using the

Seurat (v. 4.3.0.1) workflow[160] as previously described.[182] Immune cell subsets were determined based on the annotations of the clusters computed during the Seurat workflow. Comparisons of TAM gene expression between TNBC patient Responders and Nonresponders to ICB therapy were achieved by applying single-cell RNA-seq data integration tools provided by Seurat. tSNE plots were generated using the RunTSNE package with Seurat object inputs. Gene set enrichment analysis (GSEA) was performed using the gseGO package. Generation of the antigen presentation gene set signature (**Figure 4.1F**) was achieved using the UCell package.

Results

PAD4 negatively correlates with IFNγ signaling and impairs therapeutic response to ICB

Finally, we sought to demonstrate the clinical significance of these studies on PAD4 in macrophages. We aimed to assess whether PAD4 regulated IFNγ signaling and HLA-DR expression in human macrophages as we observed in the mouse system and whether the manipulation of PAD4 could affect the response to immunotherapy *in vivo*. First, we sought to assess the effect of PAD4 inhibition in the human tumor microenvironment. We processed primary ovarian cancer patient tumor tissue into a single cell suspension and isolated the immune cells via density gradient centrifugation. We then treated the suspension with IFNγ with or without GSK484. Flow cytometry enabled the observation that the ovarian tumor–associated macrophages ($CD45^+CD14^+HLA\text{-}DR^+$) treated with IFNγ and GSK484 exhibited significantly enhanced HLA-DR expression across multiple donors compared the IFNγ–stimulated macrophages (**Figure 4.1A**). When we enriched macrophages from the blood of human donors, stimulated cells with IFNγ and then treated cells with GSK484 or DMSO control, we observed that GSK484 inhibited the citrullination of STAT1 and enhanced HLA-DR protein expression, recapitulating our observations

in the mouse system (**Figure 4.1B**). We analyzed a single cell RNA-sequencing dataset featuring the $CD45^+$ immune cells from triple negative breast cancer (TNBC) patients treated with PDL1 blockade[199]. First, when we separated patient TAMs according to *PADI4*^{low} versus *PADI4*^{high} TAMs, we observed higher expression of *CIITA* and *HLA-DRA* in the *PADI4*^{low} patient TAMs recapitulating what we demonstrated previously, that the loss of PAD4 enhances MHC-II transcriptional machinery (**Figure 4.1C**). GSEA reveals that the pathways including Response to interferon-γ and Antigen presentation and processing of peptide antigen via MHC-II were negatively enriched in the *PADI4*^{high} patient TAMs (**Figure 4.1D**). To summarize, GSEA reveals that the positively enriched pathways are expectedly those associated with PAD4 enzymatic activity whereas the pathways which are most negatively enriched are those associated with MHC-II–mediated antigen presentation, T-cell activation and interferon-γ signaling (**Figure 4.1E**). In the whole population of patient TAMs, *PADI4* significantly negatively correlates with an HLA-DR–mediated antigen presentation signature in TAMs (**Figure 4.1F**). Given the importance of MHC-II expression in the activation of $CD4^+$ T-cells and given the indispensable contribution of effector $CD4^+$ T-cells in the maintenance of anti-tumor immunity, we then sought to demonstrate the relationship between TAM *PADI4* expression and the $CD4^+$ T-cell expression of effector genes. We show that TAM expression of *PADI4* was significantly negatively correlated with $CD4^+$ T-cell expression of *TBX21* and *IL12RB*, two key effector genes (**Figure 4.1G**). *TBX21* codes for transcription factor Tbet, which is required for T_h1 polarization, critical for the maintenance of systemic anti-tumor immunity[200,201,202]. Thus, we demonstrate that human PAD4 restrains HLA-DR expression and thus limits T-cell activation.

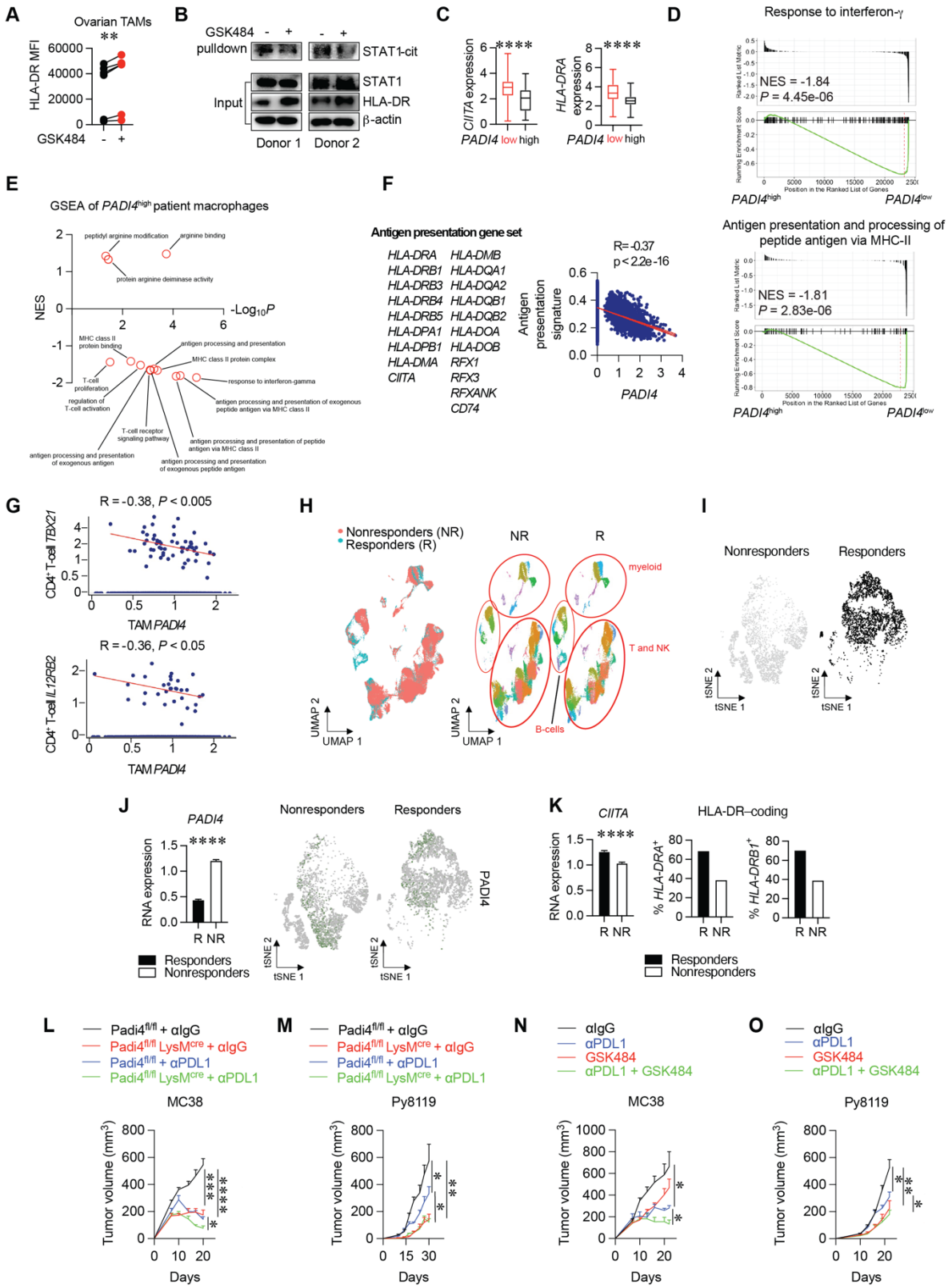
A
Ovarian TAMs
HLA-DR MFI
GSK484
B
GSK484
pulldown
STAT1-cit
Input
STAT1
HLA-DR
β-actin
Donor 1
Donor 2
C
CIITA expression
HLA-DRA expression
PADI4 low high
D
Response to interferon-γ
NES = -1.84
P = 4.45e-06
PADI4high
PADI4low
Antigen presentation and processing of peptide antigen via MHC-II
NES = -1.81
P = 2.83e-06
E
GSEA of PADI4high patient macrophages
NES
-Log10P
peptidyl arginine modification
arginine binding
protein arginine deiminase activity
MHC class II protein binding
antigen processing and presentation
MHC class II protein complex
T-cell proliferation
response to interferon-gamma
regulation of T-cell activation
antigen processing and presentation of exogenous peptide antigen via MHC class II
T-cell receptor signaling pathway
antigen processing and presentation of peptide antigen via MHC class II
antigen processing and presentation of exogenous antigen
antigen processing and presentation of exogenous peptide antigen
F
Antigen presentation gene set
HLA-DRA HLA-DMB
HLA-DRB1 HLA-DQA1
HLA-DRB3 HLA-DQA2
HLA-DRB4 HLA-DQB1
HLA-DRB5 HLA-DQB2
HLA-DPA1 HLA-DOA
HLA-DPB1 HLA-DOB
HLA-DMA RFX1
CIITA RFX3
RFXANK
CD74
R=-0.37
p<2.2e-16
Antigen presentation signature
PADI4
G
R = -0.38, P < 0.005
CD4+ T-cell TBX21
TAM PADI4
R = -0.36, P < 0.05
CD4+ T-cell IL12RB2
TAM PADI4
H
Nonresponders (NR)
Responders (R)
NR
R
myeloid
T and NK
B-cells
UMAP 1
UMAP 2
I
Nonresponders
Responders
tSNE 1
tSNE 2
J
PADI4
RNA expression
R NR
Responders
Nonresponders
Nonresponders
Responders
PADI4
K
CIITA
HLA-DR–coding
RNA expression
% HLA-DRA+
% HLA-DRB1+
R NR
Responders
Nonresponders
L
Padi4fl/fl + αIgG
Padi4fl/fl LysMcre + αIgG
Padi4fl/fl + αPDL1
Padi4fl/fl LysMcre + αPDL1
MC38
Tumor volume (mm3)
Days
M
Padi4fl/fl + αIgG
Padi4fl/fl LysMcre + αIgG
Padi4fl/fl + αPDL1
Padi4fl/fl LysMcre + αPDL1
Py8119
Tumor volume (mm3)
Days
N
αIgG
αPDL1
GSK484
αPDL1 + GSK484
MC38
Tumor volume (mm3)
Days
O
αIgG
αPDL1
GSK484
αPDL1 + GSK484
Py8119
Tumor volume (mm3)
Days

Figure 4.1.0: PAD4 negatively correlates with IFNγ signaling and impairs therapeutic response to ICB. (A) Primary human ovarian cancer mononuclear cells were isolated from patient tumors, treated with 10 ng/mL IFNγ and 10 μM GSK484 or DMSO, and then processed to detect $CD45^+CD14^+$HLA-DR levels via flow cytometry (n = 6). (B) Primary human macrophages were enriched and derived from PBMCs of blood buffy coats and treated with 10 ng/mL IFNγ and 10 μM GSK484 or DMSO. Proteins were lysed and processed to detect STAT1 citrullination and HLA-DR levels (n = 2). (C) *CIITA* and *HLA-DRA* expression in PAD4–deficient ($PADI4^{low}$) versus PAD4–expressing ($PADI4^{high}$) macrophages in patients with TNBC. (D) GSEA was conducted on $PADI4^{high}$ macrophages and the normalized enrichment scores (NESs) were assessed for the Response to interferon-γ and Antigen presentation via MHC-II pathways. (E) A GSEA summary of key pathways significantly regulated in $PADI4^{high}$ patient macrophages. (F) Pearson correlation between an MHC-II/HLA-DR–specific antigen presentation gene set and *PADI4* in macrophages from patients with TNBC. (G) Pearson correlations were conducted between TAM *PADI4* expression and the expression of effector $CD4^+$ T-cell genes including *TBX21* and *IL12RB2* in patients with TNBC. (H) UMAP projections of single-cell RNA-sequencing data featuring total $CD45^+$ cells from TNBC patients receiving anti-PDL1 therapy (GSE169246). Responders and Nonresponders to ICB treatment are indicated. (I) Macrophages were isolated from the total $CD45^+$ population of sequenced single-cells from patients with TNBC treated with anti-PD-L1 mAb (GSE169246). (J) $CD33^+$ TAMs were further filtered from total Responder (R) and Nonresponder (NR) macrophages and *PADI4* expression was assessed between R and NR TNBC patients (n = 5 Responders, n = 6 Nonresponders) (left). tSNE projection of *PADI4* expression in the macrophages from Responder and Nonresponder patients with TNBC (right). (K) Assessment of *CIITA* expression in the $CD33^+$ TAMs of the Responders and the Nonresponders. The proportion of $HLA\text{-}DRA^+$ and $HLA\text{-}DRB1^+$ patient macrophages in Responders versus Nonresponders. (L) MC38 tumor progression in $Padi4^{fl/fl}$ versus $Padi4^{fl/fl}\,LysM^{cre}$ mice treated with or without 100μg anti-PD-L1 mAb treatment (n = 5/group). (M) Py8119 tumor progression in $Padi4^{fl/fl}$ versus $Padi4^{fl/fl}\,LysM^{cre}$ mice treated with or without 100μg anti-PD-L1 mAb treatment (n = 5/group). (N) MC38 tumor progression in wild-type mice treated with or without 4mg/kg GSK484 or 100μg anti-PD-L1 mAb treatment (n = 5/group). (O) Py8119 tumor progression in wild-type mice treated with or without 4mg/kg GSK484 or 100μg anti-PD-L1 mAb treatment (n = 5/group). Data are shown as mean ± S.E.M. (A, C and J-O). Paired two-tailed Student's T-test (A). Unpaired two-tailed Student's T-test (C and J-O). *$p < 0.05$; **$p < 0.01$; ****$p < 0.0001$.

Next, we sought to examine how PAD4 expression in macrophages affects the response to ICB therapy. Clinical information was provided in the TNBC patient dataset indicating the Responders (R) versus the Nonresponders (NR) to PDL1 blockade (**Figure 4.1H**). We then filtered out the macrophages from the whole $CD45^+$ population of Responders and Nonresponders (**Figure 4.1I**). We observed that human *PADI4* was significantly more highly expressed in the Nonresponders compared to the Responders (**Figure 4.1J**). Higher expression of *PADI4* in the Nonresponders to immunotherapy indicates that PAD4 activity in human TAMs may be associated with poor prognosis during cancer. As we expect, HLA-DR machinery expression is enhanced in the Responders versus the Nonresponders. We examined the patient TAMs from Responders versus the Nonresponders and observed that *CIITA* mRNA expression was enhanced in the Responders compared to the Nonresponders; and that the Responders' TAMs contained a higher proportion of HLA-DR–coding gene expression (**Figure 4.1K**). Together, we show that in human

context – and importantly, in the patient context – PAD4 activity is associated with the restraint of IFNγ signaling in human macrophages and associated with the poor response to immunotherapy.

Finally, to further demonstrate that macrophage PAD4 impairs the response to ICB therapy, we asked whether the genetic deletion or pharmacological inhibition of PAD4 could enhance the therapeutic effect of PDL1 blockade treatment *in vivo*. We inoculated male *Padi4*$^{fl/fl}$ versus *Padi4*$^{fl/fl}$ *LysM*^{cre} and female male *Padi4*$^{fl/fl}$ versus *Padi4*$^{fl/fl}$ *LysM*^{cre} mice with MC38 colorectal and Py8119 breast cancer cells, respectively. In both models, the genetic loss of PAD4 synergized with PDL1 blockade resulting in significantly reduced tumor growth (**Figure 4.1L-M**). Next, we inoculated male wild-type mice and female wild-type mice with MC38 and Py8119, respectively. Within each model, mice were either treated with IgG isotype control, PDL1 antibody, GSK484 (PAD4–specific inhibitor) or PDL1 antibody combined with GSK484. Similar to the genetic deletion of PAD4, the specific pharmacological inhibition of PAD4 synergized with PDL1 blockade resulting in mice developing the smallest tumors compared to the other treatment groups (**Figure 4.1N-O**). This demonstrates that blocking PAD4 enhances the response to immunotherapy. Interestingly, the loss of PAD4 via genetic deletion or pharmacological inhibition alone in the Py8119 model resulted in tumor volumes smaller than those of mice treated with PDL1 blockade, suggesting that breast cancer might be particularly sensitive to blocking PAD4 in macrophages. Here, we demonstrate the clinical significance of targeting PAD4 in macrophages and the benefit of inhibiting PAD4 for the improved response to immunotherapy.

Discussion

Here, we show the clinical importance of our PAD4 studies in macrophages through demonstrating that PAD4 negatively regulates STAT1 signaling and, consequently, restrains HLA-DR machinery

expression in patients with cancer. Through the analysis of single-cell RNA-sequencing data featuring the immune cells of TNBC patients, we observed that *PADI4*^{low} patient TAMs exhibited significantly higher expression of HLA-DR–coding genes and pathways associated with critical anti-tumor responses, including response to interferon-γ, antigen presentation and T-cell activation. Further, we demonstrate that PAD4 expression in macrophages is associated with poor response to immunotherapy via (1) the observation in single-cell RNA-sequencing analysis that Nonresponders to PDL1 blockade exhibited significantly higher expression of PAD4 and (2) our *in vivo* mouse tumor model study showing that the genetic and pharmacological inhibition of PAD4 synergized with PDL1-blockade resulting in the significant reduction of tumor growth compared to the other treatment groups. Together, we recapitulate in the human context that PAD4 negatively correlates with IFNγ/STAT1 signaling and we demonstrate that PAD4 impairs the therapeutic response to ICB therapy.

Chapter 5: Computational Methods Applied in the Analysis of Bulk and Single-cell Transcriptomic Data

Throughout the work composed in this Dissertation, we apply bioinformatic methods to provide support for our findings made in the wet lab as well as to make inferences regarding the relationship between gene expression and transcription factor activity. Analysis of bulk and single-cell RNA sequencing data played an indispensable role in investigating the function of PAD4 in macrophages. The key foci of analyses included determining the cells in which PAD4 was most highly expressed, the gene signatures in low versus high PAD4–expressing cells, pathway analysis of high PAD4–expressing macrophages and to assess the association of macrophage PAD4 expression with clinical response to immunotherapy and cancer outcomes. In this chapter, we will discuss the bioinformatic strategies implemented to address the key questions which directed our research trajectories.

Differential expression analysis

We began the PAD4 studies by showing that this particular PTM enzyme was among the most important PTM enzymes upregulated in TAMs. To establish the importance of PAD4 citrullination in the regulation of TAM functions, we needed to first demonstrate through a screening process that *Padi4* (in mice) or *PADI4* (in human) expression was particularly enriched in TAMs compared to normal macrophages. Analysis of bulk RNA-sequencing datasets which feature: (1) normal macrophages vs TAMs harvested from breast cancer patients (2) normal macrophages vs TAMs harvested from breast cancer–bearing mice (3) $CSF1R^{high}$ vs $CSF1R^{low}$

TAMs sorted from colorectal cancer patients and (4) Tim-4^{high} vs Tim-4^{low} TAMs sorted from ovarian cancer–bearing mice, offers the opportunity to infer which post-translational modification enzymes may play a dominant role in the pro-tumor TAM subsets. With these data, we performed differential expression (DE) analysis between the opposing groups featured in each of these datasets to reveal the genes which are most significantly associated with the tumor-promoting macrophages. Before performing DE analysis, we first processed the raw RNA-sequencing counts, applying quality control measures such as removing duplicate genes or genes that are lowly expressed. We then transformed the data from the raw scale to that of $\log_2$ counts per million (CPM). Transformation of the raw bulk RNA-seq counts stabilizes the variance of the data therein, allowing the data to be more amenable to parametric statistical methods. We then performed trimmed mean of M values (TMM) normalization provided by the *edgeR* (empirical analysis of digital gene expression data R) algorithm which provides a robust approach to account for differences in library sizes among samples and variability in gene expression. The last step before executing the formal DE analysis is to perform unsupervised clustering of the samples, generating a multi-dimensional scaling (MDS) plot to visualize similarities and dissimilarities between samples demonstrating the extent to which differential expression can be detected. Ideally, when comparing replicates of two different experimental groups, the replicates within each group should cluster close to each other while each group as a whole should cluster far from each other.

Performance of differential expression was achieved via *edgeR* which models count data using an overdispersed Poisson model and uses empirical Bayes methods to moderate the degree of overdispersion across genes[203]. Further, edgeR estimates the genewise dispersions by conditional maximum likelihood, conditions on the total count for that gene[204]. An empirical

Bayes procedure is used to reduce the dispersions toward a consensus value, essentially borrowing information between genes[203,205]. Finally, differential expression is assessed for each gene using an exact test similar to Fisher's exact test, but adapted for overdispersed data[203,206].

The output results generated by DE analysis consists of a list of genes ranked by their statistical significance (p-value), FDR–adjusted p-values and log-fold changes. To assess which PTM enzymes exhibit the highest and most significant expression in the pro-tumor TAM subsets described above, we subset or filter the list of genes to include only those of the major post-translational modification enzymes such as deiminases, kinases, methyltransferases, acetyltransferases, acyltransferases and deacetylases. Results show that in both human and in mouse breast cancer, *PADI4* (or *Padi4*) mRNA is significantly enhanced in the TAMs as well as in the pro-tumor CSF1R^{high} and Tim-4^{high} subsets (**Figure 2.1A-D**). The *edgeR–limma* workflow is a robust method for the performance of DE analysis and for the discovery of key genes which separate experimental groups.

Single-cell data visualization

We analyzed multiple single-cell RNA-seq datasets to show that *PADI4* (or *Padi4*) was particularly enriched in TAMs versus other immune cells for the purpose of establishing the importance of PAD4 citrullination specifically in macrophages and not in T-cells, B-cells, NK cells or DCs. Common methods for the visualization of genes at the single-cell resolution include t-distributed stochastic neighbor embedding (t-SNE) and uniform manifold approximation and projection (UMAP). Unlike, bulk RNA-sequencing, single-cell RNA-sequencing enables the analysis of gene expression in specific cell subsets. The data processing preceding visualization involves first performing quality control measures to filter out low quality cells,

doublets/multiplets and cells with high mitochondrial or ribosomal gene contamination which indicates dying cells. Given that in each cell in the single-cell RNA-sequencing data, there will be a different number of reads, we need to normalize these data such that we can draw accurate comparisons of gene expression between cells.

After normalization, we then perform scaling on the data which shifts the expression of each gene so that the variance across cells is 1 and so that the mean gene expression across cells is 0; this mitigates the variability in single-cell data and facilitates comparisons in gene expression across cells. On the scaled data, we perform linear dimensional reduction in preparation for data visualization. Before generating the UMAP or the tSNE visualization, we need to cluster the cells or group them according to their identity. We construct a k-Nearest Neighbor (kNN) graph based on the reduced-dimensional representation of the cells whereby each cell is connected to it k nearest neighbor. The Louvain modularity optimization algorithm is then applied to the kNN graph as a means to identify clusters of cells. While UMAP is a dimension reduction technique, it also serves as a common method for the visualization of single-cell data. Following this optimization, the cells are then projected onto a 2–dimensional space and this representation is then used for visualization. Cells which are close to each other in the UMAP plot are more similar according to their transcriptional profiles, reflecting a biological relationship detected in the original high–dimensional data. Similar to UMAP, tSNE is also dimensionality reduction and visualization technique commonly used in the analysis of single-cell data. For each pair of data points or cells, tSNE calculates the probability that the points would “choose” each other as neighbors in the high–dimensional space. The similarity between points is measured using a Gaussian distribution centered at each point[207]. Some of the key differences between tSNE– and UMAP–mediated visualization are that UMAP is often

computationally faster than tSNE and scalable to larger datasets; that UMAP robustly balances the preservation of both local (cell-to-cell similarity) and global (cluster-to-cluster similarity) structures while tSNE may often be inferior in the representation of global structures in the low–dimensional space; and that tSNE–generated visualization may suffer from the artificial crowding of data points making the data sometimes difficult to interpret. Nevertheless, to show simple gene expression across different immune cell clusters can be successfully achieved using either tSNE or UMAP as shown in **Figure 2.1F** and **I**.

Simulation of low and high expression of *PADI4* (or *Padi4*) in single cell data

In the wet lab, to understand how a particular gene affects cellular functions, common experimental tools include the genetic or pharmacological inhibition of the gene of interest. Similar strategies can be applied in the analysis of single-cell data. In our studies, we investigate the effect of PAD4 activity on macrophage phenotype and function. We demonstrate via wet lab *in vitro*, *ex vivo* and *in vivo* experiments that the loss or inhibition of PAD4 significantly enhances MHC-II (or human HLA-DR)–coding gene expression and protein function. We then sought to validate these findings via the analysis of single cell RNA-sequencing data of mouse and human macrophages. Firstly, in **Figure 2.3**, we analyze single cell RNA-sequencing data featuring the immune cells present in the murine peritoneal lavage. We first subset for just the macrophages by identifying the macrophage clusters and then filtering for those only. We then designate *Padi4*^{high} macrophages to be those which have a normalized expression value of *Padi4* greater than 1 and *Padi4*^{low} to be the macrophages with a normalized expression of *Padi4* lower than 1. Once we separate cells according to *Padi4* expression, we can then assess the expression of other key genes in the *Padi4*^{low} vs *Padi4*^{high} macrophages. As aforementioned, we sought to

validate via the analysis of single cell RNA-sequencing data our original finding the that low PAD4 activity results in enhanced MHC-II expression. After we separated *Padi4*^{low} vs *Padi4*^{high} macrophages, we then assessed the expression levels of the key MHC-II–coding genes including genes which code for protein subunits supporting the transcriptional expression of MHC-II (**Figure 2.3 H-I**). We performed the same method when analyzing the TAMs from TNBC patients in **Figure 4.1 C**. We aimed to show that in humans – particularly cancer patients – PAD4 activity was negatively associated with type II interferon signaling and MHC-II–mediated antigen presentation. Sub-setting specifically for TAMs from patient CD45^{+} cells in the single cell data, we distinguished *PADI4*^{low} and *PADI4*^{high} patient TAMs and observed significantly higher *CIITA* and *HLA-DRA* expression in the *PADI4*^{low} TAMs. Upon distinguishing *PADI4*^{low} and *PADI4*^{high} macrophages, we can then perform further analyses enabling comprehensive characterization of macrophage phenotype in the conditions of low versus high PAD4 activity.

Pathway enrichment analysis via gene set enrichment analysis (GSEA)

Despite the limited reach of transcriptomic data to describe biological phenomena which are actually carried out by proteins, analysis of gene sets or networks along signaling pathways enables a more comprehensive demonstration of the cell's phenotype in a particular condition. Using GSEA, we examined the pathways most positively or negatively enriched in the *Padi4*^{high} macrophages. Results showed that in the *Padi4*^{high} mouse peritoneal macrophages, the pathways most significantly downregulated are those associated with the MHC-II–mediated antigen presentation, the response to interferon-γ and T-cell activation. Neatly, this recapitulates what we observed in our original wet lab experiments.

Use of the gene set enrichment analysis (GSEA) algorithm allows for the determination of whether a particular gene set shows statistically significant differences between two biological states. First, genes in the gene set are ranked based on the correlation between their expression and the class distinction such as phenotype. GSEA tools include *a priori* defined sets of genes encoding for particular pathways or processes stored in the Gene Ontology (GO) database. When we run the enrichment analysis, the GSEA tools test each predefined gene set from the GO database to determine whether the genes in the set are randomly distributed throughout the ranked list of genes or if they tend to occur at the top or the bottom of the list. GSEA iterates down the ranked list and calculates an enrichment score for each gene set. Enrichment scores reflect the degree to which a particular gene set is overrepresented at the extremes (top or bottom) of the entire ranked list. As GSEA iterates or "walks down" the ranked list to calculate the enrichment score, a running-sum statistic is increased when a gene from the predetermined gene set is encountered; and contrarily, a running-sum statistic is decreased when a gene is not encountered. Together, the enrichment score is the maximum deviation from zero encountered in the "random walk" and corresponds to a weighted Kolmogorov–Smirnov-like statistic[208]. Finally, statistical significance is assessed by comparing the observed enrichment score for each gene set to a score generated from randomly shuffled or permuted data. This generates a null distribution against which the observed scores are compared. To calculate the normalized enrichment score (NES), the observed enrichment score is normalized based on the means and standard deviation of the scores obtained from the permuted datasets[208]. Together, using the GSEA computational tools, we were able to ascribe key biological pathways and processes to the *Padi4*^{high} macrophage gene set which provides some key insight into the function and role of PAD4 in macrophages. When we performed GSEA on mouse *Padi4*^{high} (**Figure 2.3N**) or human *PADI4*^{high}

(**Figure 2.3O, 4.1D-E**) macrophages, we receive strikingly consistent results showing indeed that the most significantly negatively enriched pathways are those associated with MHC-II–mediated antigen presentation. These results validate our original results generated in the wet lab showing that PAD4 restrains IFNγ/STAT1 signaling and MHC-II expression and functions.

Binding analysis for regulation of transcription (BART)

Through our work, we showed that the citrullination of STAT1 enforces the STAT1–PIAS1 interaction which consequently restrains STAT1 binding to key promoter regions in the *CIITA* gene. In our investigations, we sought to determine the molecular mechanism through which PAD4 controls MHC-II. It has already been established that the transcription factor STAT1 binds to multiple promoter regions in the class II transactivator (*CIITA*) gene propagating the transcription and then translation of CIITA, resulting in the CIITA protein binding to promoter regions of MHC-II–coding genes leading to MHC-II expression[179]. Moreover, it has also been shown that PADs can directly citrullinate transcription factors regulating their activity as a consequence[49,139]. Given these insights, we asked whether STAT1 could be a direct target of PAD4 citrullination. Preceding the performance of the wet lab experiments needed to demonstrate this mechanism, we first sought to determine whether there existed a significant relationship between macrophage PAD4 expression and STAT1 transcriptional activity. Therefore, we resorted to using the binding analysis for regulation of transcription (BART) computational method as a means to provide some inference into a possible regulatory relationship between PAD4 and STAT1. Primarily, the BART software is designed to predict the functional transcription factors which regulate a query gene set or which associate with a query

genomic profile for epigenetic analysis. Although BART can be used across broad range of applications, a major limitation of the BART tools is that they are not particularly designed to make predictions regarding a gene set based on the high expression of a gene coding for a protein *upstream* of transcription factors such as PAD4[161]. Nevertheless, the BART results can still serve to at least infer that a regulatory relationship exists between PAD4 and the transcription factor of interest. In this scenario, further validation was required to confirm whether PAD4 regulated STAT1.

Chapter 6: Discussion

Summary of Thesis Work

Through this body of work, we discovered that PAD4–mediated citrullination of STAT1 in tumor–associated macrophages negatively regulates STAT1 transcriptional activity and that this mechanism restrains MHC-II–mediated antigen presentation affecting tumor growth outcomes. Importantly, we demonstrated that the citrullination of STAT1 is required for the physical inhibitory interaction between STAT1 and PIAS1. In the context of the regulatory systems controlling the expression and function of MHC-II, the STAT1–PIAS1 interaction restrains STAT1 binding to the promoter regions of the *CIITA* gene and thereby negatively fine-tunes MHC-II expression in response to IFNγ. We demonstrated that the genetic loss or the pharmacological inhibition of PAD4 significantly enhanced MHC-II expression and function and

that this enabled enhanced anti-tumor T-cell function, enhanced anti-tumor immunity and reduced tumor growth.

Our work elucidating the role of PAD4 citrullination in macrophages contributes to the growing body of studies which seeks to determine the ways in which macrophages can be targeted for the maintenance of anti-tumor immunity. Macrophages make up the majority of the immune cell compartment in the tumor microenvironment[9]. Current common immunotherapies such as immune checkpoint blockade (ICB) have been developed mostly to target T-cell activation, blocking immunosuppressive checkpoints on tumor cells or APCs[209,210]. While ICB and other T-cell–based therapies have shown to be efficacious in prolonging patient survival for a number of cancers, still some key components of the TME pose formidable challenges in the maintenance of durable anti-tumor immunity. Within the past 100 years, substantial knowledge has been gained regarding the pro- and anti-tumor functions of macrophages alike[40]. On the one hand, macrophages can promote tumor growth through the production of anti-inflammatory, immunosuppressive cytokines, angiogenesis and the downregulation of antigen presentation molecules. On the other hand, macrophages can prevent tumor growth through the production of proinflammatory cytokines, phagocytosis and the upregulation of antigen presentation molecules[36]. The high abundance and vast functional heterogeneity of macrophages in the TME endows macrophages with multiplexed capabilities to control immunity in the TME and therefore cancer outcomes[37,38,39]. In our work, we identify an intrinsic mechanism whereby PAD4 inhibits macrophage STAT1 signaling and demonstrate that blocking PAD4 results in enhanced STAT1 binding to the *CIITA* gene promoting the expression of MHC-II downstream.

Through this work, we also demonstrate an understudied strategy in targeting macrophages to fight cancer: targeting post-translational modifications (PTMs). Post-

translational modifications compose the final conformations of protein structure and therefore determine the ultimate protein functions. We showed that the citrullination of STAT1 reinforces the STAT1-PIAS1 interaction restraining STAT1 signaling in macrophages. This mechanism enables for the blocking of citrullination rather than the blocking of PIAS1 an essential protein which likely has other key roles apart from antagonizing *CIITA* mRNA expression. Targeting PTMs as a treatment strategy may allow for a finer refinement of protein function and more durable outcomes.

PAD4 regulation of STAT1 transcriptional activity and tumor immunity

We began our investigations into the role of PAD4 in tumor–associated macrophages upon observing that PAD4 was among the most highly and significantly expressed PTM enzymes in TAMs compared to normal macrophages. Moreover, we observed that primary ovarian cancer patient ascites fluid – as well as various tumor-associated factors and cytokines, including TLR agonists, ATRA, VEGF, IL6 and GM-CSF – directly induced PAD4 protein expression in primary human monocytes as well as in the human myeloid cell line, HL60 (**Figure 2.1N-Q**). These initial findings suggested that PAD4 may have a critical role in the immunosuppressive and tumor–promoting functions of macrophages. We then sought to determine which macrophage functions PAD4 could be regulating such that the enzyme's expression was enhanced in TAMs compared to in normal macrophages.

We first investigated the major cell surface proteins on macrophages involved in immune activation. Initially, we examined freshly harvested macrophages from wild-type versus *Padi4*$^{-/-}$ mice and observed consistently that the loss of PAD4 resulted in the significant enhancement of both intracellular and surface MHC-II expression. This phenomenon occurred in macrophages

across tissues in healthy mice and in the tumors of tumor–bearing mice alike. The expression of surface proteins including MHC-I, CD80, CD86 and PD-L1 showed neither significant nor consistent differences between the wild-type and the PAD4–deficient macrophages. Importantly, we determined that the restraint of MHC-II by PAD4 occurred at the transcriptional level. Primary mouse macrophages were harvested from wild-type and *Padi4*$^{-/-}$ mice and RNA was extracted for the performance of quantitative PCR. The PCR results revealed that the loss of PAD4 significantly enhanced multiple interferon–responsive and MHC-II–associated genes including *Stat1*, *Ciita*, *H2-Aa*, *Cd74* and *Gbp2*. This demonstrates that the enhanced MHC-II expression and interferon signaling due to the deficiency in PAD4 occurs on the transcriptional level. We further validated these findings through the analysis of publicly available single-cell RNA-seq datasets. First, we analyzed a single-cell RNA-sequencing dataset featuring the CD45^{+} cellular compartment of the mouse peritoneal lavage. We then filtered the immune cell clusters to subset only for the macrophages. When we separate the macrophage population into *Padi4*^{low} and *Padi4*^{high} subsets and then examine the expression levels of MHC-II–coding genes as well as other genes critical for the transcriptional activation of MHC-II. We observed that in the *Padi4*^{low} macrophages, MHC-II–associated genes were significantly and consistently enhanced compared to in the *Padi4*^{high} macrophages, recapitulating our finding that PAD4–deficiency results in enhanced MHC-II transcription. While we observed higher MHC-II expression levels on both the RNA and protein level, we next needed to demonstrate enhanced MHC-II function.

We performed *in vitro* antigen presentation assays to assess OT-II T-cell activation due specifically to MHC-II–mediated antigen presentation. Culturing OT-II T-cells with soluble OVA protein and *Padi4*$^{-/-}$ macrophages resulted in significantly higher T-cell activation compared to that with wild-type macrophages. We received similar results when we cultured OT-II T-cells

with OVA^+ MC38 colorectal cancer cells and *Padi4*$^{-/-}$ macrophages. These experiments demonstrate that the loss of PAD4 in macrophages results in enhanced MHC-II–mediated antigen presentation.

Further, we observed that PAD4–deficient macrophages exhibited heightened STAT1 signaling which we reasoned may underly the enhanced MHC-II functioning. Returning to the analysis of single-cell RNA-sequencing datasets, we assessed STAT1 signaling in *Padi4*^{low} versus in *Padi4*^{high} mouse peritoneal macrophages. As described above, we first separated mouse peritoneal macrophages into *Padi4*^{high} versus *Padi4*^{low} macrophages. We then perform gene set enrichment analysis (GSEA) on just the *Padi4*^{high} macrophages to determine which pathways were most significantly up- and downregulated depending on *Padi4* expression. We observed that the pathways most significantly upregulated were those associated with PAD4–mediated citrullination such as peptidyl-arginine modification and protein-arginine deiminase activity for example. The pathways most significantly downregulated included those such MHC class II protein complex, antigen processing and presentation via MHC-II and response to interferon-gamma. When we analyzed another single-cell RNA-seq dataset featuring human peripheral blood mononuclear cells (PBMCs), we filtered the data just to include monocytes and then separated cells between *PADI4*^{low} versus *PADI4*^{high} blood monocytes. We then performed GSEA on the *PADI4*^{high} monocytes and this analysis revealed similar results as we found with the mouse dataset, that the most significantly downregulated pathways were those associated with MHC-II functions.

Finally, we observed markedly enhanced STAT1 protein expression in the TAMs harvested from ID8 ovarian cancer–bearing *Padi4*$^{-/-}$ compared to those harvested from the wild-type counterparts, suggesting that the loss of PAD4 *in vivo* results in enhanced STAT1 signaling

and can contribute to reduced tumor growth. These results suggested that the restraint of MHC-II by PAD4 occurred due to an inhibitory mechanism by PAD4 onto STAT1 signaling. Since it has been established that (1) MHC-II expression is controlled by STAT1 binding to the *CIITA* promoter, activating CIITA protein to then bind to MHC-II–coding gene promoters[179]; and (2) that PADs can directly citrullinate transcription factors regulating their functions[49,139], we hypothesized that PAD4 directly citrullinated STAT1, inhibiting its transcriptional activity of STAT1 and – consequently – restraining MHC-II functions. Using a bioinformatic method to predict the transcription factors most associated with a *Padi4*^{high} macrophage gene set revealed that STAT1 was among the most highly enriched transcription factors indicating a significant relationship between STAT1 and high PAD4 expression in macrophages. Taken together, our initial investigations revealed that TAMs express high levels of PAD4 and that PAD4 restrains MHC-II–mediated antigen presentation via negatively regulating STAT1 signaling.

We next investigated the mechanism by which PAD4 regulates STAT1 transcriptional activity and how this regulation controls MHC-II expression. We demonstrated that PAD4 does citrullinate STAT1 in mouse and human macrophages in response to IFNγ or LPS. Importantly, we showed that the citrullination of STAT1 was required for the inhibitory physical interaction between STAT1 and PIAS1. The genetic loss or pharmacological inhibition of PAD4 resulted in the complete abolishment of the STAT1–PIAS1 interaction suggesting that the citrullination of STAT1 serves as an inhibitory mechanism via the facilitation of the STAT1-PIAS1 interaction. We found that PAD4 citrullinated STAT1 at arginine 121 and that the citrullination of this site was required for the STAT1-PIAS1 interaction under IFNγ signaling conditions. Furthermore, we demonstrated that the citrullination of this site modulated HLA-DR expression in human cells. As aforementioned, the STAT1-PIAS1 interaction regulates STAT1 binding to key DNA regions

to propagate downstream STAT1 signaling. For the particular regulation of MHC-II expression, STAT1 binds to multiple promoter regions in the *CIITA* gene. We performed chromatin immunoprecipitation (ChIP) on IFNγ–treated cells from wild-type versus *Padi4*$^{-/-}$ mice to detect STAT1 protein binding to multiple IFNγ–responsive promoters in the *CIITA* gene and observed significantly higher STAT1 binding in the *Padi4*$^{-/-}$ cells. We found similar results when treating IFNγ–stimulated HL60 cells with the PAD4–specific inhibitor GSK484. Together, we elucidate the mechanism by which the citrullination of STAT1 controls STAT1 transcriptional activity and consequently MHC-II expression and function.

Clinical significance of Thesis Work

We sought to demonstrate the clinical applications of our work elucidating the role of PAD4 in macrophages. We demonstrated previously that the loss of PAD4 in macrophages resulted in the significant reduction of tumor growth or metastasis across murine tumor models including MC38 colorectal cancer, Py8119 breast cancer and B16F10 melanoma. We then asked whether this *in vivo* phenomenon could be harnessed to enhance already existing immunotherapeutic strategies. To address this question, we tested whether the genetic deletion or the pharmacological inhibition of PAD4 could synergize with PD-L1 blockade to result in further reduced tumor size compared to the condition of PDL1 blockade treatment alone. First, we conducted two separate tumor models, inoculating MC38 tumor cells into *Padi4*$^{fl/fl}$ and *Padi4*$^{fl/fl}$ *LysM*^{cre} male mice and Py8119 tumor cells into *Padi4*$^{fl/fl}$ and *Padi4*$^{fl/fl}$ *LysM*^{cre} female mice. In each experiment, once tumors reached a minimum volume, mice received either PD-L1 blocking antibody or IgG isotype control. We observed in both experiments that the *Padi4*$^{fl/fl}$ *LysM*^{cre} mice treated with PD-L1 blockade therapy developed the smallest tumors indicated by the reduced tumor volume.

Second, to show whether the pharmacological inhibition of PAD4 could synergize with PD-L1 blockade, we performed an additional set of *in vivo* experiments whereby we inoculated wild-type male mice with MC38 and wild-type female with Py8119 tumor cells. In both experiments, mice received either IgG isotype control along with vehicle, PD-L1 blockade along with vehicle, PAD4 inhibitor GSK484 with IgG isotype control or GSK484 combined with PD-L1 blockade. In both experiments, we observed the smallest tumor volume in the mice which received the combination treatment of GSK484 and PD-L1 blockade, indicating synergy between the pharmacological inhibition of PAD4 and checkpoint blockade. These preclinical experiments suggest the potential efficacy in targeting PAD4 in macrophages as a means to enhance checkpoint blockade therapy. We next sought to examine (1) the relationship between PAD4 and IFNγ signaling in human macrophages and (2) the relationship between PAD4 expression in TAMs and the response to checkpoint blockade. Firstly, we demonstrated that primary IFNγ–stimulated human PBMC–derived macrophages treated with the PAD4–specific inhibitor GSK484 exhibits reduced STAT1 citrullination and enhanced HLA-DR expression, recapitulating results from our previous mouse experiments. Further, we stimulated primary TAMs from ovarian cancer patient tumors with IFNγ and then treated cells with either GSK484 or DMSO and observed that IFNγ and GSK484 synergize to enhance HLA-DR compared to the condition of IFNγ treatment alone, demonstrating that in primary patient TAMs, PAD4 negatively regulates HLA-DR expression. To further validate these initial findings and to investigate the associations of PAD4 expression with the response to immunotherapy, we analyzed a single-cell RNA-sequencing dataset featuring the $CD45^+$ cells from the triple negative breast cancer (TNBC) patients treated with PD-L1 blockade. Patient outcomes of complete response (CR) or partial response (PR) were classified as Responders; and those with the

outcomes of progressive disease (PD) or stable disease (SD) were classified as Nonresponders. We first assessed *PADI4* mRNA expression in the TAMs in Responders versus Nonresponders and found that *PADI4* was significantly more highly expressed in the TAMs of the Nonresponders to PD-L1 blockade demonstrating that PAD4 activity in macrophages impairs the response to immunotherapy. Importantly, we show that *PADI4* expression in patient TAMs is significantly negatively correlated with the HLA-DR–coding gene signature. As we expected, the Responders' TAMs exhibited higher *CIITA* and therefore higher HLA-DR–coding gene expression. Separating patient TAMs into $PADI4^{high}$ versus $PADI4^{low}$ TAMs revealed again albeit in this clinical context that *CIITA* and *HLA-DRA* expression was enhanced in the $PADI4^{low}$ TAMs compared to $PADI4^{high}$ TAMs. Further, we performed GSEA on the $PADI4^{high}$ patient TAMs to examine the pathways which are up- or downregulated in the $PADI4^{high}$ patient TAMs. GSEA results revealed (as we observed in previous single-cell RNA-sequencing dataset analyses) that the most significantly upregulated pathways included peptidyl arginine modification and protein arginine deiminase activity as we expect. However, the most significantly downregulated pathways included MHC class II protein binding, antigen process and presentation via MHC class II, response to interferon-γ, T-cell receptor signaling pathway and more pathways associated with IFNγ signaling and anti-tumor responses indicating that the high expression of PAD4 in patient TAMs is associated with the restraint of antigen presentation, T-cell activation and other proinflammatory immune pathways. MHC-II–mediated antigen presentation activates and polarizes $CD4^+$ T-cells which are indispensable for the maintenance of systemic anti-tumor immunity in the TME[200,201,202]. We show that the TAM expression of *PADI4* is significantly negatively correlated with key effector $CD4^+$ T-cell genes. These data generated through the

analysis of this single-cell RNA-seq data recapitulates what we have shown in previous analyses as well as what we have shown through our own independent investigations.

Future directions

Targeting PAD4 in human cancers

Through our work, we demonstrate that the inhibition of PAD4 in macrophages results in the enhanced antigen presentation, T-cell activation and abrogated tumor growth. The results suggest that PAD4 may constitute a durable target to enhance anti-tumor immunity in patients with cancer. Implementation of a practical strategy to inhibit PAD4 in human macrophages requires several more comprehensive studies. Two reasonable PAD4–focused treatment avenues may include (1) the use of already–existing PAD4 inhibitors originally meant to treat rheumatoid arthritis or (2) the engineering of future CAR-macrophages with PAD4 deficiency to promote enhanced antigen presentation and STAT1 signaling. Use of PAD4 inhibitors in the clinic need not target PAD4 in macrophages specifically since PAD4 in neutrophils and PAD4 in tumor cells have been shown to promote tumor growth. Therefore, the inhibition of PAD4 in macrophages, neutrophils and tumor cells would constitute a solid and durable treatment strategy. Future strategies may include the use of antibody–drug conjugates whereby the antibody, covalently attached to a PAD4 inhibitor, would specifically identify macrophages and then deliver the inhibitor, constituting a targeted therapy. More work is needed to connect our studies presented in this Dissertation to future strategies of exploiting macrophage PAD4 for the treatment of human cancers in the clinic.

Expanding the field of PADs: PAD2 in lymphocytes (T and B-cells)

Early investigations into the role of PAD2 in T-cells

While this Dissertation presents our focused investigation into a novel role for PAD4 in macrophages, we have continued our studies on nuclear PADs in other mononuclear immune cell subsets. As aforementioned, while PAD4 is the only PAD isozyme which bears the canonical nuclear localization sequence (NLS), PAD2 has also been shown to translocate to the nucleus and citrullinate nuclear targets[49,211,212,213]. Few studies have reported that PAD2 is a dominant PAD isozyme in T-cells[49]. However, whether PAD2 plays a role in the regulation of effector T-cell activation has not been comprehensively shown. In our initial investigations, we asked whether the loss of PAD2 could regulate tumor growth and anti-tumor immunity. We inoculated MC38 murine colorectal cancer cells subcutaneously in *Padi2*$^{+/+}$ and *Padi2*$^{-/-}$ mice, monitored tumor growth, excised tumors at endpoint and then processed tumors for FACS analysis to detect T-cell cytokine production. First, we observed that the loss of PAD2 resulted in the significant reduction in tumor growth and tumor weight in two experiments (**Figure 6.1A**). We then confirmed that the loss of PAD2 in macrophages had no effect on MHC-II expression contrary to PAD4 suggesting that the loss of PAD2 enhances anti-tumor immunity by affecting immune cell subsets other than macrophages (**Figure 6.1B**). Importantly, we observed that both $CD4^+$ and $CD8^+$ T-cells from the tumor and the tumor–draining lymph nodes (TDLNs) exhibited enhanced activation indicated by the significantly higher proportion $IFN\gamma^+$, $IL\text{-}2^+$, $TNF\alpha^+$ and granzyme B^+ T-cells (**Figure 6.1C**). These results prompted the further investigation on the potential role of PAD2 in regulating the process of T-cell activation. We sought to determine the potential mechanism by which PAD2 may regulate T-cell functions. Previous literature has shown that PAD2 can citrullinate transcription factors, regulating cellular functions[49]. Moreover, our studies

on PAD4 in this Dissertation further suggest that transcription factors may serve as common substrates for nuclear PADs. Interestingly, close analysis of the results from the *in vivo* tumor model revealed that the loss of PAD2 particularly enhanced granzyme B (GranB) and IL-2 production in T-cells. GranB and IL-2 signaling requires the transcriptional activity of STAT5. Following a similar approach that we took in our PAD4 studies, we asked whether PAD2 could physically interact with STAT5 during T-cell activation, suggesting that PAD2 may regulate STAT5 transcriptional activity in such a way that controls T-cell activation. When we stimulated Jurkat cells (human T-cell line) with αCD3/αCD28, we observed via Western blotting following co-immunoprecipitation that 1 hour of TCR stimulation induced PAD2 to physically interact with STAT5 (**Figure 6.1D**). In primary mouse T-cells enriched from the spleen and lymph nodes of healthy wild-type or Padi2$^{-/-}$ mice, we observed that during T-cell activation, PAD2–deficient T-cells exhibited higher levels of STAT5 phosphorylation indicating higher STAT5 signaling compared to the wild-type T-cells (**Figure 6.1E**). These data altogether suggest that PAD2 may negatively regulate or restrain T-cell effector functions via the physical interaction and citrullination of STAT5. Much work is needed to further elucidate the connection between the molecular mechanism and the T-cell effector phenotype which we believe shaped the enhanced tumor immunity in the PAD2–deficient tumor–bearing mice.

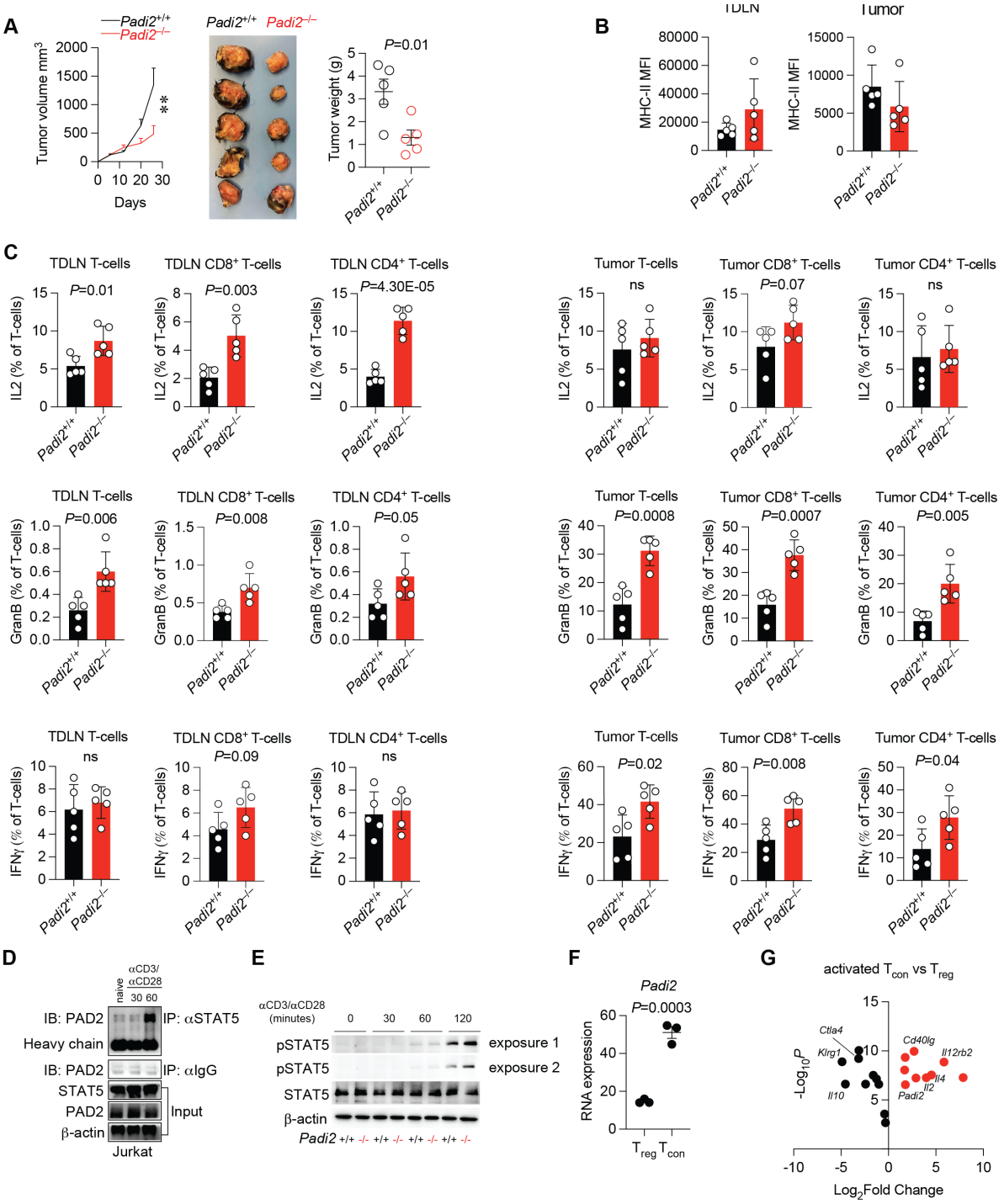

Figure 6.1.0: Preliminary investigations on the role of PAD2 in lymphocytes. (A) Growth kinetics of subcutaneous MC38 murine colorectal cancer in *Padi2*$^{+/+}$ and *Padi2*$^{-/-}$ mice (n = 5) (left). At endpoint, MC38 tumors from *Padi2*$^{+/+}$ and *Padi2*$^{-/-}$ mice were excised (n = 5) (center). Weight of the tumors excised from *Padi2*$^{+/+}$ and *Padi2*$^{-/-}$ MC38–bearing mice (right). (B) Mean fluorescence intensity (MFI) of MHC-II expression on macrophages from the tumor and TDLNs of MC38–bearing *Padi2*$^{+/+}$ and *Padi2*$^{-/-}$ mice. (C) CD4^{+} and CD8^{+} T-cell activation phenotype of the tumor and TDLN T-cells from MC38–bearing *Padi2*$^{+/+}$ and *Padi2*$^{-/-}$ mice. (D) Jurkat cells were stimulated with 2 µg/mL αCD3 and 1µg/mL αCD28 for 1hr and proteins were lysed and processed for the co-immunoprecipitation with anti-STAT5. (E) *Padi2*$^{+/+}$ and *Padi2*$^{-/-}$ cells were stimulated with 2 µg/mL αCD3 and 1µg/mL αCD28 for 2hrs. (F) *Padi2* mRNA expression in activated T_{regs} and T_{con} cells (GSE154680). Differential expression analysis of activated T_{con} vs T_{reg} (GSE154680).

To further validate our *in vitro*, *ex vivo* and *in vivo* observations, we performed some preliminary, exploratory bioinformatic analyses as a means to gain some additional insights regarding the role of PAD2 in T-cells so as to support our findings. We analyzed multiple RNA sequencing datasets (bulk and single-cell) as a means to associate PAD2 expression in T-cells with a particular effector T-cell phenotype. First, we sought to establish whether PAD2 was particularly expressed in conventional T-cells (T_{con}) versus regulatory T-cells (T_{regs}). We analyzed a bulk RNAseq dataset[214] which featured activated mouse T_{con} versus T_{regs} and we assessed PAD2 expression in each group. Results showed that PAD2 was more highly expressed in activated T_{con} compared to in activated T_{regs} (**Figure 6.1F**). Upregulation of PAD2 in the conventional $CD4^+$ T-cells in particular was associated with upregulation of other effector genes including *Il12rb*, *Il2* and *Cd40lg* (**Figure 6.1G**). Analyzing another dataset featuring $CD8^+$ T-cells stimulated with αCD3/αCD28 treated with or without IL-2 revealed that *Padi2* was upregulated in the IL-2 treatment condition along with other T-cell effector genes including granzyme B, Lag3, Tnfrsf8 and Tnfrsf9 while stem-like, quiescence genes Tcf7 and Lef1 were downregulated (**Figure 6.1H**). This suggests that PAD2 may be associated with cytotoxic or exhaustion transcriptional programs in T-cells. These findings compose a preliminary foundation upon which further studies will be required to elucidate how potentially the regulation of STAT5 by PAD2 might restrain STAT5 transcriptional activity limiting *Il2* and *Gzmb* transcription in effector T-cells.

Early investigations into the role of PAD2 in B-cells and the PAD2 specific inhibitor

PAD2 is more promiscuously expressed across immune cell subsets compared to PAD4 which is restricted to myeloid cells. Previous research reports combined with the analysis of publicly available transcriptomic data validated that PAD2 could be expressed in lymphocytes, T and B-cells alike[215] (**Figure 6.1I**). Our preliminary investigations into the potential role for PAD2 in effector T-cells revealed that PAD2 physically interacts with STAT5, regulating pSTAT5 levels and T-cell activation *in vivo*. Continuing our studies, we included the use of a PAD2–specific inhibitor called AFM32a as research tool to investigate how the pharmacological inhibition of PAD2 could affect cell phenotypes (**Figure 6.1J**).

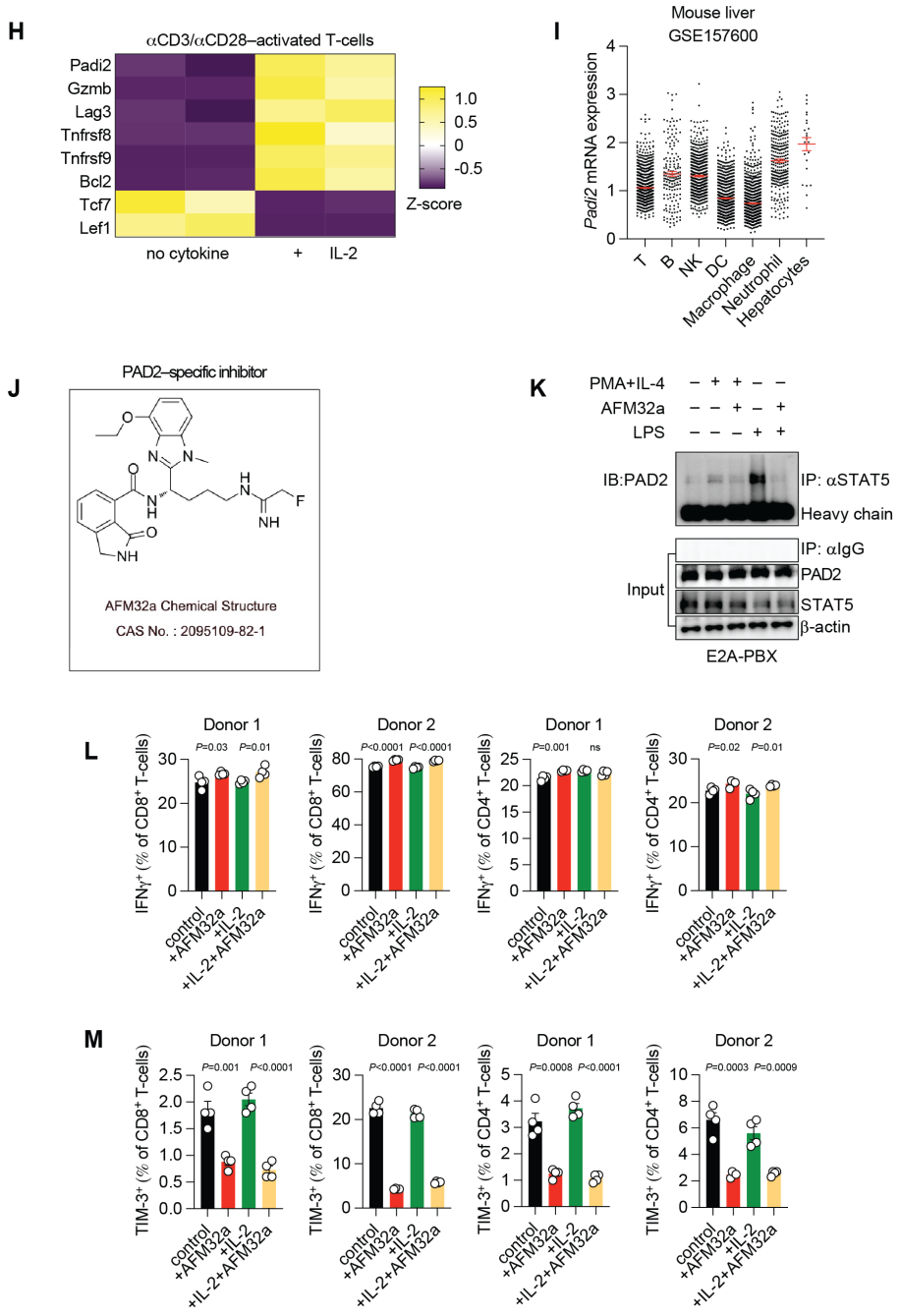

Figure 6.1.1: Preliminary investigations on the role of PAD2 in lymphocytes. (H) Heatmap showing gene expression of αCD3/αCD28–stimulated CD8$^+$ T-cells with or without IL-2 supplementation (GSE143903). (I) *Padi2* mRNA expression across cell types in murine liver metastasis (GSE157600). (J) Chemical structure of AFM32a, a PAD2–specific inhibitor. (K) E2A-PBX B-cells were stimulated with a PMA–IL-4 cocktail or LPS with or without AFM32a and proteins were lysed and processed for the co-immunoprecipitation with anti-STAT5. (L and M) Percentages of IFNγ$^+$CD4$^+$ and CD8$^+$ T-cells enriched from human PBMCs stimulated with αCD3/αCD28, treated with or without AFM32a, with or without IL-2 or with AFM32a and IL-2 combined. (M) Percentages of TIM-3$^+$CD4$^+$ and CD8$^+$ T-cells enriched from human PBMCs stimulated with αCD3/αCD28, treated with or without AFM32a, with or without IL-2 or with AFM32a and IL-2 combined.

In B-cells, STAT5 signaling is also important, regulating differentiation and effector functions[216,217]. We first asked whether PAD2 could physically interact STAT5 in B-cells and whether that could have an impact on B-cell functions. We performed a co-IP experiment in which we sought to detect and confirm PAD2 binding to STAT5 in conditions of B-cell activation. We stimulated $CD19^+$ E2a-PBX leukemia cells with a PMA–IL-4 cocktail known to activate B-cells[218] and with LPS. In addition, we included conditions in which we activated B-cells and simultaneously treated them with AFM32a. Firstly, in response to the PMA–IL-4 cocktail, we do observe that PAD2 physically interacts with STAT5 (**Figure 6.1K**). Interestingly, LPS treatment resulted in a stronger signal, perhaps indicating a higher level of physical interaction between PAD2 and STAT5 (**Figure 6.1K**). When we activated B-cells and inhibited PAD2 simultaneously, we observed clearly that the PAD2–specific inhibitor completely abolished the PAD2–STAT5 interaction (**Figure 6.1K**). In B-cell biology, STAT5 plays a variety of roles and therefore further investigation is needed.

Lastly, we sought to determine how the pharmacological inhibition of PAD2 with AFM32a affected human T-cell activation. We harvested T-cells from human PBMCs of two donors, stimulated them with αCD3/αCD8 and then treated with or without IL-2 and/or AFM32a. We observed that in both donors PAD2 inhibition resulted in enhanced IFNγ production in the $CD8^+$ and $CD4^+$ T-cells treated with AFM32a with or without IL-2 (**Figure 6.1L**). Strikingly, proportions of TIM-3^+CD8^+ and $CD4^+$ T-cells were significantly reduced upon treatment with AFM32a regardless of IL-2 treatment (**Figure 6.1M**). These results suggest that the specific inhibition of PAD2 in T-cells renders the cells more activated and less exhausted. While these results are encouraging, a substantial amount of work is required to comprehensively elucidate the role of PAD2 in regulating T-cell activation processes.

Conclusions

This body of work has focused on identifying a novel role for PAD4 in macrophages providing valuable insights into how citrullination can control key immune cell functions critical for immune responses during cancer. These studies expand our understanding of how immune cells function and impact health. As a result, we hope that they may inform future strategies for clinical intervention whether for cancer or infectious disease.

Appendix: Graphical Schematic

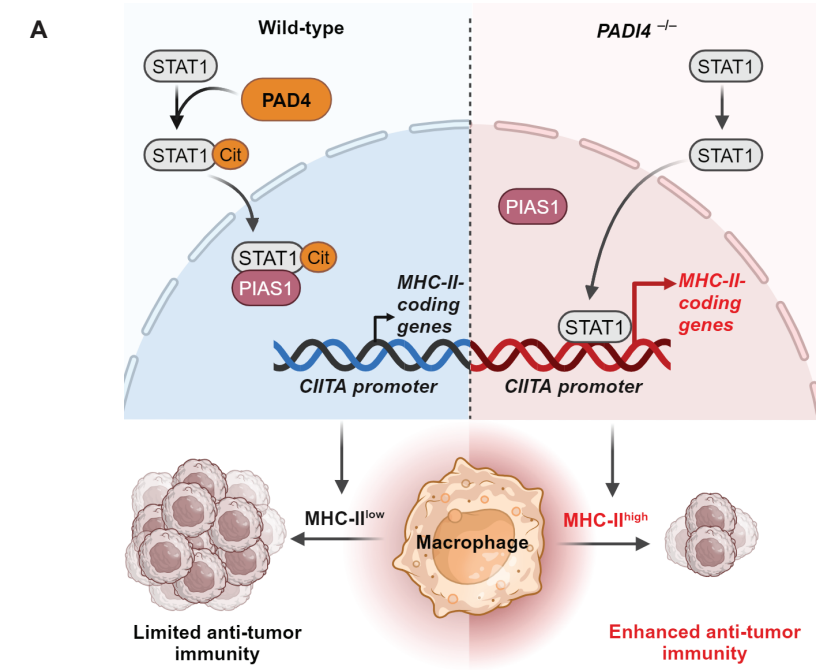

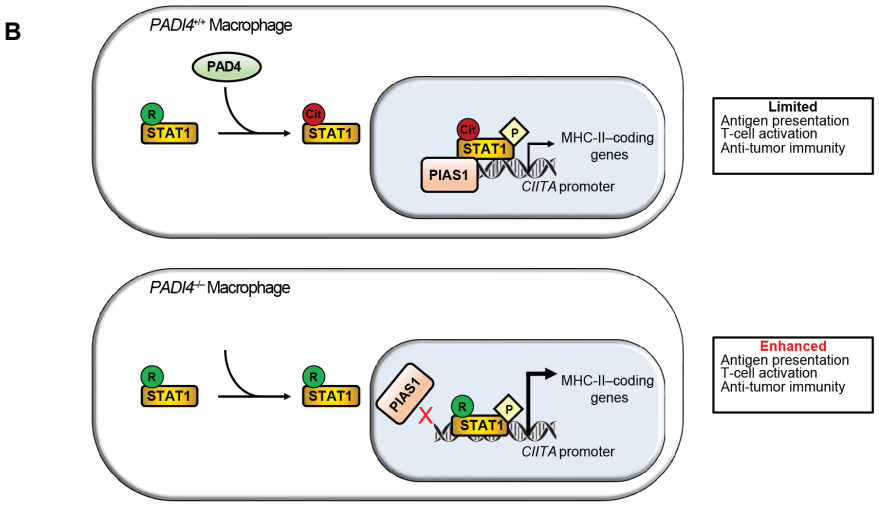

Appendix Figure A.1: (A) Graphical Schematic. (B) Mechanistic schema

Bibliography

[1] Palucka et al. The Basis of Oncoimmunology. *Cell* **164**, 1233-1247 (2016)
[2] Zou. Immunosuppressive networks in the tumour environment and their therapeutic relevance. *Nat. Revs. Cancer* **5**, 263-274 (2005)
[3] Hanahan and Weinberg. Hallmarks of Cancer: The Next Generation. *Cell* **144**, 646-674 (2011)
[4] Anderson et al. The tumor microenvironment. *Current Biology* **30**, R905-R931 (2020)
[5] Chow et al. Clinical implications of T cell exhaustion for cancer immunotherapy. *Nat. Revs. Clin. Oncol.* **19**, 775-790 (2022)
[6] Leach et al. Enhancement of antitumor immunity by CTLA-4 blockade. *Science* **271**, 1734-1736 (1996)
[7] Zou et al. PD-L1 (B7-H1) and PD-1 pathway blockade for cancer therapy: Mechanisms, response biomarkers, and combinations. *Science Trans. Med.* **8**, 328rv4 (2016)
[8] Lin et al. Host expression of PD-L1 determines efficacy of PD-L1 pathway blockade–mediated tumor regression. *JCI* **128**, 805-815 (2018)
[9] Cassetta et al. Human tumor–associated macrophage and monocyte transcriptional landscapes reveal cancer–specific reprogramming, biomarkers, and therapeutic targets. *Cancer Cell* **35**, 588-602 (2019)
[10] Pathria et al. Targeting tumor–associated macrophages in cancer. *Trends Immunol.* **40**, 310-327 (2019)
[11] Klichinsky et al. Human chimeric antigen receptor macrophages for cancer immunotherapy. *Nat. Biotech.* **38**, 947-953 (2020)
[12] Hung et al. The central role of CD4+ T cells in the antitumor immune response. *J Exp Med.* **188**, 2357-2386 (1998)
[13] Waldman et al. A guide to cancer immunotherapy: from T cell basic science to clinical practice. *Nat. Revs. Immunol.* **20**, 651-668 (2020)
[14] Zhang et al. CD8(+) T cells: foot soldiers of the immune system. *Immunity* **35**, 161-168 (2011)
[15] Golstein et al. An early history of T cell–mediated cytotoxicity. *Nat. Rev. Immunol.* **18**, 527-535 (2018)
[16] Sandu et al. Exhausted $CD8^+$T cells exhibit low and strongly inhibited TCR signaling during chronic LCMV infection. *Nat. Commun.* **11**, 4454 (2020)
[17] Ferris et al. Too much of a good thing? Tim-3 and TCR signaling in T cell exhaustion. *J Immunol.* **193**, 1525-1530 (2014)
[18] Wherry. T cell exhaustion. *Nat. Immunol.* **12**, 492-499 (2011)
[19] Whiteside. The tumor microenvironment and its role in promoting tumor growth. *Oncogene* **27**, 5904-5912 (2008)
[20] Reina-Campos et al. $CD8^+$ T cell metabolism in infection and cancer. *Nat. Revs. Immunol.* **21**, 718-738 (2021)
[21] Ho et al. Phosphoenolpyruvate Is a Metabolic Checkpoint of Anti-tumor T Cell Responses. **162**, 1217-1228 (2015)
[22] Roche et al. The ins and outs of MHC class II–mediated antigen processing and presentation. *Nat. Revs. Immunol.* **15**, 203-216 (2015)
[23] Tortorella et al. Viral subversion of the immune system. *Annu Rev Immunol.* **18**, 861-926 (2000)
[24] Yang et al. FoxO1 is a regulator of MHC-II expression and anti-tumor effect of tumor–associated macrophages. *Oncogene* **37**, 1192-1204 (2018)
[25] Rosenberg. IL-2: The First Effective Immunotherapy for Human Cancer. *J Immunol.* **192**, 5451-5458 (2014)
[26] June et al. Chimeric Antigen Receptor Therapy. *NEJM* **379**, 64-73 (2018)
[27] Brown et al. CAR T cell therapy: inroads to response and resistance. *Nat. Revs. Immunol.* **19**, 73-74 (2019)
[28] Yang et al. Diverse Functions of Macrophages in Different Tumor Microenvironments. *Cancer Research* **78**, 5492-5503 (2018)
[29] Christofides et al. The complex role of tumor–infiltrating macrophages. *Nat. Immunol.* 23, 1148-1156 (2022)
[30] Robinson et al. Monocyte Regulation in Homeostasis and Malignancy. *Trends in Immunology* **42**, 104-119 (2021)
[31] Vakkila et al. Inflammation and necrosis promote tumour growth. *Nat. Revs. Immunol.* 4, 641-648 (2004)
[32] Mantovani et al. Macrophages polarization: tumor–associated macrophages as a paradigm for polarized M2 mononuclear phagocytes. *Trends in Immunology* **23**, 549-555 (2002)

[33] Jerrells et al. Increased monocyte–mediated cytostasis of lymphoid cell lines in breast and lung cancer. *Int. J. of Cancer* **23**, 768-776 (1979)
[34] Mantovani et al. Cytolytic activity of circulating human monocytes on transformed and untransformed human fibroblasts. *Int. J. of Cancer* **23**, 28-31 (1979)
[35] Mantovani et al. Cytolytic and cytostatic activity on tumor cells of circulating human monocytes. *Int. J. of Cancer* **23**, 18-27 (1979)
[36] Pathria et al. Targeting Tumor–Associated Macrophages in Cancer. *Trends in Immunology* **40**, 310-327 (2019)
[37] DeNardo et al. Macrophages as regulators of tumour immunity and immunotherapy. *Nat. Revs. Immunol.* **19**, 369-382 (2019)
[38] Mantovani et al. Macrophage Checkpoint Blockade in Cancer – Back to the Future. *N Engl J Med* **379**, 1777-1779 (2018)
[39] Cassetta et al. Targeting macrophages: therapeutic approaches in cancer. *Nat. Revs. Drug Discovery* **17**, 887-904 (2018)
[40] Cassetta et al. A timeline of tumour–associated macrophage biology. *Nat. Revs. Cancer* **23**, 238-257 (2023)
[41] A Study of Emactuzumab and RO7009789 Administered in Combination in Participants With Advanced Solid Tumors, NCT02760797. Hoffmann-La Roche, 2018.
[42] Liu et al. CD47 blockade triggers T cell–mediated destruction of immunogenic tumors. *Nat. Med.* **21**, 1209-1215 (2015)
[43] IMM2902, a HER2/SIRPa Bispecific mAb-Trap Antibody-receptor Fusion Protein, in Patients with HER2–expressing Advanced Solid Tumors , NCT05076591. ImmuneOnco Biopharmaceuticals (Shanghai) Inc., 2021. https://classic.clinicaltrials.gov/ct2/show/NCT05076591
[44] Akula et al. Protein prenylation restrains innate immunity by inhibiting Rac1 effector interactions. *Nat. Commun.* **10**, 3975 (2019)
[45] van Loosdregt et al. Post-translational modification networks regulating FOXP3 function. *Trends in Immunology* **35**, P368-378 (2014)
[46] Doyle et al. Post-translational protein modification in antigen recognition and autoimmunity. *Trends in Immunology* **22**, P443-449 (2001)
[47] Liu et al. Post–Translational Modification Control of Innate Immunity. *Immunity* **45**, 15-30 (2016)
[48] Yu et al. Modulation of M2 macrophage polarization by the crosstalk between Stat6 and Trim24. *Nat. Commun.* **10**, 4353 (2019)
[49] Sun et al. Reciprocal regulation of Th2 and Th17 cells by PAD2–mediated citrullination. *JCI Insight* **4**, e129687 (2019)
[50] Rogers & Simmonds. Content of citrulline and other amino-acids in a protein of hair follicles. *Nature* **182**, 186-187 (1958)
[51] Smith & Young. The combine amino acids in several species of marine algae. *J of Biological Chemistry* **217**, 845-853 (1955)
[52] György et al. Citrullination: A posttranslational modification in health and disease. *Int. J of Biochem. And Cell Biol.* **38**, 166201677 (2006)
[53] "Citrullination Research Tools." *Cayman Chemical*, 21 Apr 2017, https://www.caymanchem.com/news/citrullination-research-tools. Accessed 23 May 2019.
[54] Zhang et al. Peptidylarginine deiminase 2–catalyzed histone H3 arginine 26 citrullination facilitates estrogen receptor α target gene activation. *PNAS* **109**, 13331-13336 (2012)
[55] Coleman et al. Metal ion dependent binding of sulphonamide to carbonic anhydrase. *Nature* 2**14**, 193-194 (1967)
[56] Arita et al. Structural basis for Ca^{2+}-induced activation of human PAD4. *Nat. Structural & Molec. Biology* 11, 777-783 (2004)
[57] Takahara et al. Calcium-dependent properties of peptidylarginine deiminase from rabbit skeletal muscle. *Agri. And Biological Chem.* 50, 2899-2904 (1986)
[58] Papayannopoulos et al. Neutrophil extracellular traps in immunity and disease. *Nat. Revs. Imunol.* **18**, 134-147 (2018)
[59] Schauer et al. Aggregated neutrophil extracellular traps limit inflammation by degrading cytokine and chemokines. *Nat. Med.* **20**, 511-517 (2014)
[60] Castoldi et al. TLR2, TLR4 and the MYD88 Signaling Pathway Are Crucial for Neutrophil Migration in Acute Kidney Injury Induced by Sepsis. *PLoS One* **7**, e37584 (2012)
[61] Kuwabara et al. NADPH Oxidase-Dependent Production of Reactive Oxygen Species Induces Endoplasmatic Reticulum Stress in Neutrophil-Like HL60 Cells. *PLoS One* **10**, e0116410 (2015)
[62] Damage-associated molecular patterns in cancer: a double-edge sword. *Oncogene* **35**, 5931-5941 (2016)

[63] Jang et al. Interactions between tumor-derived proteins and Toll-like receptors. *Exp. & Mol. Med.* **52**, 1926-1935 (2020)
[64] Bawadekar et al. Peptidylarginine deiminase 2 is required for tumor necrosis factor alpha-induced citrullination and arthritis, but not neutrophil extracellular trap formation. *J Autoimmun.* **80**, 39-47 (2017)
[65] Keshari et al. Cytokines induced neutrophil extracellular traps formation: implication for the inflammatory disease condition. *PLoS One* **7**, e48111 (2012)
[66] Brandolini et al. IL-1 beta primes IL-8-activated human neutrophils for elastase release, phospholipase D activity, and calcium flux. *J Leukoc Biol* **59**, 427–434 (1996)
[67] Zhu et al. PAD4 and its inhibitors in cancer progression and prognosis. *Pharmaceutics* **14**, 2414 (2022)
[68] Lee et al. Extracellular CIRP Induces Macrophage Extracellular Trap formation via Gasdermin D Activation. *Front. Immunol.* **12**, 780210 (2021)
[69] Zhou et al. Thioredoxin-interacting protein links oxidative stress to inflammasome activation. *Nat. Immunol.* **11**, 136-141 (2010)
[70] Wen et al. A role for the NLRP3 inflammasome in metabolic diseases—did Warburg miss inflammation? *Nat. Immunol. Rev.* **13**, 352-357 (2012)
[71] Zhong et al. TRPM2 links oxidative stress to NLRP3 inflammasome activation. *Nat. Communications* **4**, 1-11 (2013)
[72] Wu et al. Peptidylarginine Deiminase 2 Mediates Caspase-1-Associated Lethality in *Pseudomonas aeruginosa* Pneumonia-induced Sepsis. *J Inf. Dis.* **223**, 1093-1102 (2021)
[73] Franciosi et al. Interferon-γ acutely induces calcium influx in human microglia. *J of Neuro. Research* **69**, 607-613 (2002)
[74] Koide et al. Calcium influx and the Ca2+–calmodulin complex are involved in interferon-γ–induced expression of HLA class II molecules on HL-60 cells. *Proc. Natl. Acad. Sci. USA* **85**, 3120-3124 (1988)
[75] June et al. Role of the CD28 receptor in T-cell activation. *Immunology Today* **11**, 211-216 (1990)
[76] Kim et al. Targeted calcium influx boosts cytotoxic T lymphocytes function in the tumour microenvironment. *Nat. Commun.* 8, 15365 (2017)
[77] Treback & Kinet. Calcium signaling in T cells. *Nat. Revs. Immunol.* **19**, 154-169 (2019)
[78] Dominguez-Villar et al. TLR7 induces anergy in human $CD4^+$ T cells. *Nat. Immunol.* **16**, 118-128 (2014)
[79] Schenten et al. Signaling through the Adaptor Molecule MyD88 in $CD4^+$ T cells Is Required to Overcome Suppression by Regulatory T Cells. *Immunity* **40**, 78-90 (2014)
[80] Liu et al. Peptidylarginine deiminases 2 and 4 modulate innate and adaptive immune responses in TLR-7–dependent lupus. *JCI Insight* 3, e124729 (2018)
[81] Wood et al. The isolation, characterization, and lipid-aggregating properties of a citrulline containing myelin basic protein. *J of Biol Chem.* **264**, 5121-5127 (1989)
[82] Knipp et al. A colorimetric 96-well microtiter plate assay for the determination of enzymatically formed citrulline. *Anal. Biochem.* **286**, 257-264 (2002)
[83] Senshu et al. Detection of citrulline residues in deiminated proteins on polyvinylidene difluoride membrane. *Anal. Biochem.* **203**, 94-100 (1992)
[84] Nicholas et al. Immunohistochemical localization of citrullinated proteins in adult rat brain. *J Comp. Neurol.* **459**, 251-266 (2003)
[85] Moelants et al. Detection and quantification of citrullinated cytokines. *PLoS ONE* **6**, pe28976 (2011)
[86] Nicholas et al. Preparation of a monoclonal antibody to citrullinated epitopes: its characterization and some applications to immunohistochemistry in human brain. *Glia* **37**, 328-336 (2002)
[87] Nicholas et al. Immunohistochemical localization of citrullinated proteins in adult rat brain. *J. Comp. Neurol.* **459**, 251-266 (2003)
[88] https://www.abcam.com/products/primary-antibodies/histone-h3-citrulline-r2--r8--r17-antibody-ab5103.html
[89] Tanikawa et al. Regulation of histone modification and chromatin structure by the p53–PADI4 pathway. *Nat. Commun*. **3**, 676 (2012)
[90] Christophorou et al. Citrullination regulates pluripotency and histone H1 binding of chromatin. *Nature* **507**, 104-108 (2014)
[91] Hunt et al. Protein sequencing by tandem mass spectrometry. *Proc. Natl. Acad. Sci. USA* **83**, 6233-6237 (1986)
[92] Clancy et al. Detection and identification of protein citrullination in complex biological systems. *Current Opinion in Chem. Biol.* **30**, 1-6 (2016)
[93] Lee et al. Mining the human tissue proteome for protein citrullination. *Mol. & Cellular Proteomics* **17**, 1378-1391 (2018)

[94] Rajimakers et al. Elevated levels of fibrinogen–derived endogenous citrullinated peptides in synovial fluid of rheumatoid arthritis patients. *Arthritis Res. Ther.* 14, pR114 (2012)
[95] van Beers et al. The rheumatoid arthritis synovial fluid citrullinome reveals novel citrullinated epitopes in apolipoprotein E, myeloid nuclear differentiation antigen, and beta-actin. *Arthritis Rheum.* **65**, 69-80 (2013)
[96] De Ceuleneer et al. Quantification of citrullination by means of skewed isotope distribution pattern. *J Proteome Res.* **11**, 5245-5251 (2012)
[97] Fert-Bober et al. Citrullination of myofilament proteins in heart failure. *Cardiovasc Res*. **108**, 232-242 (2015)
[98] Holm et al. Specific modification of peptide-bound citrulline residues. *Anal. Biochem.* **352**, 68-76 (2006)
[99] De Ceuleneer et al. Modification of citrulline residues with 2,3–butanedione facilitates their detection by liquid chromatography/mass spectrometry. *Rapid Commun. Mass. Spectrom.* 25, 1536-1542 (2011)
[100] Bengelsdorf. A reaction of guanidine with glyoxals in aqueous solution. The preparation of glycocyamidines. *Am. Chem. Soc.* **75**, 3138-3140 (1952)
[101] Jong et al. Reactivity of (vicinal) carbonyl compounds with urea. *ACS Omega* **4**, 11928-11937 (2019)
[102] Bicker et al. Seeing citrulline: development of a phenylglyoxal-based probe to visualize protein citrullination. *J Am Chem Soc* 134, 17015-17018 (2012)
[103] Choi et al. Matrix-assisted laser desorption ionization-time of flight mass spectrometry identification of peptide citrullination site using Br signature. *Anal Biochem* **437**, 62-67 (2013)
[104] Tutteran et al. Assessing the citrullinome in rheumatoid arthritis synovial fluid with and without enrichment of citrullinated peptides. *J Proteome Res* **13**, 2867-2873 (2014)
[105] Tutteran et al. Specific biotinylated and sensitive enrichment of citrullinated peptides. *Anal Bioanal Chem* **405**, 9321-9331 (2013)
[106] Lewallen et al. A chemical proteomic platform to identify citrullinated proteins. *ACS Chem. Biol.*, 2520-2528 (2015)
[107] Leshner et al. PAD4 mediated histone hypercitrullination induces heterochromatin decondensation and chromatin unfolding to form neutrophil extracellular trap-like structures. *Front. Immunol.* **3**, 307 (2012)
[108] Slade et al. Citrullination unravels stem cells. *Nat. Chem. Biol.* **10**, 327-328 (2014)
[109] Nakashima et al. PAD4 regulates proliferation of multipotent haematopoietic cells by controllins c-myc expression. *Nat. Commun.* 4: 1836 (2013)
[110] Song et al. A novel PAD4/SOX4/PU.1 signaling pathway is involved in the committeed differentiation of acute promyelocytic leukemia cells into granulocytic cells. *Oncotarget* **7**, 3144-3157 (2016)
[111]Yuzhalin et al. Citrullination in Cancer. *Cancer Res* **79**, 1274-1284 (2019)
[112] Shi et al. Endogenous PAD4 in breast cancer cells mediates cancer extracellular chromatin network formation and promotes lung metastasis. *Mol. Cancer Res.* **18**, 735-747 (2020)
[113] Cuthbert et al. Histone deimination antagonizes arginine methylation. *Cell* **118**, 545-553 (2004)
[114] Bannister et al. Histone methylation: dynamic or static? *Cell* **109**, 801-806 (2002)
[115] Bauer et al. Methylation at arginine 17 of histone H3 is linked to gene activation. *EMBO Rep.* **3**, 39-44 (2002)
[116] Wang et al. Human PAD4 regulates histone arginine methylation levels via demethylimination. *Science* **306**, 279-283 (2004)
[117] Stadler et al. Dysregulation of PAD4–mediated citrullination of nuclear GSK3β activates TGF-β signaling and induces epithelial-to-mesenchymal transition in breast cancer cells. *PNAS* **110**, 11851-11856 (2013)
[118] Tillotson et al. Differential protein citrullination in human ER^- and ER^+ tumor and adjacent healthy breast tissue. Biochemistry *62*, 893-898 (2023)
[119] Yuzhalin et al. Colorectal cancer liver metastatic growth depends on PAD4-driven citrullination of the extracellular matrix. *Nat Commun.* **9**, 1-15 (2018)
[120] Zhang et al. Genome-Wide Analysis Reveals PADI4 Cooperates with Elk-1 to Activate *c-Fos* Expression in Breast Cancer Cells. *PLoS Genetics* **7**, e1002112 (2011)
[121] Tanikawa et al. Regulation of protein citrullination through p53/PADI4 network in DNA damage response. *Cancer Res.* **69**, 8761-8769 (2009)
[122] Sekhar et al. Nucleophosmin plays a role in repairing DNA damage and is a target for cancer treatment. *Cancer Res.* **83**, 1573-1580 (2023)
[123] Nakashima et al. Nuclear localization of peptidylarginine deiminase V and histone deimination in granulocytes. *J Biol Chem.* **277**, 49562-49568 (2002)
[124] Neeli et al. Histone deimination as a response to inflammatory stimuli in neutrophils. *J Immunol.* **180**, 1895-1902 (2008)
[125] Wang et al. Histone hypercitrullination mediates chromatin decondensation and neutrophil extracellular traps. *J Cell Biol.* **184**, 205-213 (2009)

[126] Tsourouktsoglou et al. Histones, DNA, and citrullination promote neutrophil extracellular trap inflammation by regulating the localization and activation of TLR4. *Cell Reports* **31**, 107602 (2020)
[127] Luo et al. Constitutive neutrophil apoptosis: mechanisms and regulation. *Am J Hematol.* **83**, 288-295 (2008)
[128] Remijsen et al. Dying for a cause: NETosis, mechanisms behind an antimicrobial cell death modality. *Cell Death & Differentiation* **18**, 581-588 (2011)
[129] Klebanoff et al. Myeloperoxidase: contribution to the microbicidal activity of intact leukocytes. *Science* **169**, 1095-1097 (1970)
[130] Segal et al. How neutrophils kill microbes. *Annu Rev Immunol.* **23**, 197-223 (2005)
[131] Brinkmann et al. Neutrophil extracellular traps kill bacteria. *Science* **303**, 1532-1535 (2004)
[132] Li et al. PAD4 is essential for antibacterial innate immunity mediated by neutrophil extracellular traps. *J Exp. Med.* **207**, 1853-1862 (2010)
[133] Curran et al. PAD enzymes in rheumatoid arthritis: pathogenic effectors and autoimmune targets. *Nat. Revs. Rheumatology* **16**, 301-315 (2020)
[134] Schellekens et al. Citrulline is an essential constituent of antigenic determinants recognized by rheumatoid arthritis-specific autoantibodies. *J Clin. Invest.* **101**, 273-281 (1998)
[135] Khandpur et al. NETs are a source of citrullinated autoantigens and stimulate inflammatory responses in rheumatoid arthritis. *Sci Transl. Med.* **5**, 178ra40 (2013)
[136] Tilvawala et al. The rheumatoid arthritis–associated citrullinome. *Cell Chem. Biol.* **25**, 691-704 (2018)
[137] Albrengues et al. Neutrophil extracellular traps produced during inflammation awaken dormant cancer cells in mice. *Science* **361**, 1-13 (2018)
[138] Yang et al. DNA of neutrophil extracellular traps promotes cancer metastasis via CCDC25. *Nature* **583**, 133-138 (2020)
[139] Sun et al. Citrullination of NF-kB p65 promotes its nuclear localization and TLR–induced expression of IL-1b and TNFa. *Sci. Immunol.* **2**, eaal3062 (2017)
[140] Sabnis et al. Novel peptidylarginine deiminase type 4 (PAD4) inhibitors. *ACS Med. Chem. Lett.* **13**, 1537-1538 (2022)
[141] Khandpur et al. NETs are a source of citrullinated autoantigens and stimulate inflammatory responses in rheumatoid arthritis. *Sci. Transl. Med.* **5**, 178ra40 (2013)
[142] Witalison et al. Protein arginine deminases and associated citrullination: physiological functions and diseases associated with dysregulation. *Curr. Drug Targets* **16**, 700-710 (2015)
[143] Martinez-Prat et al. Antibodies targeting protein-protein deiminase 4 (PAD4) demonstrate diagnostic value in rheumatoid arthritis. *Ann. Rheum. Dis.* **0**, 1-3 (2018)
[144] Wang et al. Anticancer peptidylarginine deiminase (PAD) inhibitors regulate the autophagy flux and the mammalian target of rapamycin complex 1. *J. Biol. Chem.* **287**, 25941-53 (2012)
[145] Chen et al. Inhibition of PAD4 enhances radiosensitivity and inhibits aggressive phenotypes of nasopharyngeal carcinoma cells. *Cellular & Molecular Biology Letters* **26**, 9 (2021)
[146] Deng et al. A novel selective inhibitor JBI-589 targets PAD4–mediate neutrophil migration to suppress tumor progression. *Cancer Res* **82**, 3561-3572 (2022)
[147] Zhu et al. Highly-tumor-target PAD4 inhibitors with PBA modification inhibit tumors *in vivo* by specifically inhibiting the PAD4-H3cit-NETs pathway in neutrophils. *European Journal of Med. Chem.* **258**, 115619 (2023)
[148] Casanova-Acebes et al. Tissue-resident macrophages provide a protumorigenic niche to early NSCLC cells. *Nature* **595**, 578-584 (2021)
[149] Underhill et al. Dynamic interactions of macrophages with T cells during antigen presentation. *J Exp. Med.* **190**, 1909-1914 (1999)
[150] Gordon. Alternative activation of macrophages. *Nat. Revs. Immunol.* **3**, 23-35 (2003)
[151] Xiang et al. Targeting tumor-associated macrophages to synergize tumor immunotherapy. *Sig. Transduct. Target Ther.* **6**, 75 (2021)
[152] Lin et al. Host expression of PD-L1 determine efficacy of PD-L1 pathway blockade–mediated tumor regression. *J Clin Invest* **128**, 805-815 (2018)
[153] Zhu Y, Knolhoff BL, Meyer MA, Nywening TM, West BL, Luo JQ, et al. CSF1/CSF1R Blockade Reprograms Tumor-Infiltrating Macrophages and Improves Response to T-cell Checkpoint Immunotherapy in Pancreatic Cancer Models. *Cancer Research.* **74**, 5057-5069 (2014)
[154] Vitale I, Manic G, Coussens LM, Kroemer G, and Galluzzi L. Macrophages and Metabolism in the Tumor Microenvironment. *Cell Metabolism.* **30**, 36-50 (2019)

[155] Mantovani A, Allavena P, Marchesi F, and Garlanda C. Macrophages as tools and targets in cancer therapy. *Nat Rev Drug Discov.* **21**, 799-820 (2022)
[156] Ramazi et al. Post-translational modifications in proteins: resources, tools and prediction methods. *Database* **2021**, baab012 (2021)
[157] Mann et al. Proteomic analysis of post-translational modifications. *Nat. Biotechnol.* **21**, 255-261 (2003)
[158] Ryslava et al. Effect of posttranslational modification on enzyme function and assembly. *J. Proteomics* **92**, 80-109 (2013)
[159] Lin et al. Stanniocalcin 1 is a phagocytosis checkpoint driving tumor immune resistance. *Cancer Cell.* **39**, 480-493 (2021)

[160] Satija R, Farrell JA, Gennert D, Schier AF, Regev A. Spatial reconstruction of single-cell gene expression data. *Nat. Biotechnology* **33**, 495-502 (2015)

[161] Wang et al. BART: a transcription factor prediction tool with query gene sets or epigenomic profiles. *Bioinformatics* 34, 2867-2869 (2018)
[162] Rebollo R, Horard B, Begeot F, Delattre M, Gilson E and Vieira C. A Snapshot of Histone Modifications within Transposable Elements in *Drosophila* Wild Type Strains. *PLoS One* **7**, e44253 (2023)

[163] Popadin K, Gutierrez-Arcelus M, Dermitzakis ET and Antonarakis SE. Genetic and Epigenetic Regulation of Human lincRNA Gene Expression. *AJHG* **93**, 1015-1026 (2013)

[164] Wang R, Lee JH, Kim J, Xiong F, Al Hasani L, Shi Y, et al. SARS-CoV-2 restructures host chromatin architecture. *Nat. Microbiol*. **8**, 679-694 (2023)

[165] Mann et al. Proteomic analysis of post-translational modifications. *Nat. Biotech*. **21**, 255-261 (2003)
[166] Deribe et al. Post-translational modifications in signal integration. *Nat. Structural & Mol. Biol.* **17**, 666.672 (2010)
[167] Nixon et al. Tumor-associated macrophages expressing the transcription factor IRF8 promote T cell exhaustion in cancer. *Immunity* **55**, 2044-2058 (2022)

[168] Pyonteck et al. CSF-1R inhibition alters macrophage polarization and blocks glioma progression. *Nat. Medicine* **19**, 1264-1272 (2013)
[169] Xia et al. Autophagic adaptation to oxidative stress alters peritoneal residential macrophage survival and ovarian cancer metastasis. *JCI Insight* **5**, e141115 (2020)
[170] Wang et al. Select autophagy genes maintain quiescence of tissue-resident macrophages and increase susceptibility to *Listeria monocytogenes*. *Nat. Microbiol.* **5**, 272-281 (2020)

[171] Jang et al. Interactions between tumor-derived proteins and Toll-like receptors. *Experimental & Mol. Med.* **52**, 1926-1935 (2020)
[172] Devalaraja et al. Tumor-derived retinoic acid regulates intratumoral monocyte differentiation to promote immune suppression. *Cell* **181**, 1098-1114 (2020)
[173] Kryczek et al. CXCL12 and vascular growth factor synergistically induce neoangiogenesis in human ovarian cancer. *Cancer Res.* **65**, 465-72 (2005)
[174] Kryczek et al. B7-H4 expression identifies a novel suppressive macrophage population in human ovarian carcinoma. *J Exp. Med.* **203**, 871-881 (2006)
[175] Kokubu et al. Induction of protumoral CD11c(high) macrophages by glioma cancer stem cells through GM-CSF. *Genes Cells* **21**, 241-251 (2016)
[176] Roche et al. The ins and outs of MHC class II–mediated antigen processing and presentation. *Nat. Revs.Immunol.* **15**, 203-216 (2015)
[177] Wang et al. Transition of tumor-associated macrophages from MHC class II^{hi} to MHC class II^{low} mediated tumor progression in mice. *BMC Immunol.* **12**, 43 (2011).
[178] Geeraerts et al. Macrophages are metabolically heterogeneous within the tumor microenvironment. *Cell Reports* **37**, 110171 (2021)
[179] Ting et al. Genetic control of MHC class II expression. *Cell* **109**, S21-33 (2002)
[180] Shuai et al. Regulation of gene-activation pathways by PIAS proteins in the immune system. *Nat. Revs. Immunol.* **5**, 593-605 (2005)

[182] Li et al. Metabolism drives macrophage heterogeneity in the tumor microenvironment. *Cell Reports* **39**, 110609 (2022)
[183] Baker and Clauser. Protein Prospector. http://prospector.ucsf.edu. (1996-2023)
[184] Chen et al. Crystal structure of a tyrosine phosphorylated STAT-1 dimer bound to DNA. *Cell* **93**, 827-839 (1998)
[185] Vinkemeier et al. Structure of the Amino-Terminal Protein Interaction Domain of STAT-4. *Science* **279**, 1048-1052 (1998)
[186] Ota et al. N-domain–dependent nonphosphorylated STAT4 dimers required for cytokine-driven activation. *Nat. Immunol.* **5**, 208-215 (2004)
[187] Reich and Liu. Tracking STAT nuclear traffic. *Nat. Rev. Immunol.* **6**, 602-612 (2006)
[188] Göder et al. STAT1 N-terminal domain discriminatively controls type I and type II IFN signaling. *Cytokine* **144**, 155552 (2021)

[189] Mowen et al. Arginine methylation of STAT1 modulates IFNalpha/beta–induced transcription. *Cell* **104**, 731-741 (2001)
[190] Mowen and David. Unconventional post-translational modification in immunological signaling. *Nat. Immunol.* **15**, 512-520 (2014)
[191] Hu et al. The JAK/STAT signaling pathway: from bench to clinic. *Signal Trans. And Targeted Therapy* **6**, 402 (2021)
[192] Hoeve et al. Identification of a nuclear Stat1 protein tyrosine phosphatase. *Mol Cell Biol* **22**, 5662-5668 (2002)
[193] Croker et al. SOCS Regulation of the JAK/STAT Signaling Pathway. *Semin Cell Dev Biol.* **19**, 414-422 (2008)
[194] Liu et al. PIAS1 selectively inhibits interferon–inducible genes and is important in innate immunity. *Nat. Immunol.* **5**, 891-898 (2004)
[195] Buxadé et al. Macrophage–specific MHCII expression is regulated by a remote *Ciita* enhancer controlled by NFAT5. *J Exp Med* **215**, 2901-2918 (2018)
[196] Lei et al. A second-generation M1-polarized CAR macrophage with antitumor efficacy. *Nat. Immunol.* 25, 102-116 (2024)
[197] Cedervall et al. Pharmacological targeting of peptidylarginine deminase 4 prevents cancer–associated kidney injury in mice. *OncoImmunology* **6**, e1320009 (2017)

[199] Zhang et al. Single-cell analyses reveal key immune cell subsets associated with response to PD-L1 blockade in triple-negative breast cancer. *Cancer Cell* **39**, 1578-1593 (2021)
[200] Kruse et al. $CD4^+$ T cell–induced inflammatory cell death controls immune-evasive tumours. *Nature* **618**, 1033-1040 (2023)
[201] Cachot et al. Tumor-specific cytolytic CD4 T cells mediate immunity against human cancer. *Sci. Advances* **7**, eabe3348 (2021)
[202] Oh and Fong. Cytotoxic $CD4^+$ T cells in cancer: Expanding the immune effector toolbox. *Immunity* **54**, 2701-2711 (2021)
[203] Robinson et al. edgeR: a Bioconductor package for differential expression analysis of digital gene expression data. *Bioinformatics* **26**, 139-140 (2010)
[204] Smyth and Verbyla. A conditional likelihood approach to residual maximum likelihood estimation in generalized linear models. *J. R. Statist. Soc.* **58**, 565-572 (1996)
[205] Love et al. Moderated estimation of fold change and dispersion for RNA-seq data with DESeq2. *Genome Biology* 15, 550 (2014)
[206] Robinson and Smyth. Small-sample estimation of negative binomial dispersion, with applications to SAGE data. *Biostatistics* **9**, 321-332 (2008)
[207] Hao et al. Integrated analysis of multimodal single-cell data. *Cell* **184**, 3573-3587 (2021)
[208] Subramanian et al. Gene set enrichment analysis: a knowledge-based approach for interpreting genome-wide expression profiles. *PNAS* **102**, 15545-15550 (2005)
[209] Hirano et al. Blockade of B7-H1 and PD-1 by monoclonal antibodies potentiates cancer therapeutic immunity. *Cancer Res.* **65**, 1089-1096 (2005)
[210] Pitter et al. Uncovering the immunoregulatory function and therapeutic potential of the PD-1/PD-L1 axis in cancer. *Cancer Res.* **81**, 5141-5143 (2021)
[211] Cherrington et al. Potential role of PAD2 in gene regulation in breast cancer cells. *PLoS One* **7**, e41242 (2012)
[212] Zheng et al. Calcium regulates the nuclear localization of protein arginine deiminase 2. *Biochemistry* **58**, 3042-3056 (2019)

[213] Falcão et al. PAD2–mediated citrullination contributes to efficient oligodendrocyte differentiation and myelination. *Cell Reports* **27**, 1090-1102 (2019)
[214] van der Veeken et al. The transcription factor FOXP3 shapes regulatory T cell identity by tuning the activity of trans–acting intermediaries. *Immunity* **53**, 971-984 (2020)
[215] Yu et al. Liver metastasis restrains immunotherapy efficacy via macrophage–mediated T cell elimination. *Nat. Medicine* **27**, 152-164 (2021)
[216] Scheeren et al. STAT5 regulates the self-renewal capacity and differentiation of human memory B cells and controls Bcl-6 expression. *Nat. Immunol.* **6**, 303-313 (2005)
[217] Malin et al. Role of STAT5 in controlling cell survival and immunoglobulin gene recombination during pro-B cell development. *Nat. Immunol.* **11**, 171-179 (2010)
[218] Lundgren et al. Interleukin 4 induces synthesis of IgE and IgG4 in human B cells. *Eur J Immunol.* **19**, 1311-1315 (1989)